

UMTRI-83-10-2

INFLUENCE OF SIZE AND WEIGHT VARIABLES ON THE STABILITY
AND CONTROL PROPERTIES OF HEAVY TRUCKS

Final Report

Contract Number FH-11-9577

Volume II

R.D. Ervin
R.L. Nisonger
M. Sayers
T.D. Gillespie
P.S. Fancher

April 1983

Prepared for the Department of Transportation, Federal Highway Administration under Contract FH-11-9577. The opinions, findings, and conclusions expressed in this publication are those of the authors and not necessarily those of the Federal Highway Administration.

Technical Report Documentation Page

1. Report No. FHWA/RD-83/030	2. Government Accession No.	3. Recipient's Catalog No.	
4. Title and Subtitle INFLUENCE OF SIZE AND WEIGHT VARIABLES ON THE STABILITY AND CONTROL PROPERTIES OF HEAVY TRUCKS - Volume II		5. Report Date April 1983	
		6. Performing Organization Code	
7. Author(s) R.D. Ervin, R.L. Nisonger, M. Sayers, T.D. Gillespie, P.S. Fancher		8. Performing Organization Report No. UMTRI-83-10/2	
9. Performing Organization Name and Address Transportation Research Institute The University of Michigan 2901 Baxter Road Ann Arbor, Michigan 48109		10. Work Unit No. 31U4-044	
		11. Contract or Grant No. FH-11-9577	
12. Sponsoring Agency Name and Address Federal Highway Administration U.S. Department of Transportation Washington, D.C. 20590		13. Type of Report and Period Covered Final 4/5/79 - 5/18/83	
		14. Sponsoring Agency Code	
15. Supplementary Notes Contract Manager - Dr. R. Hegmon (HNR-20)			
16. Abstract <p>This study has determined the influence of variations in truck size and weight constraints on the stability and control properties of heavy vehicles. The size and weight constraints of interest include axle load, gross vehicle weight, length, width, type of multiple-trailer combinations, and bridge formula allowances. Variations in location of the center of gravity of the payload were also considered as a separate subject. The influence of these parametric variations on stability and control behavior was explored by means of both full-scale vehicle tests and computer simulations.</p> <p>In volume I, the findings of the study were presented in a manner which is intended to inform the non-technical reader and, specifically, the persons concerned with formulating policies and laws regarding truck size and weight.</p> <p>Volume II presents the methodology and summary results from the full-scale test program. The test findings relating size and weight variables to vehicle dynamic behavior are compared with those derived from simulation results. Volume II also presents the results of a special set of experimental measurements showing the dynamic loads which heavy trucks impose on the pavement. Volume III contains appendices of test and simulation data.</p>			
17. Key Words size and weight, heavy trucks, stability and control, traffic safety, pavement loading, dynamic wheel load tests, simulation		18. Distribution Statement UNLIMITED	
19. Security Classif. (of this report) NONE	20. Security Classif. (of this page) NONE	21. No. of Pages 179	22. Price

TABLE OF CONTENTS

CHAPTER

1	INTRODUCTION.	1
2	TEST PROGRAM.	4
	2.1 Test Methodology.	4
	2.2 Overview of Test Results.	35
	2.3 Comparison of Test and Simulation Results	60
3	ANALYTICAL METHODS.	85
	3.1 Previously-Developed Models	85
	3.2 Simplified Method of Analyzing Vehicle Braking Performance	94
	3.3 Simplified Method for Analyzing Rearward Amplification Level	100
	3.4 Low-Speed Offtracking Calculation	101
	3.5 High-Speed Offtracking Calculation.	117
	3.6 Conventions for Fixing Typical Vehicle Parameters	121
4	DYNAMIC WHEEL LOAD.	125
	4.1 Measurement of Dynamic Wheel Load	126
	4.2 Road Test Sites	134
	4.3 Results	136
	4.4 Corroboration with Sweatman's Findings.	142
	4.5 Relative Importance of Dynamic Loads to Pavement Damage	146
	4.6 The Role of Vehicle Dynamics in Pavement Load	148
	4.7 Conclusions	152
	4.8 Recommendations	155
	REFERENCES.	157
	APPENDIX A.	161

ACKNOWLEDGEMENTS

A number of parties contributed vehicles and hardware in support of the full scale test program. In particular we wish to acknowledge the following organizations:

- International Harvester Company, Truck Division
(for the loan of road tractors and the provision of technical advice)
- Yellow Freight Lines
(for the loan of trailers and converter dollies)
- Central Transport Inc.
(for the loan of a tandem axle converter dolly)
- The Fruehauf Corporation, R & D Division
(for the loan of semitrailers)
- The Chrysler Corporation
(for the loan of test loading weights--and for their gracious cooperation in the use of the Chelsea Proving Grounds)
- The Holland Hitch Company
(for the contribution of pintle hitch assemblies)
- Union Carbide Corporation - Linde Division
(for the loan of a road tractor for use in the dynamic wheel load experiments)
- Western Highway Institute
(for arrangement of industry contacts through which Rocky Mountain doubles combinations were defined)

CHAPTER 1
INTRODUCTION

This volume of the report covers the test program which was conducted to measure the influences of size and weight variations on the stability and control of heavy vehicles. Also, an overview is given of the various analytical methods used to calculate vehicle response under differing size and weight configurations. Additionally, a set of field measurements are reported concerning the dynamic wheel loads experienced by heavy vehicles during travel at highway speeds. Although this last subject did not relate directly to the primary objectives of the study, vis-a-vis size and weight influences, it was undertaken here as an efficient means of accomplishing an experiment which required the same basic data recording system that was used in the stability and control tests.

The study of the influence of size and weight variables on stability and control was first envisioned by FHWA as a full-scale test activity. Later in the project, it was desired that the depth of the research be expanded to provide for computerized simulations which would explore the same size and weight issues more thoroughly as well as address certain additional subjects.

Since the simulation results provided a much more comprehensive treatment of the size and weight influences of interest here, and since, in general, the simulation and test results were not produced under identical pavement and velocity conditions, it was determined that simulation results would be used by themselves to provide the format for presenting the great bulk of the study findings in Volume I. This approach was based also upon the observation that the test data generally confirmed the simulation results and that the few "discrepancies" could be easily traced to parametric differences in vehicles.

Thus, the question arises, "What role do the test data play in achieving the objectives of the study?" Clearly, the fact that test results

are commonly looked upon as "hard data" suggests that the proper role of these results is to serve as the reference or benchmark illustrations of the influences of size and weight variables on stability and control. Assuming that the test data are to play this role, the reader is advised to consider the following observations which tend to qualify the adequacy of the test results:

1) The test program, though very ambitious in sheer number of tests performed, provides a rather sparse treatment of the size and weight issues. The problem is simply that a broad set of subjects is involved, and with each subject, there are a large set of levels of variation and vehicle configurations which are of interest. It was possible to address only a modest sampling of these subjects by way of full-scale tests.

2) The test vehicles were obtained on loan from manufacturers and from trucking fleets. Since no parameter measurements were made on each vehicle, the extent to which the mechanical properties of the suspensions, brakes, steering systems, etc., were actually representative of typical hardware is unknown. Nevertheless, inspection of the vehicles suggests that no unusual component configurations were present.

3) The full-scale test procedures were constrained by certain practicalities which make the results more of an approximation than is attainable by means of simulation. For example, consider that:

- a) The rollover limit is determined by observing the maneuver severity at which the test vehicle "touches down" its protective outrigger. Since, due to safety considerations, the outrigger is adjusted to touch the ground after the trailer tires have lifted off the pavement, whether tractor tires have lifted off or not, the touchdown does not precisely determine an incipient rollover condition.
- b) The representativeness of braking performance test results is seen to be undefineable, here, since the torque output of brakes employed on heavy vehicles is generally poor in repeatability.

- c) Tire wear is accrued rapidly during the type of maneuvers conducted here. Further, truck tires are relatively expensive such that a practice of changing test tires so as to avoid appreciable treadwear is prohibitively expensive. Thus, the testing process suffers to some degree from variations in vehicle performance accompanying the changes in tire behavior which result from treadwear.
- d) The maximum test speed was limited by the layout of the test facility to 45 mph (72 km/h) such that the higher levels of so-called "rearward amplification" seen with multiple-trailer combinations at highway speeds could not be illustrated.

Moreover, the greatest value of the test results is seen by the authors to be that of providing a qualitative basis for confirming the simulation results. On the strength of the qualitative agreement seen between simulation and the experiments conducted here, and with the experience of having, in the past [1,2,3,4,5,6], proven the ability of the simulations to accurately reproduce the response of vehicles whose mechanical parameters were known in detail, the simulation results produced in this study were seen as the ideal means of displaying the influences of size and weight variables on stability and control performance.

In Chapter 2 of this volume, the test program will be outlined in terms of the conditions covered, the vehicles and test procedures employed, and the results obtained. The test and simulation results will also be compared. In Chapter 3, the various analytical methods used in the study will be identified and discussed. Certain of these methods which were developed specifically for application to this study will be documented with reference to appended material in Volume III.

Finally, in Chapter 4, the limited study of dynamic wheel loads will be discussed. This portion of the effort should be of interest to those concerned with the extent to which trucks having differing suspension types impose dynamically-fluctuating loads on the pavement. The results are presented in the context of their implications for pavement damage.

CHAPTER 2

TEST PROGRAM

During the May-to-November periods of 1980 and 1981, full-scale tests were conducted at the Chrysler Corporation's Chelsea Proving Grounds in Chelsea, Michigan. The test program consisted of braking and steering experiments designed to evaluate the stability and control characteristics of a wide range of heavy vehicle configurations. Each of these configurations was tested in some baseline, fully-loaded state and certain of the vehicles were also examined with variations in loading. Altogether, some 25 cases of vehicle configuration and loading condition were represented in the tests. The vehicle response data were measured and recorded using an instrumentation system which was assembled under a previous FHWA-sponsored project [7]. The collected data was processed using the central computing system of The University of Michigan.

The test program will be discussed below in terms of the elements making up the test methodology and by means of an overview of the results. Detailed plots of test data are provided in Volume III.

2.1 Test Methodology

In this section, the test methodology will be described. The methodology discussion will include:



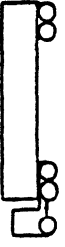
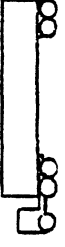
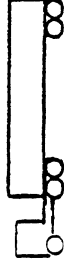

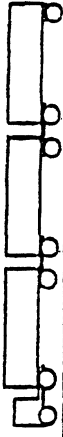
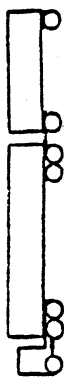

- the matrix of vehicles and loading conditions used
- the equipment with which the test vehicles were outfitted
- the procedures employed
- the data processing method

2.1.1 Test Matrix. Shown in Table 1 is the matrix of vehicles and loading conditions employed in full-scale testing. Each vehicle and loading condition is represented by a code number which identifies the power unit, trailer, and vehicle condition by separate designations. For example, the

Table 1

Matrix of Test Vehicle Configurations

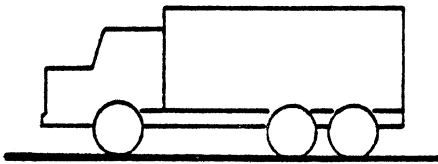
Payload

Code No.	Vehicle	Description	Power Unit		Trailers Axles Lgth.	Special Conditions	C.G. Hgt. in.	Axle Loads/1000 lb									GVW 1000 lb
			GAWRF	GAWRR				1	2	3	4	5	6	7	8	9	
ST2-C1 ST2-C2 ST2-C3 ST2-C4		3-axle Truck	12 K	38 K	—	Baseline High C.G. Radials fr., bias rear	70.5 79.0 93.0 70.5	34 38 34 34									46 50 50 50
T1-TR1-C1 T1-TR1-C2 T1-TR1-C3		3-axle tractor semi	12 K	23 K	1 27'	Baseline Radials fr., bias rear	72 80 80	20 22 22									52 56 56
T3-TR6-C1 T3-TR6-C2 T3-TR6-C3 T3-TR6-C4 T3-TR5-Empty		5-axle tractor semi	12 K	34 K	2 45'	Baseline Radials fr., bias rear Empty	70 78.5 70 70	34 38 35 35	34 38 35 35								80 88 80 80 80
T7-TR6-C1 T7-TR6-C2 T7-TR6-C3 T7-TR6-C4		5-axle tractor semi	12 K	38 K	2 45'	Baseline Partial Loading High C.G. 80K High C.G. 88K	70 70 95 99	34 30 34 38	34 16 34 38								80 58 80 88
T5-TR6-C1 T5-TR6-C2 T5-TR6-C3 T5-TR6-C4		5-axle tractor semi	12 K	38 K	2 45'	Baseline Radials fr., bias rear	70 78.5 70 70	34 38 35 35	34 38 35 35								80 88 80 80
T1-TR1-TR2-C1 T1-TR1-TR2-C2 T1-TR1-TR2-Empty		5-axle double	12 K	23 K	1 27'	Baseline Empty	73 83	18 20	17.5 19.5	17.5 19.5							80 88
T1-TR1-TR2-TR3-C1		7-axle triple	12 K	23 K	1 27'	Baseline	69	16	15.5	15.5	15.5						103
T7-TR6-TR7-C1		Rocky Mountain Double	12 K	38 K	2 45' 1 27'	Baseline	68	10	32	30	15	15					102
T3-TR5-TR6-C1		Turnpike Double	12 K	34 K	2 45'	Baseline	67	10	28	25	25						113

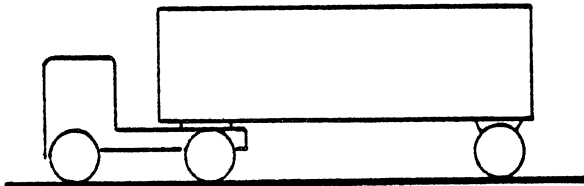
U)

tractor designated as "T1" coupled to semitrailer, "TR1," loaded to the level described as condition "C1" is listed on the table and elsewhere in the report as "T1-TR1-C1."

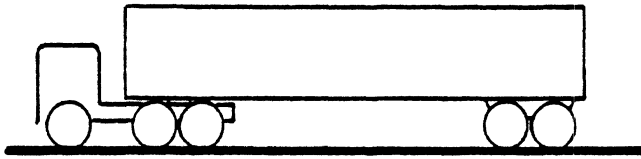
The table shows the following basic vehicle configurations:



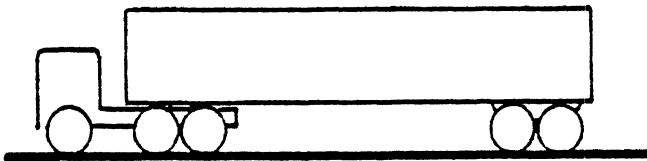
ST2 (straight truck, three-axle, 209-inch (531-cm) wheelbase -- This truck is the same physical vehicle as the tractor, T5, cited below but is outfitted with a flat load bed for fastening loading racks. The truck is an International Harvester COE design which was loaned from IH's engineering fleet. This test vehicle and all others having tandem axles incorporated a four-spring type of tandem suspension.)



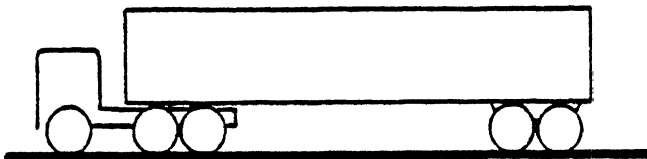
T1-TR1 (a two-axle tractor coupled to a single-axle semitrailer. The tractor was a Ford W-9000 COE with 135-inch (343-cm) wheelbase and the semitrailer was a 27-foot (8.2-m) van—one of three on loan from Yellow Freight Lines.)



T3-TR6 (a three-axle tractor coupled to a tandem-axle semitrailer. The tractor was an International Harvester COE 4070B with 142-inch (361-cm) wheelbase and the trailer was a 45-foot (13.7-m) van on load from the Fruehauf Company's R & D fleet.)



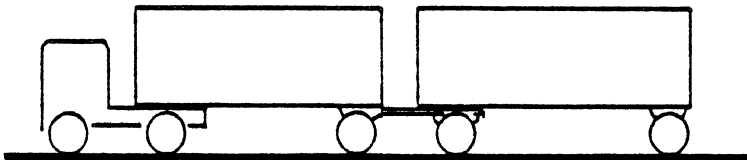
T3-TR5 (the above, T3, tractor coupled to another tandem-axle semitrailer. This semitrailer was a rented unit, also 45 feet (13.7 m) in length.)



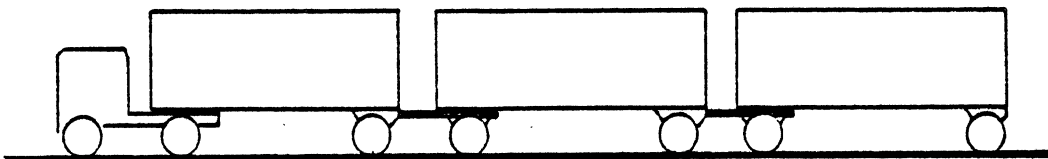
T7-TR6 (a three-axle tractor coupled to the TR6 tandem-axle semitrailer cited above. The tractor was the same basic International Harvester COE power unit identified above in the straight truck configuration except that it was first obtained from IH in a short wheelbase (145-inch (368-cm)) layout. After tests using this power unit in the short-wheelbase, T7, configuration, the frame was lengthened to produce the configurations T5 (below) and the straight truck, ST2.)



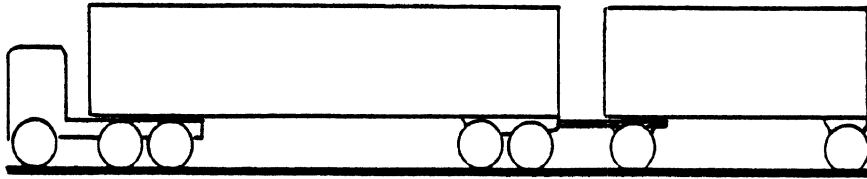
T5-TR6 (a three-axle tractor coupled to the TR6 tandem-axle semi-trailer cited above. The tractor is simply the long-wheelbase (209-inch (531-cm)) version of tractor T7.)



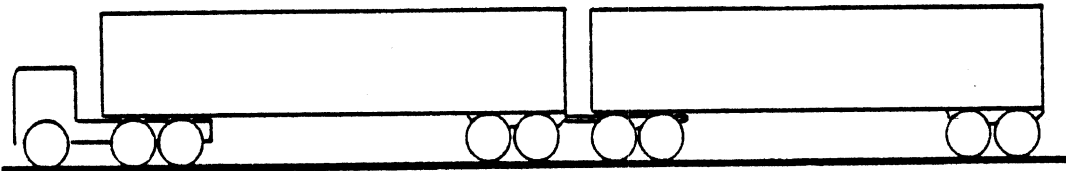
T1-TR1-TR2 (a conventional doubles configuration consisting of the two-axle tractor, T1, plus two of the 27-foot (8.2-m), single-axle, van semitrailers. The second trailer was hitched via a standard single-axle converter dolly.)



T1-TR1-TR2-TR3 (a triple comprised of the above unit plus an additional 27-foot (8.2-m) trailer with dolly.)



T7-TR6-TR7 (a so-called "Rocky Mountain Double" comprised of the above-described three-axle tractor, T7, and 45-foot (13.7-m) tandem-axle semitrailer, TR6, coupled to a short full trailer. The full trailer is comprised of a 27-foot (8.2-m) single-axle van semitrailer with single-axle converter dolly identical to the units TR2 and TR3 cited above.)



T3-TR5-TR6 (a so-called "Turnpike Double" comprised of a three-axle tractor coupled to two 45-foot (13.7-m) tandem-axle trailers. Each of the constituent elements of this vehicle have been described above except that the second trailer was hitched by means of a tandem-axle converter dolly.)

Each of the loading configurations selected for the various vehicles was designed to represent one of the following cases:

1) A baseline case in which the vehicle reached the maximum loading allowed on the federal interstate highway system. For the straight truck, the tractor-semitrailers, and the five-axle double, this case appears with the code designation "C1." The primary constraints determining these load levels were the following:

- 20,000 lbs (9.07 m tons), single-axle load
- 34,000 lbs (15.42 m tons), tandem-axle load
- 80,000 lbs (36.28 m tons), gross weight

Also, a convention was established for assigning a baseline loading to the tractor steering axle. For tandem-axle power units, this load was 12,000 lbs (5.44 m tons) and for two-axle tractors, this load was 9,500 lbs (4.31 m tons). For five-axle tractor-semitrailer combinations, this convention represents the most common scheme for attaining the 80,000-lb (36.28-m tons) gross weight level on the interstate system. For doubles the axle load limit allowed for single axles is considerably higher than needed for achieving the 80,000-lb (36.28-m tons) gross weight level. Thus, the steering axle load assumed for the double is seen as reasonably representative but, admittedly, arbitrary.

2) Other test cases representing variations in axle load and gross weight such as might be considered under some future size and weight provision. Certain cases are deserving of specific note, namely,

-Case ST2-C3 (The baseline load condition is repeated with the payload elevated to represent the higher range of placement of the payload center of gravity as prevails in service with lighter density, homogeneous freight.)

-Case ST2-C4 (The baseline load condition is repeated with radial tires mounted on the steering axle and bias-ply tires mounted on the rear axles of the truck. This condition was selected to provide a means of destabilizing the vehicle in its yaw response properties in a fashion which occurs in service due to tire mixing. Other cases in which this tire mix arrangement was employed involved tires mounted on the tractor axles of the following three tractor-semitrailer configurations:

-T1-TR1-C3 (two-axle tractor with 27-foot (8.2-m) semitrailer)

-T3-TR6-C4 (three-axle, short-wheelbase tractor with 45-foot (13.7-m) tandem-axle semitrailer)

-T5-TR6-C4 (three-axle, long-wheelbase tractor with 45-foot (13.7-m) tandem-axle semitrailer)

- Case T3-TR5-Empty (A five-axle tractor-semitrailer combination with the trailer unloaded.)

- Case T7-TR6-C2 (A five-axle tractor-semitrailer in which the rear half of the payload has been removed from the semitrailer. This "partially unloaded" case was to represent the condition which occurs in service when a portion of the freight on a given vehicle is unloaded at an intermediate destination.)

- Case T7-TR6-C3 (A five-axle tractor-semitrailer in which the 80,000-lb (36.28-m ton) gross weight condition is achieved with a high location of the payload center of gravity. This elevated payload location represents the case of a homogeneous cargo whose density is such that the trailer van is filled to its cubic capacity while reaching the full gross weight allowance at the same time. This case is looked upon as yielding the lowest level of vehicle roll stability that is found commonly in service.)

- Case T7-TR6-C4 (The same conditions as described in the above (-C3) case are achieved but with a total gross weight level of 88,000 lbs (39.91 m tons).)

The last three cases shown in Table 1, representing the triple, Rocky Mountain Double, and Turnpike Double involved loading levels which approach, but do not attain, the gross weights permitted by bridge formula "B" (for calculations showing the loads allowed by this bridge formula, see Volume I). Rather, these load conditions were determined by practical considerations concerning the need to make simple adjustments, in the field, of the payloads in individual trailers. That is, trailers were originally loaded in order to provide the specific weight levels which match the current federal limits for five-axle tractor-semitrailers and doubles. It was then efficient to reduce these weights by specific amounts in the field to attain the lower, per-trailer, weights representative of the longer combinations.

2.1.2 Test Equipment. To facilitate safe and accurate data collection, each vehicle configuration had to be equipped with specific test equipment. This equipment takes the form of occupant protection, jackknife protection, and rollover protection safety equipment, and transducers, signal conditioning devices, and on-board recording equipment.

2.1.2.1 Safety equipment. To protect the vehicle and its occupants from damage resulting from potentially unstable vehicle behavior, each vehicle was equipped with competition-style seat belts and harnesses, a rollover protection structure, anti-jackknife chains, and outriggers which were to restrain trailer rollover. Figure 1 shows a vehicle equipped with the rollover bar and outriggers. The rollover protective structure was bolted to the tractor frame immediately behind the cab. The device consisted of an outer frame of 8-inch (20.3 cm) pipe with diagonal braces of 6-inch (15.2 cm) pipe welded to a C-channel base. The outriggers were constructed of heavy pipe sections which located out-board spindles for carrying the dual wheel assemblies. Height adjustment is provided by telescoping struts mounted between the main outrigger section and a subframe installed on the underside of the trailer. Fore-aft restraint was provided by chains attached to the outrigger and the added subframe. In addition to the subframe placed beneath the trailer floor, another structure was also added inside of the trailer to carry the loads generated by outrigger touchdown. Contact with the pavement is made by the dual tire assemblies, thus the rolling interface provides minimal disturbance to the vehicle when a rollover limit is reached. Although the outriggers contributed some 10 to 20% to the roll moment of inertia, depending upon the trailer and load condition involved, the outrigger weight was included in the accounting of the test weight conditions.

The anti-jackknife chains cannot be seen in Figure 1, but their function is illustrated in Figure 2. The chains are attached to the trailer structure near its outside edge in the vicinity of the trailer's "landing gear." As the articulation angle of the vehicle increases, the slack in one of the chains is taken up. At some angle, determined by the original chain adjustments, the connection becomes taut and articulation is constrained. The angle at which the articulation becomes "locked" is determined by the maneuvering needs of the vehicle in the test area, usually in the 15- to 30-degree range, depending on trailer length.

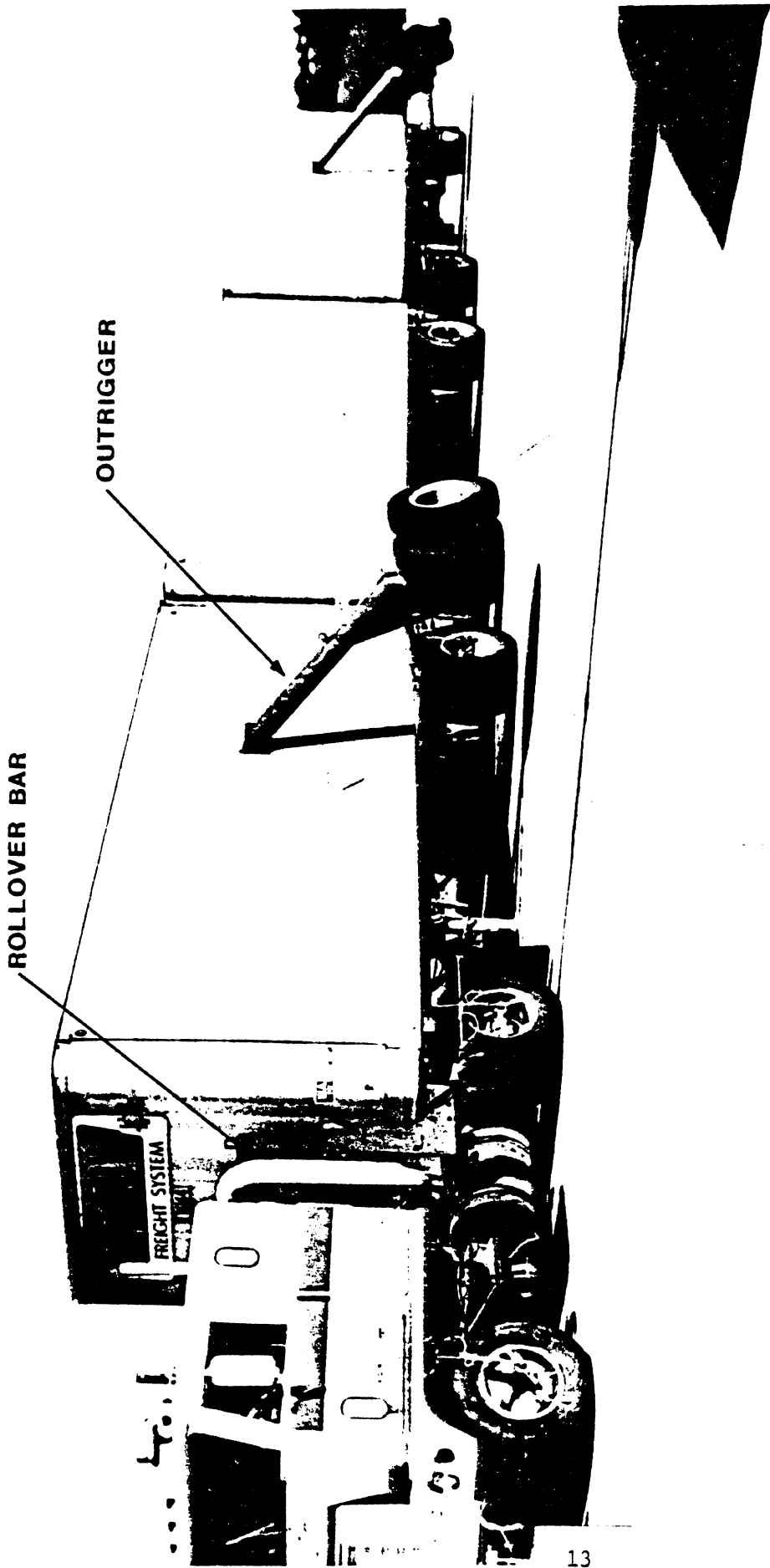


Figure 1. Safety equipment installed on triple-trailer combination.

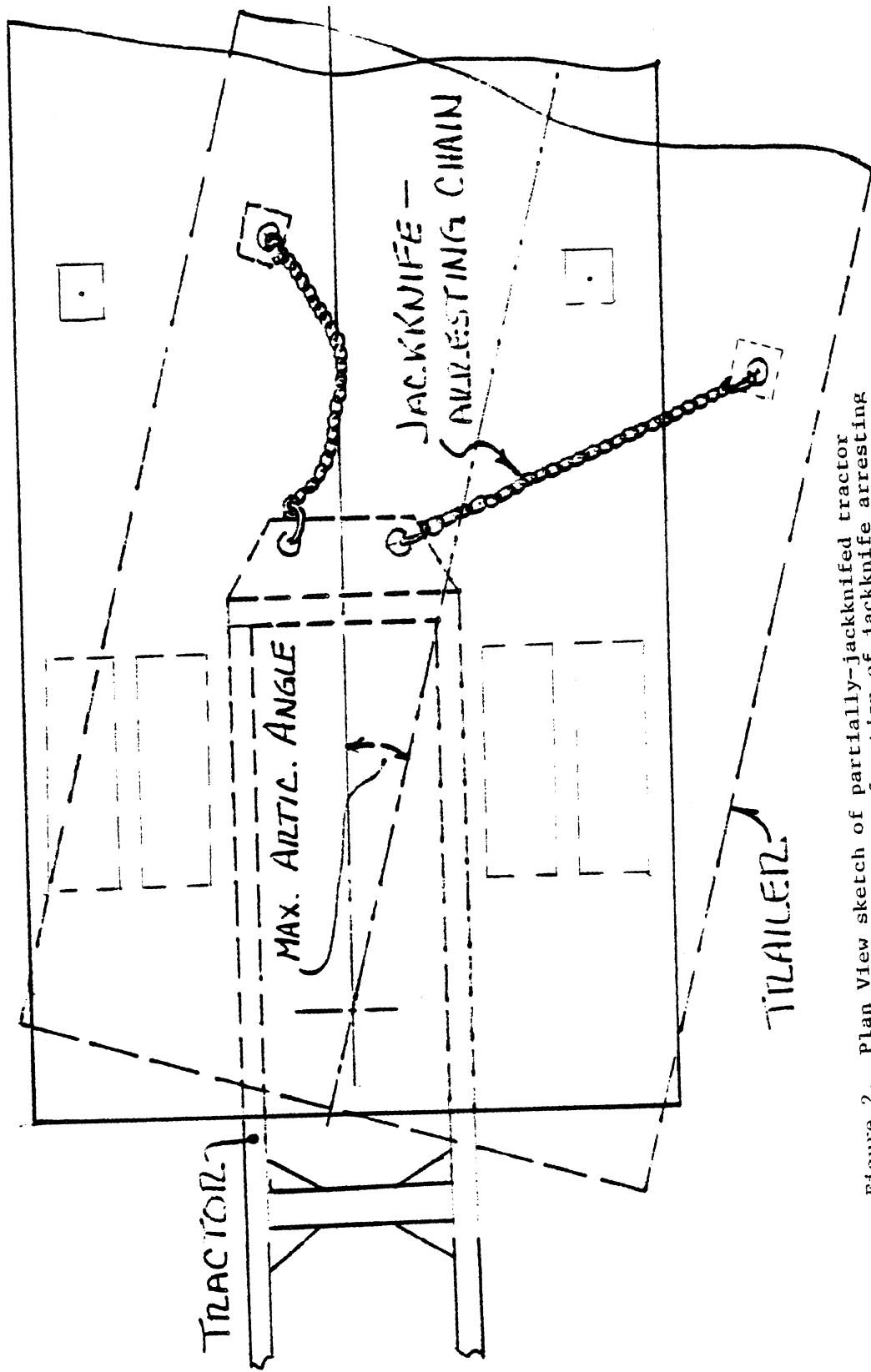


Figure 2. Plan View sketch of partially-jackknifed tractor semitrailer showing function of jackknife arresting chains.

2.1.2.2 Test equipment. Two pieces of equipment were employed to enable precise test inputs of steering-wheel angle and brake pressure. A steering wheel with mechanical stops and a system for regulating brake command pressure were used to accomplish these tasks easily and repeatably.

The instrumented steering wheel used to measure steering angle and torque was equipped with a pair of movable stops that could be adjusted to provide 330 degrees of single-sided steering input, as in a trapezoidal steer maneuver, or ± 151 degrees of two-sided input for a sine steer-like maneuver. A single body-fixed stop provided a rigid limit on steering angle excursions. The body-fixed stop was retractable to provide maneuverability in non-test or emergency situations.

Brake command pressure was used to control braking level in straight-line braking and braking-in-a-turn tests. A high-flow, pilot-operated regulator in the treadle valve supply controlled the pressure available to the brakes. Using this method, the treadle valve is always stroked to its maximum deflection. Adjustment of this type of control is easily accomplished by adjusting the regulator to supply the appropriate command pressure. This system eliminated the trial and error method associated with setting a mechanical treadle stop device and the variability of pressure observed with mechanical stops during high-command-pressure runs.

To achieve the loading conditions necessary for this testing, each trailer was loaded with racks of cast iron weights and tanks filled with water. An example loading scheme is shown in Figure 3. The racks of weights were used to provide for the nominal loading condition. In general, the baseline load for the vehicle was then achieved by the combination of the cast iron weights and filled lower tank(s) (please note that a total of only two tanks were used in each single-axle trailer). Increases in load, with attendant increases in c.g. height, were accomplished by filling the upper tanks. Each tank provided a volume of approximately 64 cubic feet (1.78 m³) for a payload increase of about 4,000 lbs (1.81 m tons) for each tank filled. (Note that, since tanks were either filled or empty, sloshing was not an issue.) With this system, the baseline and increased load conditions could be achieved without the considerable effort of rearranging the loading racks.

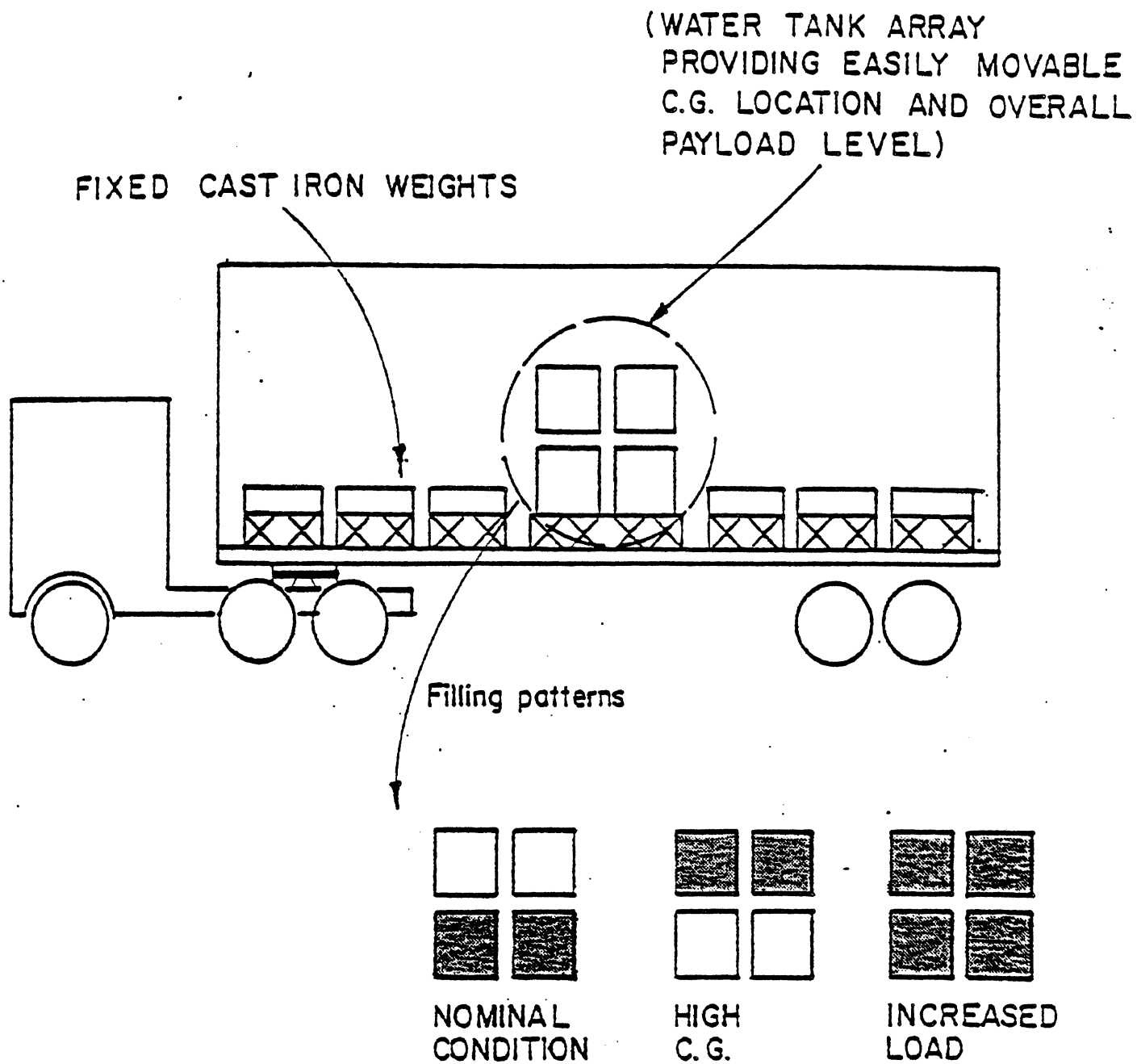


Figure 3. Scheme by which variable test loadings were achieved.

In certain cases, identified previously in Table 1 as "high c.g." configurations, the cast iron loading racks were mounted on raised platforms. The water tanks were then filled to achieve either baseline or "increased load" perturbations around that condition. Table 1 has listed the calculated values of payload c.g. height which were achieved in each vehicle configuration.

2.1.2.3 Instrumentation. The instrumentation system used in this study was developed under prior FHWA contract by Systems Technology, Inc. [7]. This system utilizes transducers to measure the input and response variables of the vehicle as outlined in Table 2. The signals from the transducers are scaled by an analog signal conditioning unit before being digitized and recorded on a nine-track digital tape. A schematic of the data acquisition system is presented in Figure 4.

Analog signals from the transducers are adjusted for zero offset and gain and are filtered to avoid aliasing, thus producing full-scale signals which are compatible with the digitizing system. The analog conditioning unit also provides zero and one volt calibration signals for checking the amplifier gains of the analog circuitry. The basic analog unit supplied by STI was expanded in this study with a wheel lock-up detection circuit which is used to identify wheels that fall below a selected value of spin velocity for more than 0.2 second. When a wheel lockup is detected, an LED on the analog unit corresponding to that particular wheel will be lit. Thus, the lockup detection circuit serves as an aid in guiding the test sequence, searching for limit braking performance.

The Digilog (DLI) 203 processor accepts transducer signals as analog voltage inputs, performs an A-D conversion, and stores the digitized signals on nine-track digital magnetic tape. The system is capable of accepting from 8 to 128 input channels and 1 to 32 output channels.

At the beginning of each test in which data is to be collected, the DLI/203 writes a 4094-byte identification record on tape which contains general information such as run number, date, and test conditions. During data collection, the DLI/203 sequentially stores the designated input channels in a 4096-byte high-speed memory. Filling of this buffer triggers

Table 2. Measured Response Variables and Transducers.

<u>Variable(s), Symbol(s)</u>	<u>Transducer</u>
Steering Wheel Angle, δ_{sw}	Rotary Potentiometer
Steering Wheel Torque, τ	Lebow Torque Sensor
Vehicle Velocity, V	Fifth Wheel with D.C. Generator
Brake Command Pressure, P_b	Potentiometric
Heading Angle, ψ	Humphrey Directional Gyro
Tractor Acceleration and Rotational Rates, a_x, a_y, a_z, p, q, r	STI Inertial Measuring Unit
Fifth Wheel Articulation Angle, η_1	Celesco String Potentiometer
Trailer Accelerations and Rotational Rates, $a_{xn}, a_{yn}, a_{zn}, p_n, q_n, r_n$	STI Inertial Measuring Unit
Pintle Hook and Dolly Articulation Angles, η_2, η_3	Celesco String Potentiometer
Wheel Rotational Speeds, $\omega_1 \dots \omega_{18}$	Servo-Tek D.C. Generators

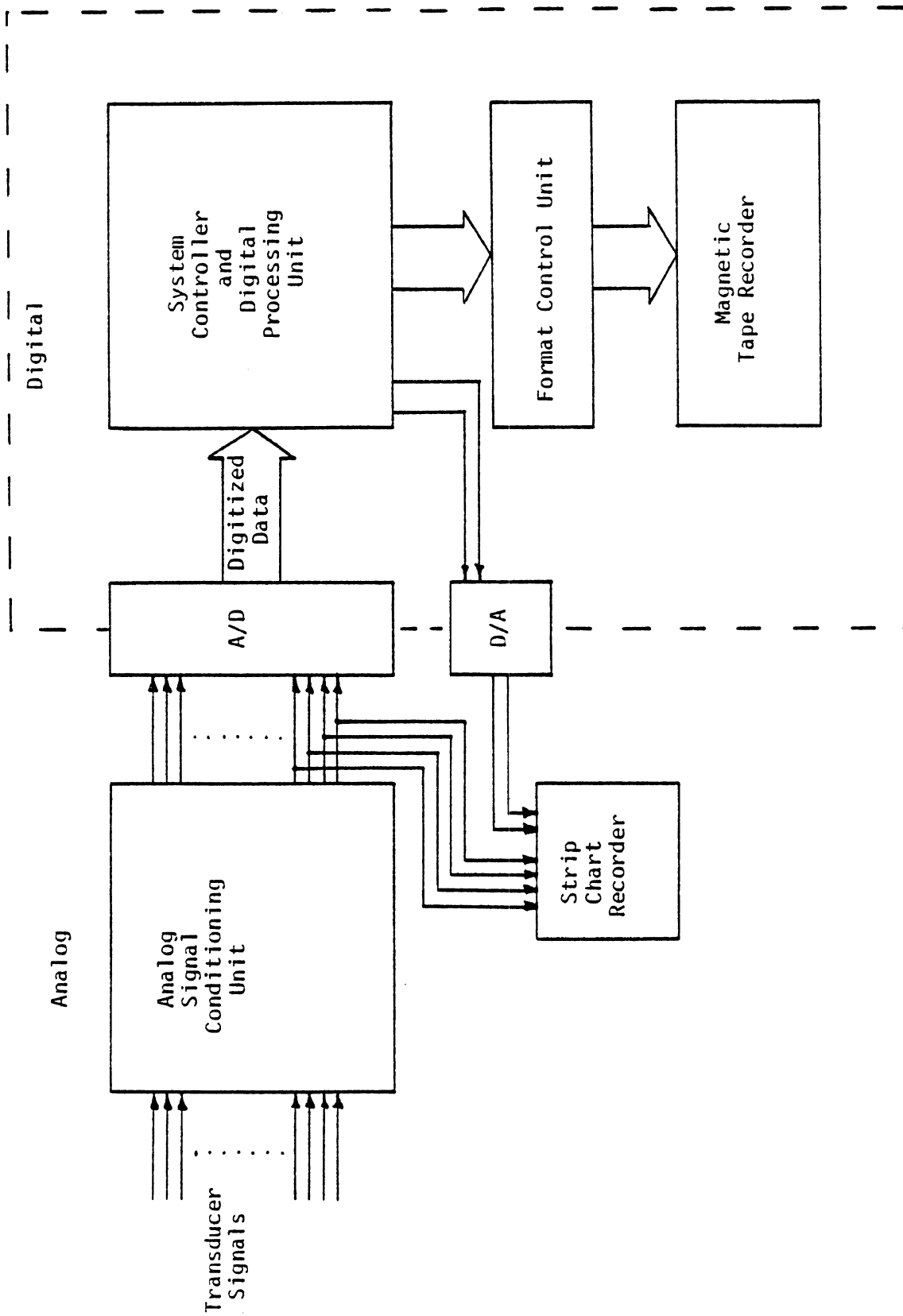


Figure 4. Data acquisition system.

transfer of the data to the nine-track magnetic tape unit as a 4096-byte data block. This process of filling the high-speed memory buffer and its periodic transfer to magnetic tape takes place continuously during the data collection period. Completion of each test and the data collection process causes the DLI/203 to write a tape mark after the last data block, thereby defining each group of data blocks on tape as a separate file. The typical arrangement of identification blocks, data blocks, and file marks on tape are shown in Figure 5. Additional details concerning the DLI/203 operation can be obtained from Reference [7].

2.1.3 Test Procedures. A total of five basic test maneuvers were conducted on the indicated test vehicles. Not all tests were performed with all vehicles, however, since certain of the vehicle configurations and size and weight variations were of interest only in the context of certain performance attributes.

Braking performance was studied by means of straight-line braking and braking-in-a-turn maneuvers on both high and low friction surfaces. Yaw and roll responses were studied by means of open-loop trapezoidal- and sinusoidal-steer tests on the high coefficient surface only, while closed-loop negotiation of a lane-change course was studied on both dry and wet surfaces.

All testing was conducted at the Chrysler Corporation Proving Ground in Chelsea, Michigan. Dry tests (high friction surface) were conducted on the Vehicle Dynamics facility which provides an oval track for reaching the test-approach speed and an 800-foot-square skid pad to facilitate cornering maneuvers. The large pad area has a dry ASTM skid number of approximately 86. Low friction tests were performed on the jennite-coated Skid-Traction facility wetted with sprinklers, giving a nominal skid number of 37.

2.1.3.1 Pre-test procedures. Prior to testing, certain standard procedures were followed to assure consistent vehicle conditions and proper functioning of the data acquisition system. Each truck or tractor began its test series with new Firestone Transport 1 tires. As tires accumulated treadwear (a very rapid process due to the severity of the maneuvers involved), they were replaced prior to exposing the "wear bar" indicators.

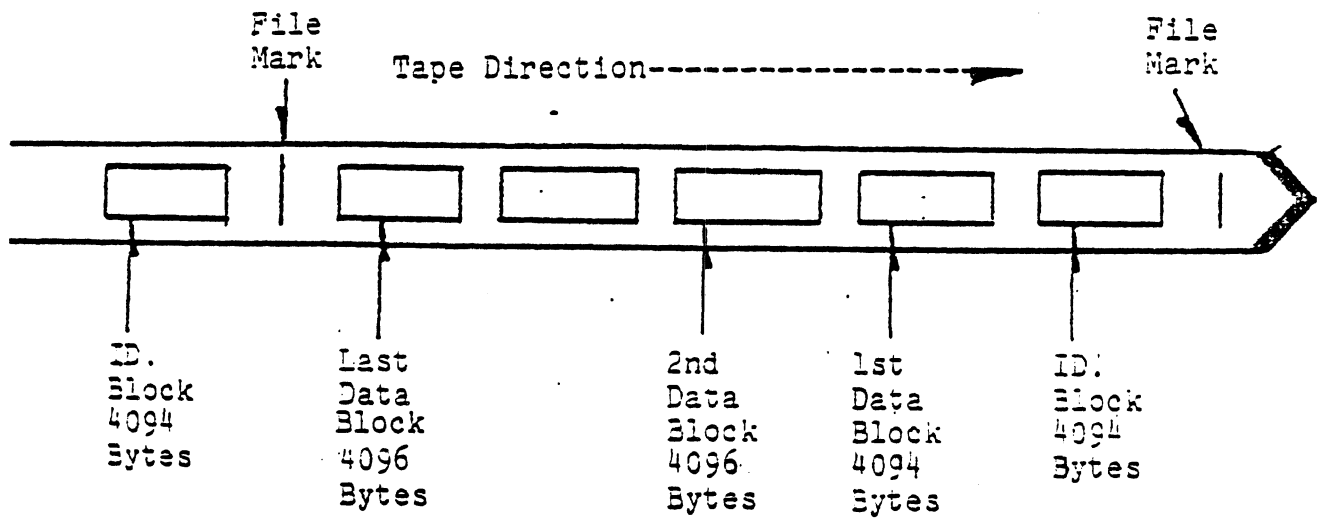


Figure 5. DLI/203 Output File Blocking Format

The brakes at each wheel were inspected to assure suitable lining thickness. Also, slack adjusters were set to provide the appropriate pre-travel dimensions.

Tire cold inflation pressure was set at 85 psi (5.78 bars) for bias tires and 105 psi (7.18 bars) for radials and checked prior to testing each day. Following a general mechanical check, the vehicle was then driven for several miles to warm the tires to operating temperature and to remove flat spots caused by standing overnight. During the vehicle check and warm up, the instrumentation system was powered up and allowed to stabilize until after the warm-up runs were completed. Amplifier gains and transducer zero values were then checked and adjusted and calibration values recorded on tape.

2.1.3.2 Straight-line braking. Straight braking tests were performed on wet and dry surfaces from initial velocities of 25 and 40 mph (40 and 64 km/h), respectively. Tests were run to study braking behavior over a wide range of deceleration levels from approximately .1 g to the braking limit of the vehicle. The braking limit was defined to be that braking input level at which (a) all wheels on either a single axle or tandem axle set exhibited lockup, or (b) the maximum brake pressure was reached. Repeat runs were made at a level just below the axle lockup condition or at the maximum pressure to provide information on the maximum braking capability of the vehicle.

The test involves bringing the vehicle to the test speed (± 1 mph (1.6 km/h)) specified for the particular surface (wet or dry) and applying a step input to the treadle valve. During braking, the driver steers to maintain a straight path in a 12-foot (3.66-m) lane. The treadle is held in a fully depressed position until the vehicle comes to a complete stop. Brake pressure is incremented by approximately 10 psi (.68 bars), using the regulator referred to in Section 2.1.2.2 and the procedure is repeated. As mentioned above, either the brake pressure limit or the occurrence of lockup on a single or tandem axle set determined the limit condition. When the lockup criterion was met, the brake input pressure was backed off to the

previous setting and two repeat stops were made. If the maximum available brake input pressure was reached, two repeats were run at that pressure value.

The results of interest obtained with this test relate to the average deceleration obtained over the duration of the stop with a given brake input pressure and the maximum deceleration level attainable with the vehicle. The format of these results are illustrated in Figure 6. The slope of the line defining the vehicle's braking response (a_x/P) is referred to as the "gain" of the braking system. This gain is a measure of the vehicle response to a given change in applied brake pressure. It can be thought of as the sensitivity of the braking system. The maximum deceleration achieved can be directly related to the minimum stopping distance obtainable.

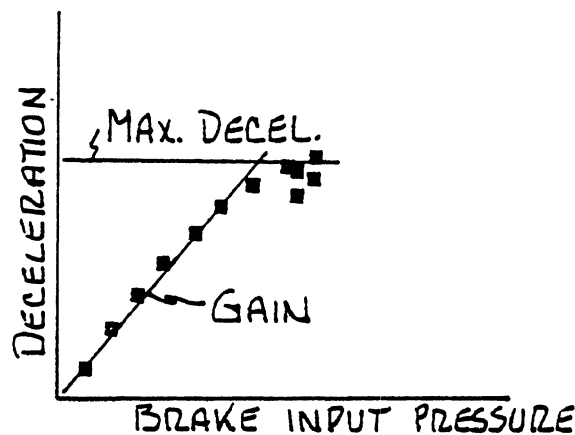


Figure 6. Format of braking test results showing performance measures.

2.1.3.3 Braking in a turn. Braking in a turn was conducted on the same surfaces used for straight-line braking. The same initial velocities, 25 mph (40 km/h) on the wet, 40 mph (64 km/h) on the dry, were used along with the brake scheme for incrementing input pressure. In this test, the vehicle is driven on a circular, 12-foot-wide (3.66-m) lane delineated by traffic cones. Once a steady turn has been established, the driver applies the brakes and steers to maintain the circular path. On the wet surface a path radius of 278 feet (84.7 m) was used (radius measured to the center of the 12-foot (3.66-m) lane), resulting in a lateral acceleration level of .15 g. A radius of 533 feet (163 m) was used on the dry surface, giving a lateral acceleration level of 0.2 g.

The braking-in-a-turn test is conducted in nominally the same fashion as the straight braking experiment, with tests run at increasing braking levels, controlled by regulating the brake input pressure, up to the limit response condition. Brake pressure and lockup limits are defined as for straight braking. Also, exceedance of the 12-foot lane is added as a limit. In many cases, the lane exceedance criteria is met in the same runs in which axle- (or tandem-) lockup occurs, causing a yaw disturbance that is likely to result in either jackknife (tractor drive axle(s) lock), plow-out (steering axle lock), or trailer swing (trailer axle(s) lock). These possible limit responses are illustrated in Figure 7. As before, repeat runs are conducted at a brake pressure level which is just under the value producing a limiting condition.

2.1.3.4 Trapezoidal steer. Transient and steady-turning responses to an abrupt steering input were examined using the trapezoidal steering input. Amplitude of the steering input was controlled using mechanical stops integrated into the instrumented steering wheel. The driver applies the steering input as quickly as possible, generating a ramp input up to the specified steering level which is then held constant until the vehicle settles into a quasi-steady-state condition. A true steady state is not achieved due to the vehicle scrubbing off speed while cornering with the transmission in neutral. This test was conducted only on the high-friction surface at a test speed of 45 mph (72 km/h).

To accomplish this test, the vehicle is first brought to a speed slightly greater than the test speed. The driver then takes the transmission out of gear and as the vehicle coasts through the test speed, the rapid steer input is applied and held until the quasi-steady turn is established or space limitations dictate a need to change trajectory. Successive tests are run with increasing steer amplitude until a limit condition is reached. Three possible limits are defined, viz., the vehicle exhibits a rollover response (restrained by the outriggers), the tractor becomes yaw divergent (tending toward a jackknife), or the front tires saturate such that further increase in lateral acceleration becomes impossible. In actual practice, the test procedure was always continued with loaded vehicles until the "rollover

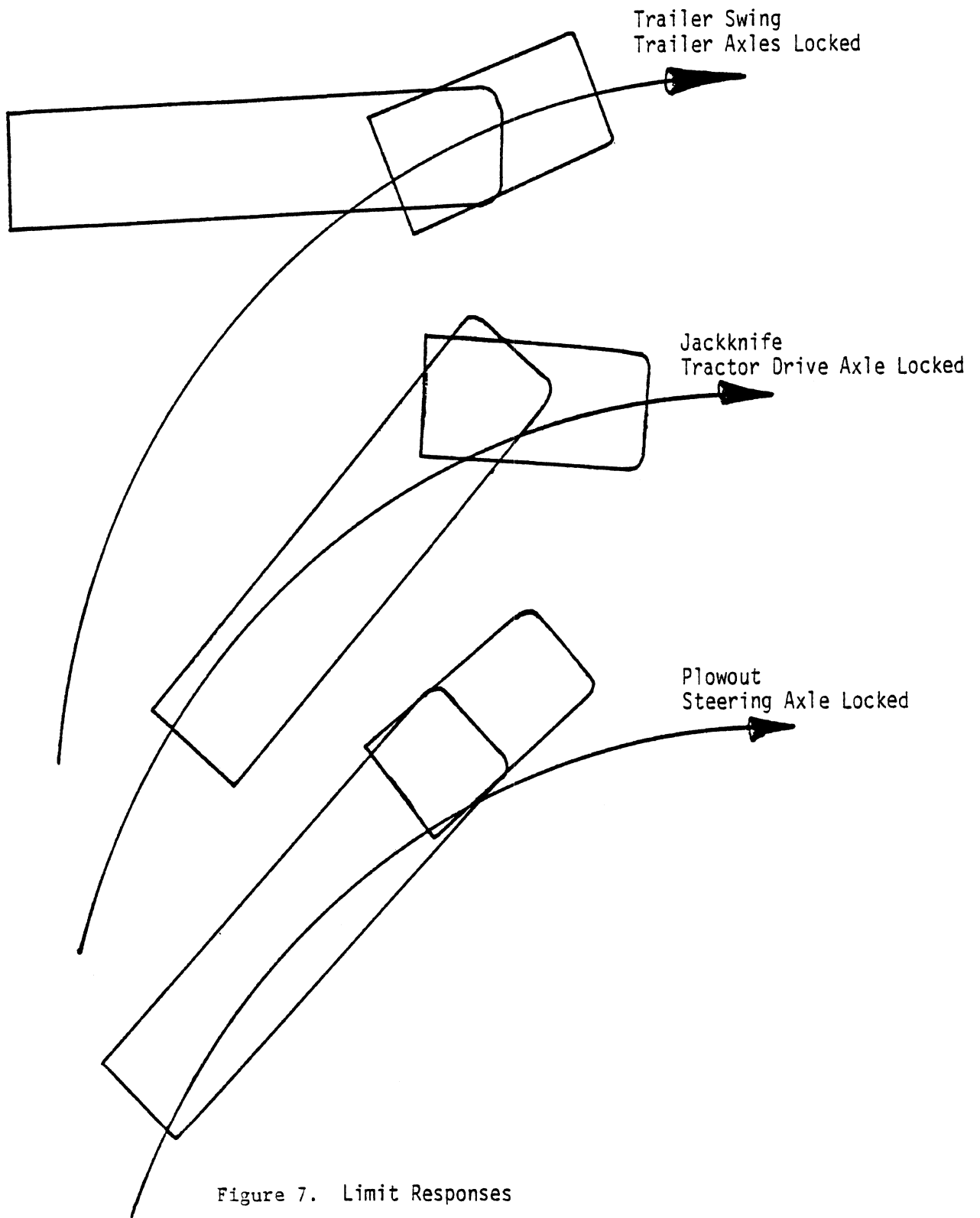


Figure 7. Limit Responses
Braking in a Turn

response" was observed. The outrigger height was adjusted so that outrigger touchdown occurs after the trailer wheels on one side have lifted from the ground by some 4 to 8 inches. The outrigger touchdown condition, then, is taken to be the indicator of an incipient rollover. Repeat runs are then made at a level just below the limit condition.

This test results in a trajectory of nominally constant radius at steady state, also referred to as a J-turn. The initial portion of the maneuver is used to describe the transient response to steering input. The quasi-steady-state portion of the maneuver approximates vehicle response to a long duration (5-6 seconds) constant steering input, such as in negotiating an off-ramp from an expressway.

Typical steering-wheel angle, lateral acceleration, and yaw rate time histories for a trapezoidal steer maneuver are shown in Figure 8. This figure illustrates the important response features of this test, involving the transient and steady-state yaw rate responses. While the steady-turning response is obvious, the yaw rate response time is given a special definition as the elapsed time between reaching 50% of the steering input and 90% of the steady-state yaw rate.

2.1.3.5 Double lane change. This obstacle-avoidance-type maneuver was conducted on high and low friction surfaces at speeds of 45 and 30 mph (64 and 48 km/h), respectively. The test involves the closed-loop negotiation of the courses illustrated in Figure 9 for the two surfaces. The gate spacing for the double-lane-change test on a dry surface was changed for the second season's testing, as shown, to provide a higher frequency input. This test is similar to that developed by the National Swedish Road and Traffic Research Institute and evaluation of performance was similarly determined by the axle path trajectories of the entire vehicle negotiating the course.

The test requires that the vehicle enter the course at the test speed and the driver maneuver through the course while holding the throttle fixed. Five repeats are run in each direction to account for variations in the driver's closed-loop control during the maneuver.

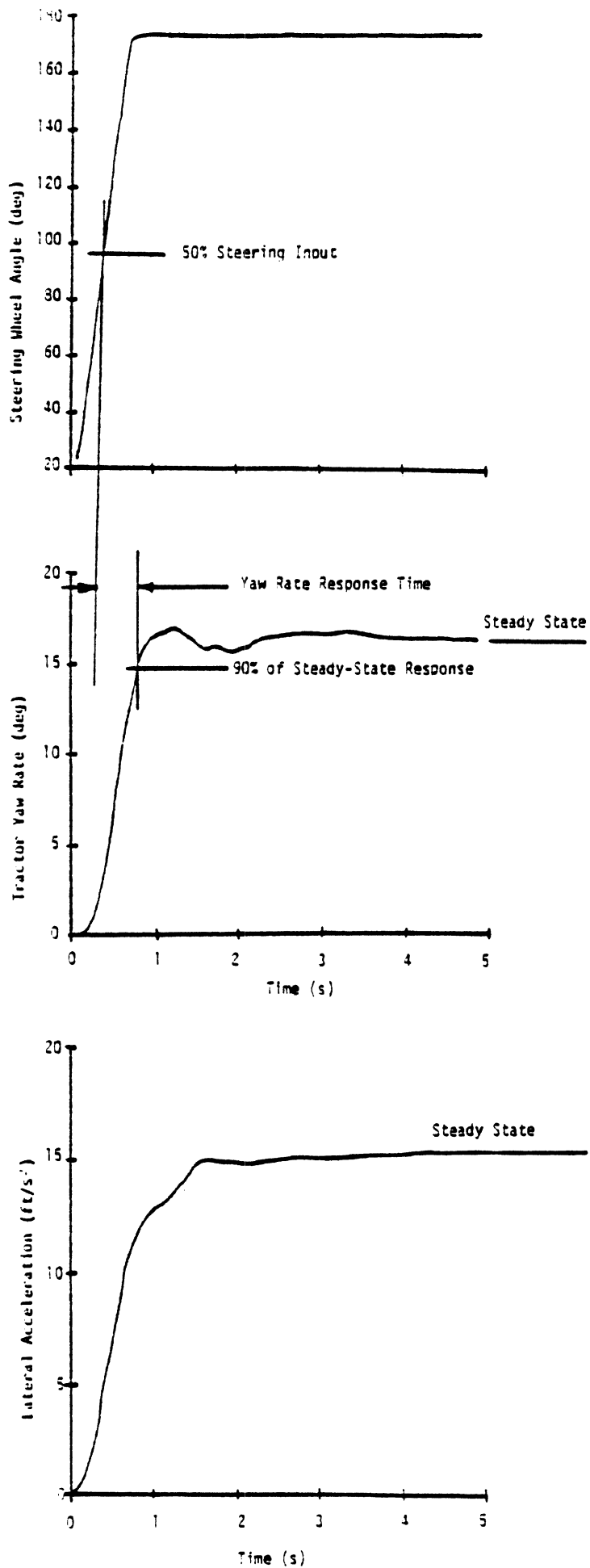
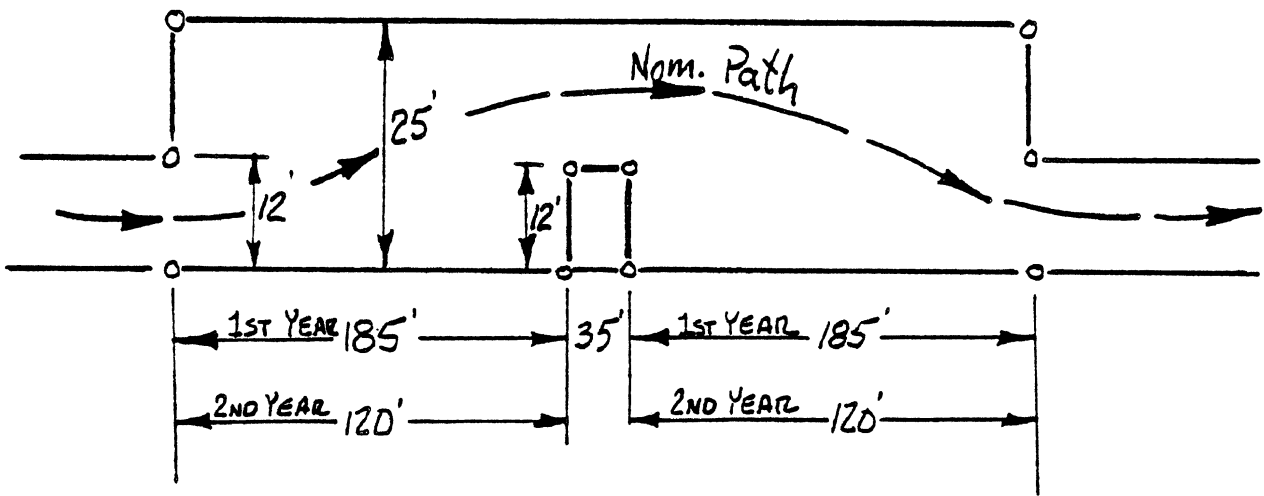
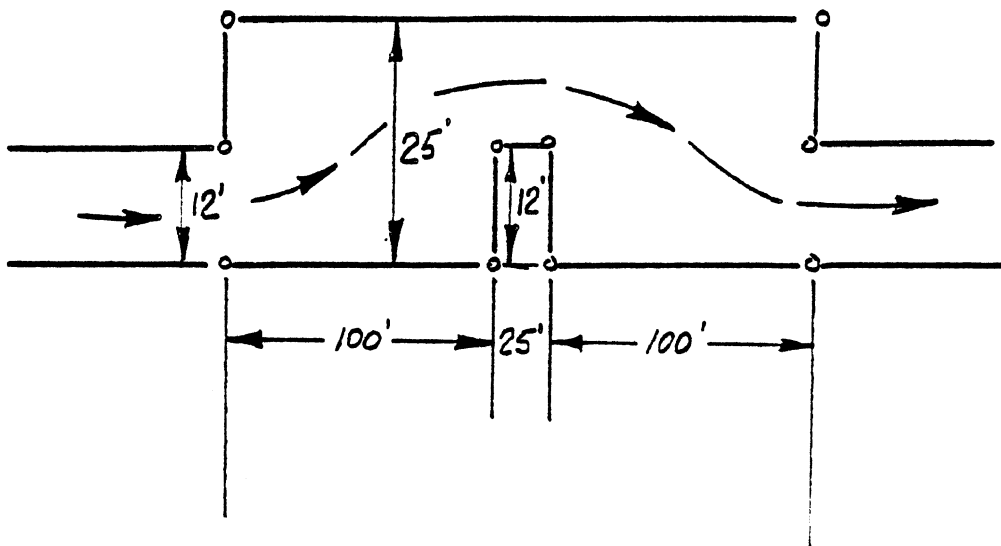


Figure 4. Example time histories for the trapezoidal steer test.



Dry Surface Lane-Change Maneuver at 45 mph.



Wet Surface Lane-Change Maneuver at 30 mph.

Figure 9

2.1.3.6 Sinusoidal steer. Previous experience with multi-trailer vehicles [5] indicates that rearward amplification of vehicle trains is best excited by a steering input of a higher frequency than that generated by means of the lane-change maneuver described above.

Thus, to investigate the rearward amplification phenomenon for the doubles and triples tested in this program, a sinusoidal-like steer input of a two-second period was used to excite the motions of interest. A single quasi-sine wave steering disturbance, shown in Figure 10, was applied by the driver to the vehicle from an initially straight-running condition at a speed of 45 mph (72 km/h).

The maneuver allows for investigation of the rearward amplification phenomenon as well as any oscillatory motion of the vehicle prevailing after the steering is returned to zero. Tests were run at increasing steer amplitudes, with the amplitude being controlled by two mechanical steering stops displaced equally about the zero position of the steering wheel. The test runs advanced in severity up to the maximum level of steering amplitudes which could be achieved with the steering stop device. Thus, the limit was determined by a steering input amplitude of approximately ± 151 degrees. Repeats were run at this maximum amplitude condition. Timing of the sine-wave-like input was monitored with each test run. Only tests in which each half-wave period was within $\pm .1$ second of the ideal 1.0 second half-period were considered valid.

The response of multi-trailer combinations in this maneuver can involve exaggerated motions at the rearmost trailer. At sufficiently high levels of steering amplitude, and with a sufficient forward velocity, the rear trailer can exhibit a rollover response.

2.1.4 Data Processing. Computer processing of the nine-track tapes produced by the DLI/203 data acquisition package was accomplished using The University of Michigan's AMDAHL 470V/8 digital computer. A main program was written to read data from the DLI/203 tapes, calibrate and smooth the data, and then to call one of five different subprograms (corresponding to each of the five basic vehicle test maneuvers) to further process the data to obtain approximate numerics and selected time histories.

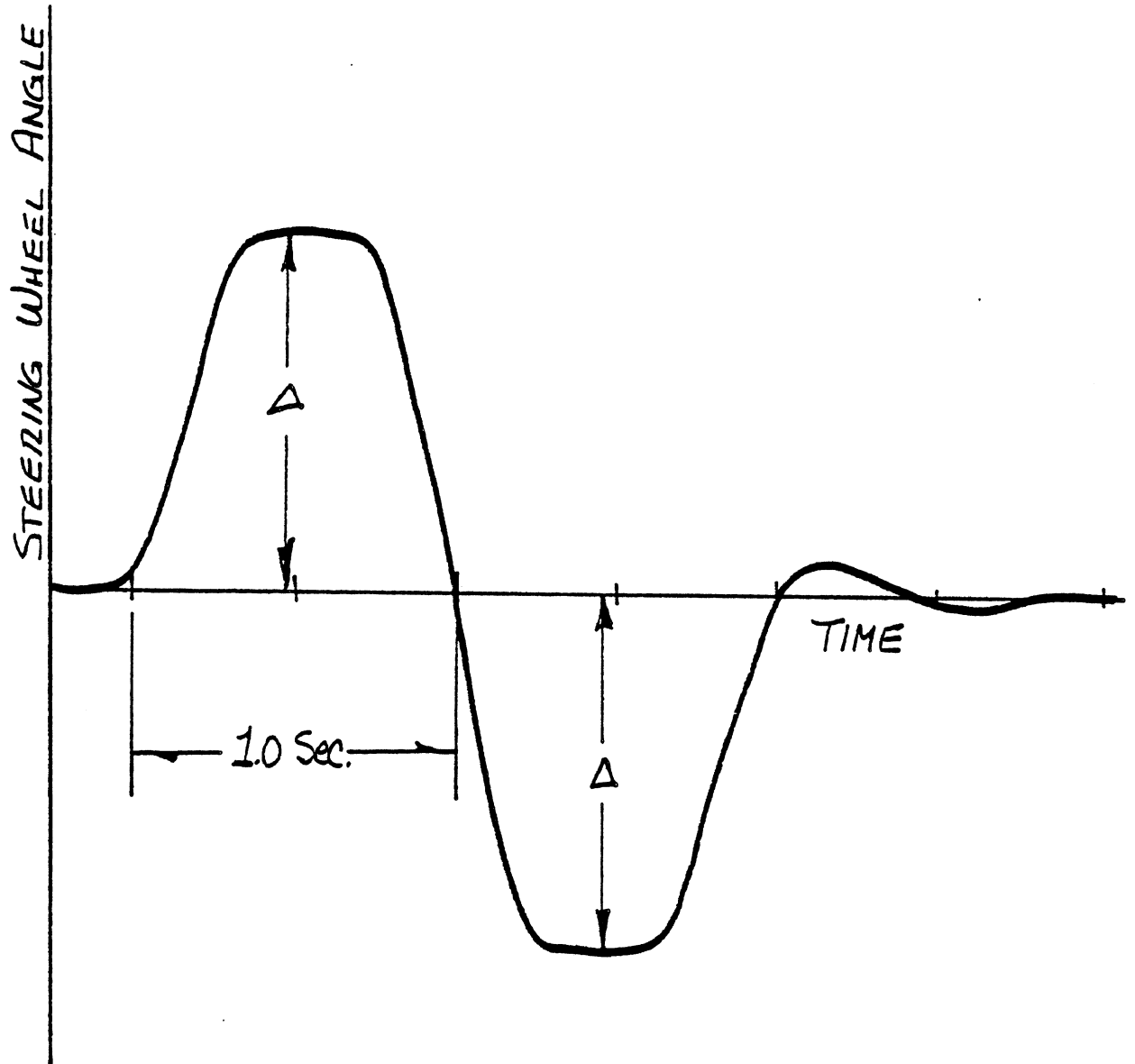


Figure 10. Quasi sine-steer waveform

The following section describes the operations and calculations performed by the main processing program and presents an example of one of the five subprograms.

**** Main Program ****

1. Reads parameters from terminal or input file which: (a) control the file processing sequence of the DLI/203 input tape and (b) define the maneuver and vehicle configuration associated with each input file.
2. Positions input tape to its starting file; output tape to its last file position.
3. Transfers data from next file of the DLI/203 input tape to the AMDAHL 470V/8 main memory for processing.
4. Manipulates data in AMDAHL memory to change format from DLI/203 format to an equivalent AMDAHL two-byte binary word format (byte reversal, masking operations).
5. Sub-sampling of data from 100 Hz (digitized rate) to 50 Hz. This step significantly reduces the volume of data for processing with little compromise to the accuracy of the subsequent calculations.
6. Performs zero calibration, full-scale calibration, and zero-data calibration calculations for any calibration files appearing on the DLI/203 input tape.
7. Identifies legitimate data files appearing on the DLI/203 input tape and calls the appropriate subprogram to further process that data.
8. Branches, upon return from a subprogram call, to Step 3, above, to continue processing; or, detects an end-of-input tape and terminates processing.

Presented below is an outline of the subprogram for processing the data from straight-line braking tests. This program is similar in general form to the other subprograms, found in Appendix 1 of this report, covering

the braking-in-a-turn, trapezoidal-steer, double-lane-change, and sinusoidal-steer tests. The subprograms are distinguished from one another, of course, insofar as they operate upon differing types of response time histories to determine differing objective measures, or numerics, characterizing the vehicle's behavior. Certain measures, such as stopping distances (c) and (e) below, were calculated by alternative means in order to assure the determination of a high quality result.

**** Subprogram #1 (Straight-Line Braking) ****

-Scales data to proper physical units.

-Smooths appropriate data channels by replacement with 5-point average (0.10-second smoothing interval).

-Detects start and end of test maneuver (brake application/forward velocity falling below 2 mph).

-Calculates the following numerics over the maneuver interval:

- a) Initial vehicle velocity, V_0 (ft/sec)
- b) Average brake line pressure, P_B (psi)
- c) Stopping distance from integration of forward velocity corrected for initial velocity variations from 40/25 mph (64/40 km/h), D^* (ft)
- d) Average longitudinal deceleration, A_X (g's)
- e) Stopping distance from double integration of longitudinal acceleration corrected for initial velocity variations from 40/25 mph (64/40 km/h), D_{AX} (ft)
- f) Stopping time, T (sec)
- g) Tractor peak yaw rate, R_{LP} (deg/sec)
- h) Last trailer peak yaw rate, R_{NP} (deg/sec)
- i) Peak tractor/trailer articulation angle, G_{AM1} (deg)
- j) Peak articulation angle of last dolly with respect to lead trailer (pintle hook angle), G_{AM2} (deg)
- k) Peak articulation angle of last dolly with respect to last trailer, G_{AM3} (deg)

- 1) Wheel lock indicator 0.0 (no) or 1.0 (yes) and the corresponding vehicle velocity at which it occurred. For wheel speeds, $\omega_2, \omega_4, \omega_6, \omega_8, \omega_{10}, \omega_1, \omega_3, \omega_5, \omega_7, \omega_9$.

-Writes a header record containing run number, file number, and maneuver information on the output tape.

-Writes the above numerics to both the line printer and the output tape.

-Writes the following variables as time histories to both the line printer and output tape:

- a) time, T (sec)
- b) forward velocity, V5 (mph)
- c) longitudinal deceleration of tractor, AX1 (g's)
- d) longitudinal deceleration of last trailer, AXN (g's)
- e) suspension deflections of tractor at wheel locations 1-6, Z1-Z6 (inches)
- f) brake line pressure, PB (psi)

-Writes a tape mark on the output tape, closing the output tape file.

-Returns to main program.

Figure 11 shows an example printout for the above subprogram.

STRAIGHT LINE BRAKING RUN NO. 300 INPUT FILE 76 OUTPUT FILE1585
 V0 = 59.5 P0 = 102.1 D* = 111.3 AX = 0.57 DAX = 108.9 T = 3.6
 RIP = -0.5 RHP = -0.3 GAM1 = -0.9 GAM2 = 0.0 GAM3 = 0.0
 VEHICLE CONFIGURATION: T3-TR6-C2
 WHEEL LOCKS:

T	V5	AX1	AXH	Z1	Z2	Z3	Z4	Z5	Z6	P0
0.0	40.026	-0.009	0.001	-0.477	-0.199	-0.030	0.006	0.099	0.078	-1.333
0.100	40.560	0.010	0.007	-0.454	-0.209	-0.021	-0.023	0.048	0.047	-1.097
0.200	40.747	0.024	0.020	-0.254	-0.096	-0.006	-0.008	0.022	0.008	-1.362
0.300	40.538	0.015	0.013	-0.182	-0.035	0.019	-0.008	0.023	-0.000	-1.127
0.400	40.727	0.014	0.008	-0.044	-0.044	0.025	0.001	0.041	0.011	-1.230
0.500	40.540	0.017	0.026	-0.307	-0.140	0.015	0.006	0.036	0.008	1.687
0.600	40.429	0.061	0.039	-3.121	0.032	0.040	0.008	-0.013	-0.054	9.128
0.700	40.072	0.116	0.120	0.228	0.376	0.078	0.093	-0.153	-0.177	18.381
0.800	39.615	0.191	0.182	0.743	0.909	0.206	0.128	-0.325	-0.332	29.255
0.900	38.980	0.286	0.284	1.453	1.733	0.260	0.218	-0.602	-0.810	44.593
1.000	38.365	0.422	0.388	2.112	2.180	0.268	0.237	-1.079	-1.234	61.846
1.100	37.799	0.478	0.459	2.345	2.162	0.296	0.269	-1.192	-1.342	74.208
1.200	36.797	0.533	0.504	2.251	2.157	0.301	0.249	-1.174	-1.308	83.358
1.300	35.239	0.588	0.533	2.335	2.158	0.290	0.280	-1.184	-1.303	90.592
1.400	34.306	0.599	0.536	2.354	2.162	0.304	0.298	-1.229	-1.357	95.646
1.500	33.075	0.581	0.575	2.332	2.158	0.303	0.259	-1.218	-1.331	98.489
1.600	31.845	0.590	0.565	2.322	2.158	0.283	0.233	-1.216	-1.355	99.698
1.700	30.664	0.506	0.565	2.391	2.162	0.334	0.293	-1.283	-1.409	101.348
1.800	29.453	0.595	0.560	2.333	2.158	0.217	0.180	-1.267	-1.402	101.333
1.900	28.103	0.573	0.572	2.348	2.160	0.290	0.231	-1.252	-1.402	101.878
2.000	26.932	0.571	0.542	2.399	2.162	0.291	0.236	-1.256	-1.404	102.217
2.100	25.533	0.584	0.561	2.322	2.158	0.260	0.193	-1.247	-1.404	102.202
2.200	23.895	0.561	0.545	2.376	2.158	0.314	0.246	-1.252	-1.407	102.188
2.300	23.151	0.586	0.557	2.605	2.162	0.321	0.274	-1.306	-1.466	102.261
2.400	21.603	0.563	0.542	2.312	2.158	0.299	0.229	-1.257	-1.417	102.247
2.500	20.432	0.574	0.543	2.384	2.162	0.296	0.228	-1.274	-1.407	102.217
2.600	19.142	0.574	0.561	2.392	2.162	0.296	0.231	-1.279	-1.427	102.291
2.700	18.020	0.555	0.524	2.286	2.160	0.280	0.215	-1.257	-1.393	102.232
2.800	16.680	0.574	0.563	2.361	2.162	0.286	0.223	-1.251	-1.397	102.232
2.900	15.609	0.559	0.527	2.387	2.162	0.299	0.229	-1.265	-1.420	102.202
3.000	14.299	0.571	0.555	2.309	2.158	0.296	0.231	-1.264	-1.417	102.217
3.100	13.078	0.567	0.543	2.366	2.160	0.304	0.234	-1.267	-1.415	102.188
3.200	11.808	0.573	0.552	2.391	2.160	0.304	0.246	-1.267	-1.415	102.232
3.300	10.627	0.567	0.530	2.341	2.158	0.299	0.237	-1.262	-1.415	102.232
3.400	9.437	0.569	0.554	2.366	2.160	0.299	0.241	-1.261	-1.412	102.202
3.500	8.314	0.579	0.552	2.400	2.162	0.299	0.249	-1.265	-1.414	102.232
3.600	6.905	0.567	0.544	2.374	2.162	0.296	0.242	-1.257	-1.407	102.202
3.700	5.635	0.570	0.552	2.369	2.158	0.293	0.239	-1.261	-1.401	102.202
3.800	4.454	0.572	0.546	2.382	2.162	0.293	0.241	-1.264	-1.402	102.276

Figure 11. Example data processing printout for straight-line braking maneuver.

2.2 Overview of Test Results

In this section a summary of the test results will be presented using measures of performance which have been derived from the real-time response data gathered using the on-board instrumentation system. The time history data was first processed by computer to produce plots containing data points representing each of the test runs made with a given vehicle configuration and loading case. For example, the braking performance data were plotted in terms of the average deceleration achieved versus the brake input pressure applied in each run. Plots of data in this run-by-run format are presented in Volume III of this report. These plots were then employed to define a single numerical measure which is then used as a summary of the vehicle's performance. These measures are defined below in Section 2.2.1.

It should be noted that not all of the test data are addressed in the summary which follows. Rather, the summary omits reference to results from the braking-in-a-turn and closed-loop lane-change experiments. These data are not discussed here since the results reveal no significant information beyond that presented through other measures. For example, the stopping distance data measured in the braking-in-a-turn tests show the same sensitivities to size and weight variables as are indicated in the straight-line braking data. The lane-change results, on the other hand, were generally disappointing insofar as this test had virtually no ability to discriminate between the various vehicle configurations examined. That is, the lane-change maneuver was selected primarily for the purpose of examining differences in vehicle trajectory exhibited in a lane change whose severity level and nominal frequency content were in the intermediate range between normal driving and emergency obstacle-avoidance maneuvering. Since negligible differences in trajectory were seen between widely differing vehicle configurations, the data are not reported here. This "negligible difference" result, however, does reveal that a skilled test driver can maneuver any of the examined test vehicles through the indicated lane change without making significant space demands beyond the nominal width of the vehicle. The result further indicates that, from a trajectory point of view, a capable, experienced driver can compensate for most tracking anomalies in his vehicle by adopting a strategy which, even unconsciously, places the vehicle on a virtually optimum path. (Note that the rearward

amplification issue was to be treated, not in the "lane-change" maneuver, per se, but rather in the sinusoidal-steer test for which the steer input period was particularly selected to excite the amplification motions of interest.)

The test data are summarized in groups which nominally address differing size and weight issues. In this presentation, the test cases involving changes in axle load and gross weight are considered together since many of the conditions involving increased gross weight were achieved by means of increases in payload beyond the current federally-allowed limits. It will be noted that while the test matrix did not provide for variations in trailer length, differing-length trailers were certainly present in the various multi-trailer combinations which were assembled. The influence of trailer length is thus represented indirectly in the presentations of data according to "combination type."

2.2.1 Measures of Performance. The summary of test data presented in the next section employs numerical measures of performance which are defined below.

Minimum stopping distance. This measure represents the minimum stopping distance achieved prior to incurring lockup on all of the wheels of a single- or tandem-axle assembly. The stopping distance measure, expressed in feet, was obtained from the "average deceleration" data by the following relationship:

$$S.D. = V^2/2A + 0.25 V$$

where V = initial velocity, ft/sec

A = average deceleration, ft/sec²

This means of determining a stopping distance measure incorporates an adjustment which reflects a particular feature of the test procedure. That is, the brake input condition was achieved by means of a procedure in which the test driver very quickly depresses the treadle valve through its full stroke, initiating the transmission of the pre-selected air pressure

condition through a quick-responding regulator. This procedure was selected for purposes of attaining a high uniformity in the pressure condition from run-to-run and throughout the duration of a single stop. Since the procedure is seen as lacking that portion of the initial transient which derives from the rate at which the typical driver applies the treadle to achieve a desired braking level, the formula shown above introduces an effective 0.25 second delay in the onset of the braking input. This adjustment has no significance, of course, to the comparison of vehicle performance under various size and weight conditions, but is introduced for the sake of realism in the quantitative results.

Understeer gradient. The understeer gradient appears in the presentation of test data as the negative inverse slope of the so-called "handling diagram," an example of which is shown in Figure 12. Plots showing handling diagrams for all of the test vehicles subjected to the trapezoidal steer test are given in Volume III. As in the reporting of simulation results in Volume I, the specific measure which was obtained from these plots was the understeer gradient occurring at a lateral acceleration condition of 0.25 g's. This measure reveals the understeer gradient in that portion of the cornering range in which the vehicle is responding in a distinctly nonlinear fashion, typically exhibiting a reduced level of understeer with respect to that exhibited in the "normal" driving regime. When the understeer gradient becomes negative, the potential for a yaw instability is present. The more negative is the gradient, the greater is the propensity for such an instability. The reader is advised to consult References [8] and [9] for more background on the understeer and yaw stability subjects.

Yaw rate response time. This measure was defined in the context of the discussion of the transient content of the trapezoidal maneuver in Section 2.1.3. The measure basically describes the time lag in yaw response which follows an abrupt steering input. This measure is of interest insofar as long values of response time generally imply that the driver must adopt a more anticipatory method of steering, since the vehicle takes longer to respond. In other words, larger values of response time are seen as degrading the control quality of the vehicle.

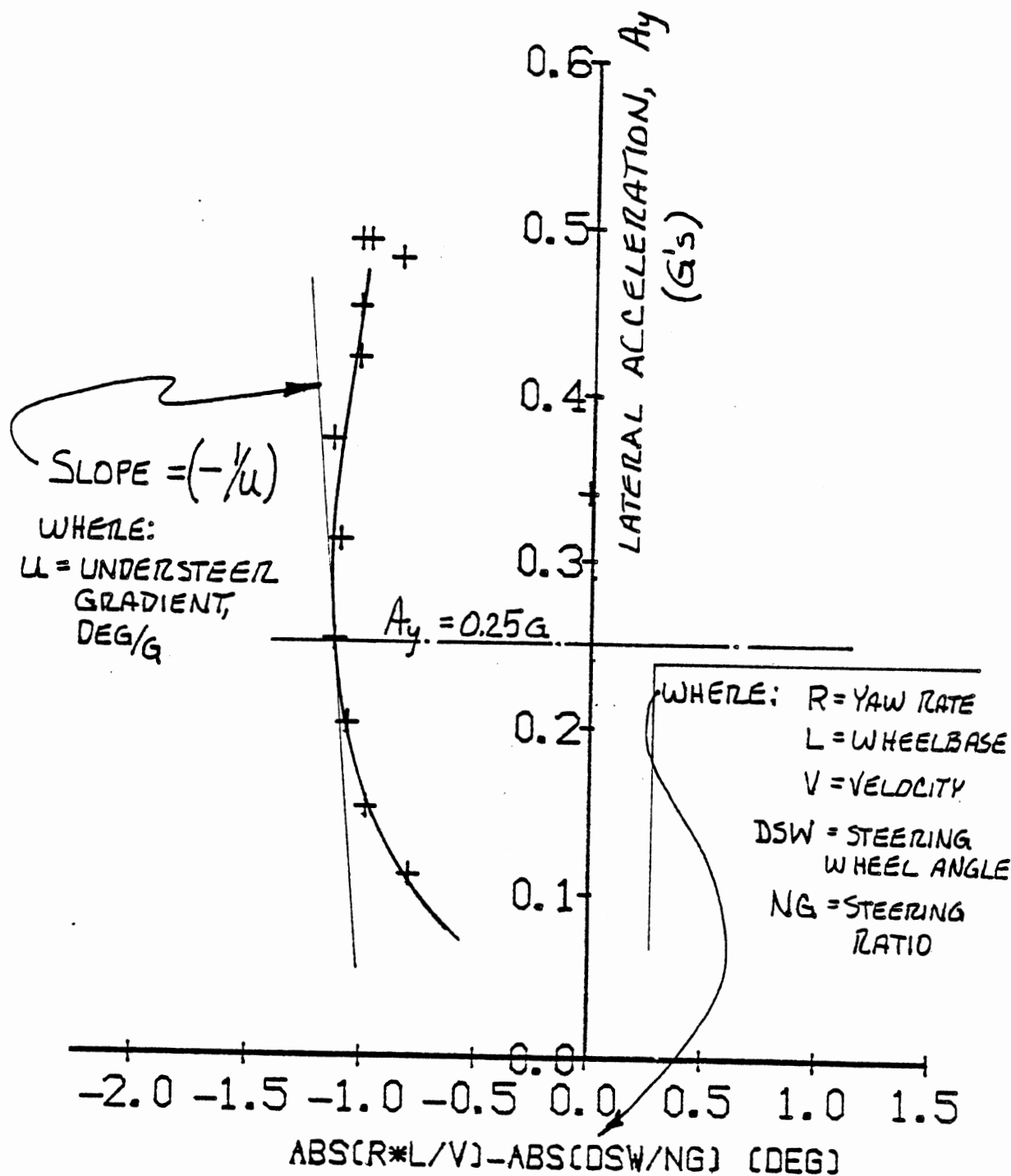


Figure 12. Example handling diagram showing definition of the understeer gradient, u , at a lateral acceleration level of 0.25 G's.

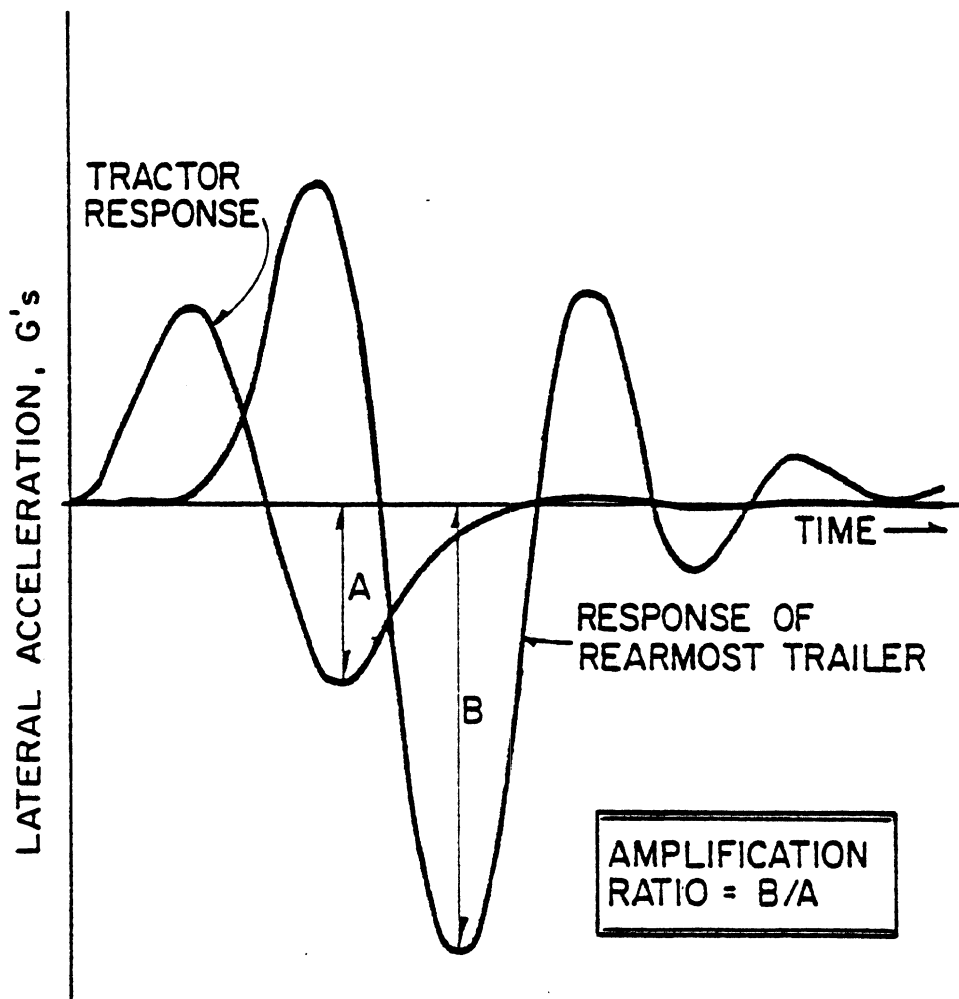


Figure 13. Lateral Acceleration Responses in an Obstacle Avoidance Maneuver Defining the Amplification Ratio.

Rollover threshold. The rollover threshold measure is defined as that minimum level of lateral acceleration which was needed in the sequence of trapezoidal steering maneuvers to cause one of the roll-arresting outriggers to touch down on the pavement. The measure corresponds, approximately, to the lateral acceleration level actually needed for rollover.

Rearward amplification. The rearward amplification measure is defined as the ratio of the peak value of lateral acceleration achieved at the rearmost trailer of a combination vehicle to the peak value of lateral acceleration achieved at the tractor. The rearward amplification measure is illustrated as the ratio, B/A, in Figure 13. As shown, the measure is derived from the lateral acceleration response signals measured in the sinusoidal steer test. This measure is seen as depicting the relative propensity of the rear trailer to approach a rollover condition in this rapid-steering maneuver which is similar to an emergency lane change. Since full-scale tests reveal that the amplification measure increases with the nominal severity of the maneuver (due to nonlinear phenomena), it was necessary, for the purposes of the summary of data in this section, to adopt the convention of evaluating the amplification ratio at a peak lateral acceleration level of 0.2 g at the tractor.

2.2.2 Summary Results. Test results will be summarized in four primary groups, namely,

- 1) Variations in loading level
- 2) Variations in payload c.g. height
- 3) Partial unloading of trailer
- 4) Type of multiple-trailer combination

The summary will be devoted simply to the data which was measured and not to a discussion of the safety significance of the findings. The reader should consult Volume I of the report for a discussion of the range of safety issues which pertain to the various categories of vehicle response.

In Section 2.3, a comparison will be made between the test and simulation data and the extent of agreement between the two sets of data will be discussed.

2.2.2.1 Variations in loading level. Test data representing the influences of variations in axle loading and gross weight are presented by means of each of the following measures:

- Stopping distance
- Understeer gradient
- Yaw rate response time
- Rollover threshold
- Rearward amplification

Stopping distance. Shown in Figure 14 are the stopping distance results for vehicles which were tested with differing loading states. In each of the baseline, "-C1," cases represented, payload c.g. height was essentially the same (see Table 1 for reference to specific values). The increased-load cases also involved increases in payload c.g. height on the order of 8 inches (20 cm).

The data show generally increasing stopping distances with increased loading. Exceptions occur only in the data taken on the wetted pavement. There are also large differences in the stopping distance values achieved among the differing vehicle samples. In general, the test vehicles were seen to be either incapable, or marginally capable, of achieving wheel lock-up on the dry surface. Thus, increases in gross weight merely resulted in lower deceleration levels for the same (saturated) level of brake torque output.

Understeer gradient. Shown in Figure 15 are data illustrating the influence of various loading configurations on the understeer gradient evaluated in the trapezoidal-steer test at a lateral acceleration level of 0.25 g's. We see that increases in gross weight, and particularly, load changes producing a more rear-biased loading on the tractor axles, cause a

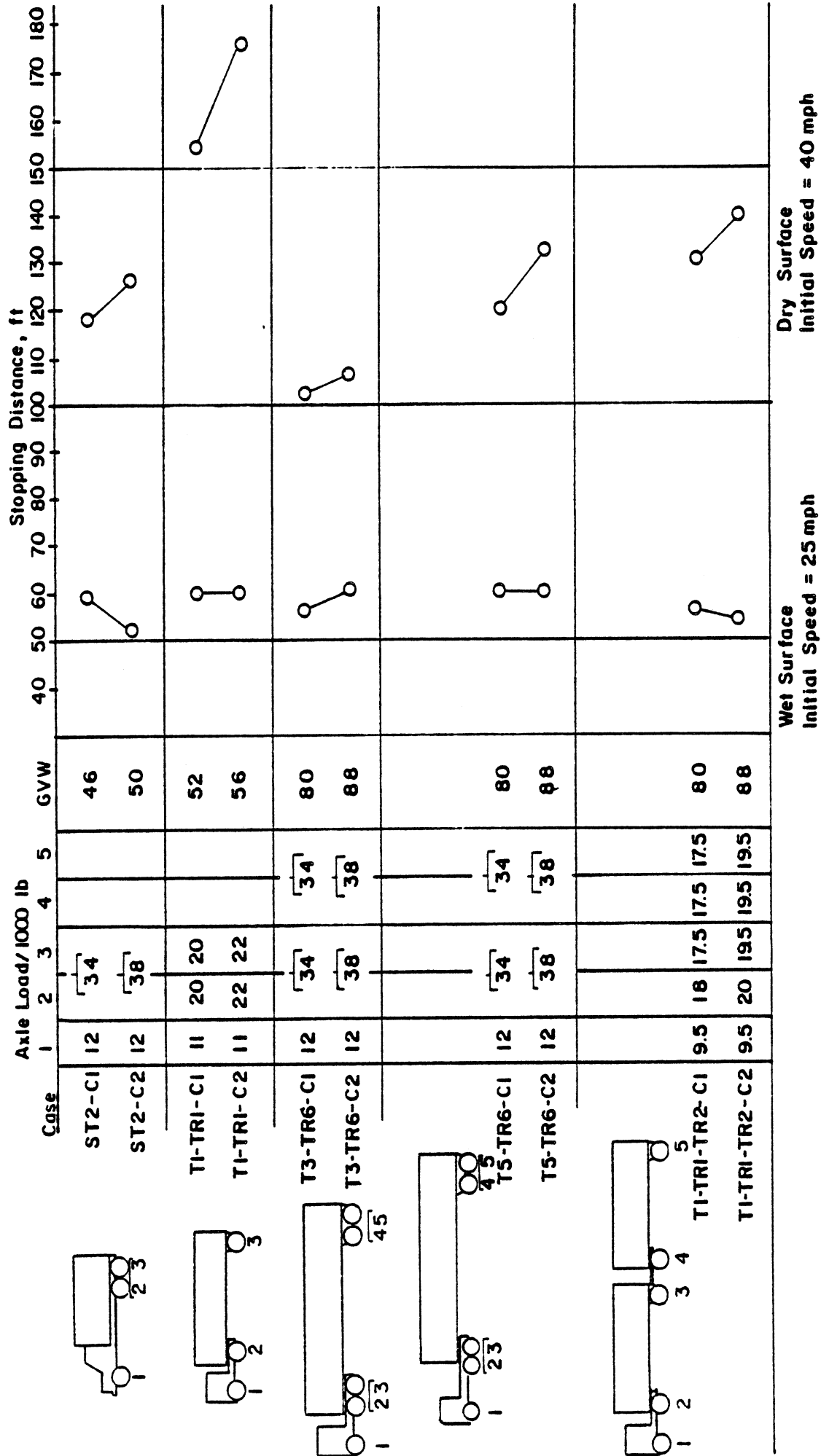


Figure 14. Influence of Variations in Axle Load and Gross Weight on Stopping Distance Performance

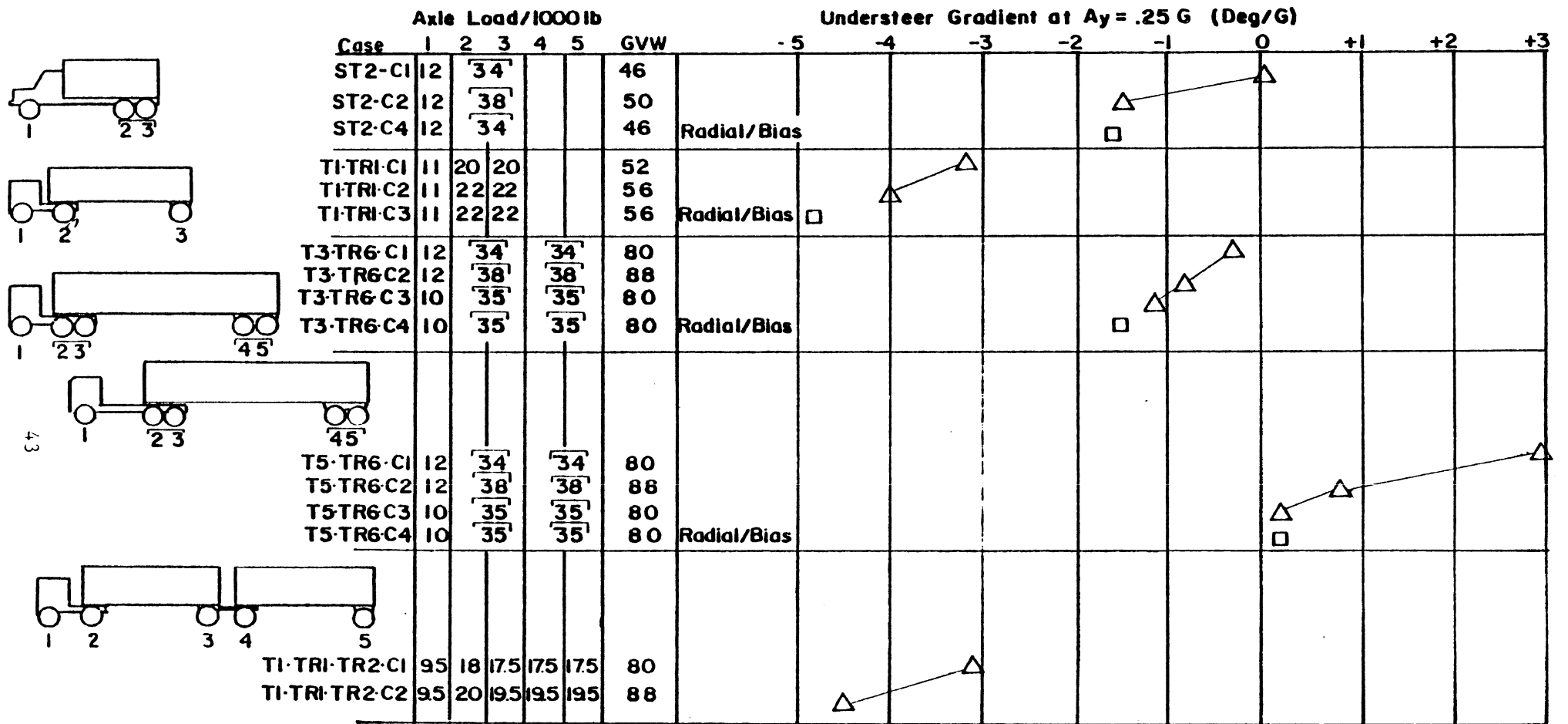


Figure 15. Influence of Variations in Axle Load and Gross Weight on Understeer Level

decline in the vehicle's understeer level. For example, the two combinations involving five-axle tractor-semitrailers (T3-TR6 and T5-TR6) show substantial reductions in understeer level with the change in gross weight from 80,000 to 88,000 lbs (36.3 to 39.9 m tons) (see cases C1 vs. C2). Somewhat larger reductions in understeer are observed, for the baseline level of gross weight, when the load is simply redistributed among the axle sets (see cases C1 vs. C3 for both of the five-axle tractor-semitrailer combinations).

Moreover, the generally meaningful implication here is that rear-biasing of the axle loads on the power unit causes a reduction in understeer level. Since increases in either axle load or gross weight allowances will typically be implemented within the trucking industry by the imposition of greater load on the non-steering axles, it can be concluded from these test data that changes in either type of weight allowance will influence the understeer level of vehicles.

In addition to variations in loading conditions, the data in Figure 15 also show the influence of a tire mix condition upon the understeer level. The tire mix condition simply involved the mounting of steel-belted radial-ply tires on the steering axle while retaining, at the other axle positions, the bias-ply tires with which all other testing was conducted. The tire mix cases were included in the test matrix for the purpose of providing some scale of reference for the interpretation of the influence of size and weight variables on the understeer characteristic. That is, since the tire mix condition is known to occur in service and produces a substantial decline in understeer level, it was seen as a convenient means of obtaining a degraded level of understeer for comparison with loading-induced degradations.

The reader should note that differing loading conditions were involved in the tire mix case with differing vehicles. For example, to assess the influence of the tire mix condition, per se, on understeer level, one should compare the data obtained under the following cases with the indicated vehicles:

Straight truck, ST2, -- cases C1 vs. C4

Three-axle tractor-semi, T1-TR1 -- cases C2 vs. C3

Five-axle tractor-semi, T3-TR6 and T5-TR6 -- cases C3 vs. C4

We see that the data show the understeer level to be reducing in the case of the tire mix conditions employed on the top three vehicles in Figure 15 and staying essentially unchanged in the case of the fourth vehicle (the T5-TR6 combination). The largest reduction in understeer level due to the tire mix is seen in the case of the straight truck for which a 1.6 deg/g loss in understeer is observed.

Results showing a degraded level of understeer in the case of the mixed tire installation had been anticipated, of course, although the extent of the degradation was less than expected. It appears, however, that the less-than-anticipated influence can be traced to an anomaly of the test procedure. That is, tests using the tire mix condition on specific vehicles were conducted at the conclusion of the other test cases on that vehicle. At that point, the bias-ply tires which had been installed as new tires on the vehicle at the beginning of the test series were at least half-worn. The radial-ply tires which were put on the steering axle to effect the "mix" condition were essentially new tires having negligible treadwear. Since there is a strong influence of the tread depth of truck tires on their cornering stiffness property (see, for example, Reference [10]), the mix condition provided only a minor disturbance in the cornering stiffness at the front axle. That is, the mix condition actually represented a combination of full-tread radials and half-tread bias tires. The contrast in the estimated [10,11] cornering stiffness levels involved is as follows:

<u>Tire</u>	<u>Cornering Stiffness</u>
New bias (Firestone T-1)	565 lb/deg (2568 N/deg)
1/2-worn bias (Firestone T-1)	745 lb/deg (3382 N/deg)
New radial (Michelin XZA)	790 lb/deg (3586 N/deg)

Accordingly, the mix condition that appears to have actually prevailed in most of the four cases shown in Figure 15 may have involved a narrow

range of cornering stiffness levels between the radial and bias tires which were installed. In retrospect, the test sequence should have been rearranged such that the mixed tire condition was run as the first case in the series, while the bias-ply tires were still at their full-tread depth.

Yaw rate response time. Shown in Figure 16 are the values of yaw rate response time obtained in the trapezoidal-steer tests with the various cases of load variation. The figure shows essentially an inverse influence from that illustrated in the understeer data presented above. That is, increases in loading, and specifically, increases in the rear-bias of load distribution on a truck or tractor will cause the yaw rate response time measure to increase. Although the increases due to load changes are substantial, they are seen to be modest in contrast with the spread of values among the various vehicles in their baseline, C1, condition.

Rollover threshold. Shown in Figure 17 are the rollover threshold values obtained over the various cases of loading. Of course, we see that the rollover threshold declines strongly with increased loading. It should be noted, however, that increases in loading were implemented, in each case, by means of the water tanks described in Section 2.1.2.2. The filling of the upper tanks to achieve the increased load levels introduced an increase in the height of the payload center of gravity as well. Since the geometry of the tank array was fixed, the resulting arbitrary variation in payload c.g. height was relatively large in cases such as T1-TR1-C2, T3-TR6-C2, T5-TR6-C2, and T1-TR1-TR2-C2, while a relatively small change in payload c.g. height was effected in the "high c.g." cases identified in the next section.

The data in Figure 17 thus show relatively large reductions in roll stability for the given variations in axle loading and gross weight. Although many common loading scenarios might involve somewhat lesser reductions in roll stability resulting from an increased load allowance, discussions presented in Volume I cite the great variety of loading situations which may occur—some producing greater disturbances in payload c.g. height than those represented in the test cases, and some producing less.

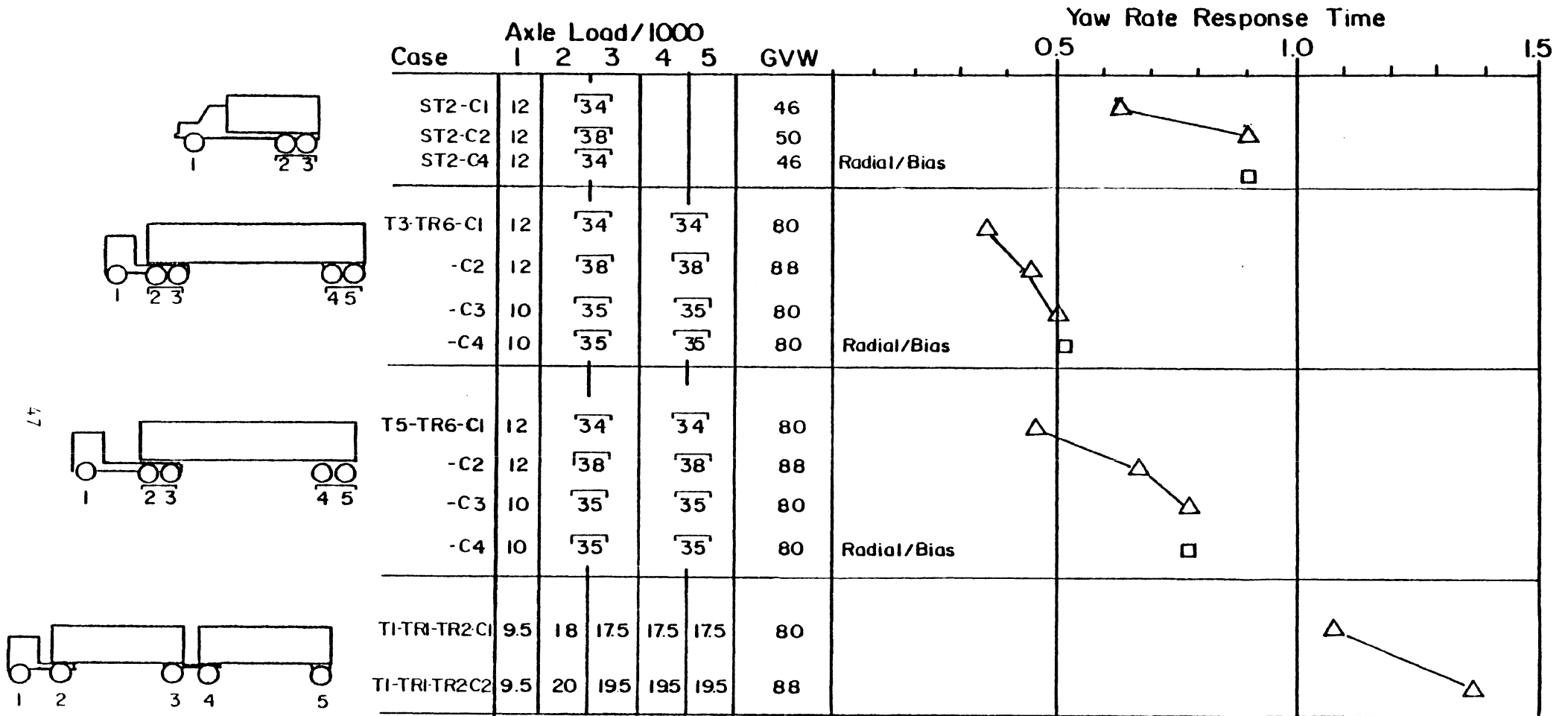


Figure 16. Influence of Variations in Axle Load and Gross Weight on Yaw Rate Response Time

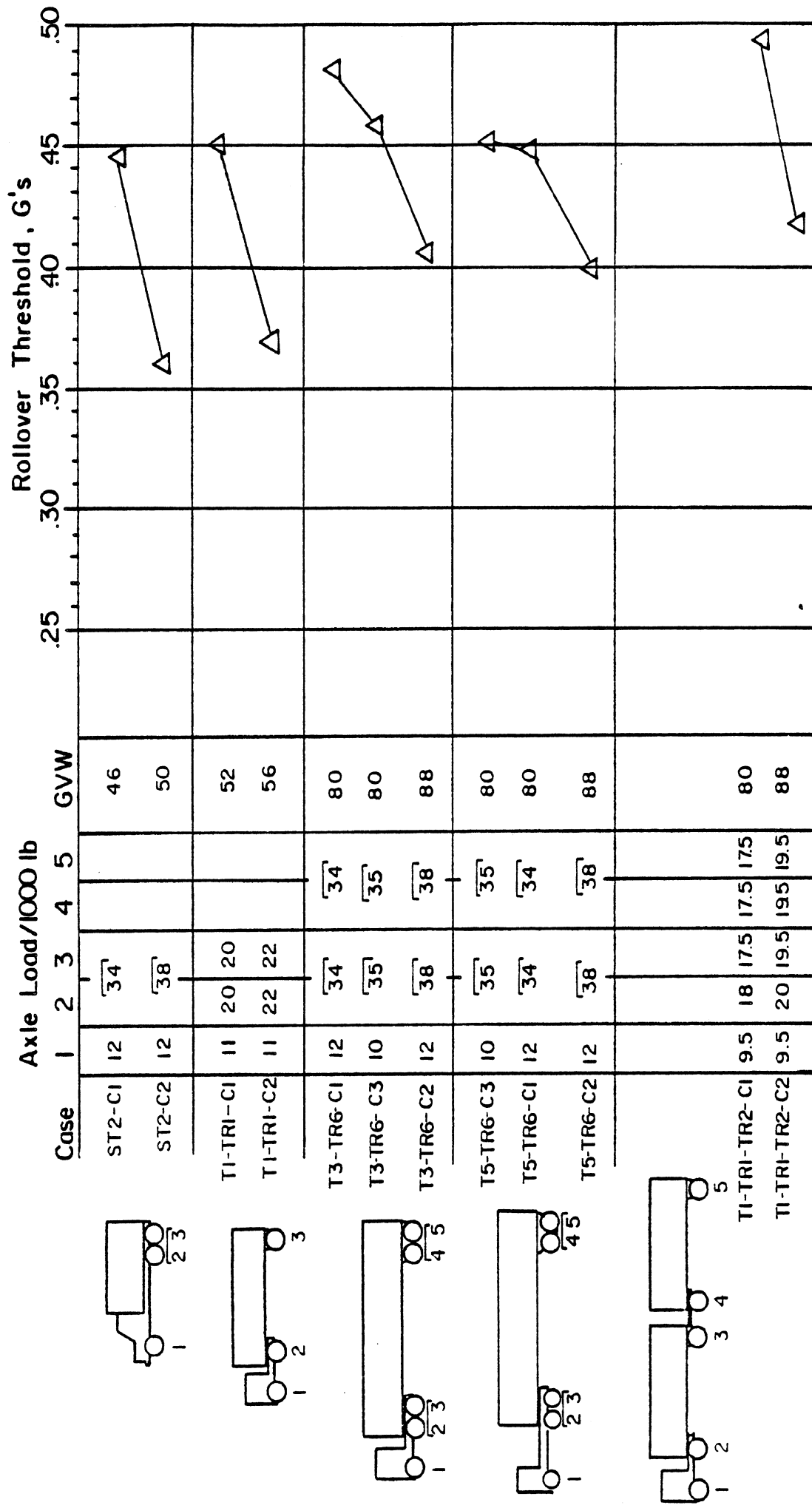


Figure 17. Influence of Variations in Axle Load and Gross Weight on Rollover Threshold

Rearward amplification. Two cases of the five-axle doubles combination permit examination of the influence of gross weight level on the rearward amplification of the vehicle in the sinusoidal-steer maneuver. Listed below are the two test cases of interest, both of which produced the same nominal rearward amplification response.

<u>Case Code</u>	<u>Axle No.</u>	<u>Axle & Gross Loads/1000 lbs</u>						<u>Amplification Ratio</u>
		<u>1</u>	<u>2</u>	<u>3</u>	<u>4</u>	<u>5</u>	<u>GVW</u>	
T1-TR1-TR2-C1		9.5	18	17.5	17.5	17.5	80	1.5
T1-TR1-TR2-C2		9.5	20	19.5	19.5	19.5	88	1.5

Although only one test case was examined for indicating the nominal influence of gross weight level on rearward amplification, the data confirm the generally-known result; namely, that gross weight changes have a negligible influence on rearward amplification.

2.2.2.2 Variations in payload c.g. height. Test results showing the influence of payload c.g. height, per se, on the dynamic performance of heavy vehicles are summarized below in terms of the following response measures:

- Stopping distance
- Understeer gradient
- Rollover threshold

The two vehicle types upon which changes in payload c.g. height were examined were the three-axle straight truck and one of the five-axle tractor-semitrailers.

Stopping distance. Braking tests involving cases with elevated payload location were done on the wet pavement only. Shown in Figure 18 are the stopping distance values obtained for cases in which a certain payload weight was located at the baseline and elevated heights. With both vehicles, the payload represented a nominally full-gross-weight load.

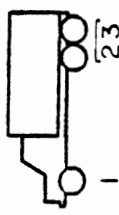
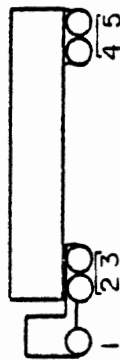
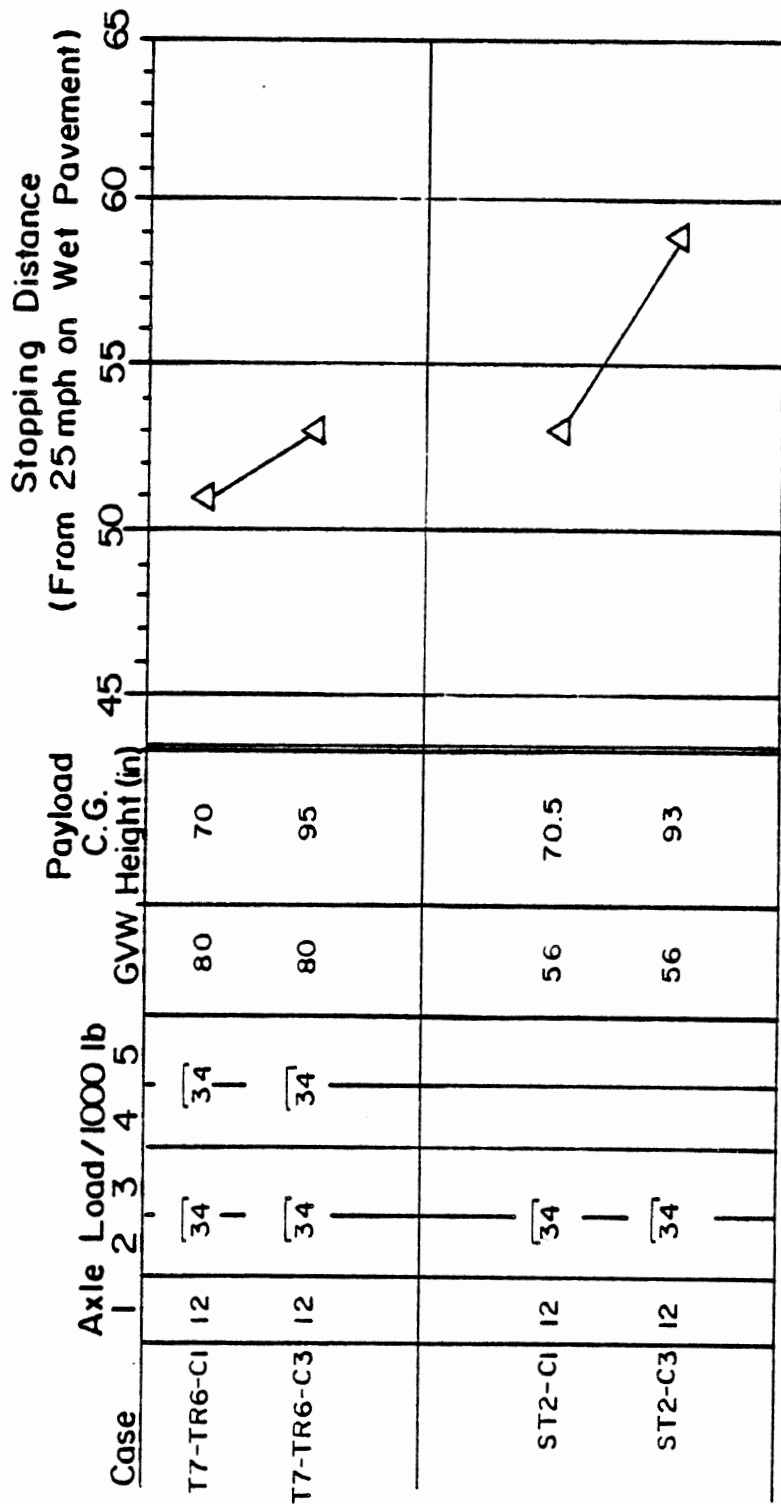


Figure 18. Influence of Payload C.G. Height on Stopping Distance

We see that the increased c.g. height condition causes the stopping distance to increase. This result is explained by observing that, even in their baseline loading states, the vehicles in question are limited in stopping distance capability on this wetted surface by the lockup of their rearmost tandem axle sets. Thus, when the c.g. position is elevated further, the dynamic load transfer occurring during braking causes these rearmost axles to unload even more, such that rear wheel lockup occurs at a lower deceleration level than in the baseline cases.

Understeer gradient. Shown in Figure 19 are the test results showing the influence of payload c.g. height on understeer level. We see that increased c.g. height causes the understeer level to reduce. In the case, C4, of the five-axle tractor-semitrailer, T7-TR6, the elevated c.g. height at the gross weight level of 88,000 lbs (39.9 m tons) has so degraded roll stability that the understeer measure cannot be meaningfully characterized. As will be shown in the following data concerning roll stability, this case is virtually unstable in roll at the 0.25 g level of lateral acceleration at which the understeer measure is evaluated here.

The basic trend indicated by the two vehicle cases shown in Figure 19 confirms the result which would be predicted by theoretical considerations. Namely, the increased c.g. height causes a greater degree of lateral load transfer during cornering, thus further increasing the difference between the loads borne on left- and right-side tires. Since the strong trend toward a decreasing level of understeer in heavy trucks as lateral acceleration increases depends primarily upon the left/right differences in tire loading, increases in payload c.g. height should be generally expected to further reduce the understeer level.

Rollover threshold. Shown in Figure 20 are the rollover threshold values exhibited by test vehicles operated with differing values of c.g. height. Clearly, there is a profound reduction in roll stability with the levels of payload height increase represented here. Nevertheless, the represented cases should not be looked upon as being unusual. Rather, these cases represent conservative values of payload c.g. height falling well

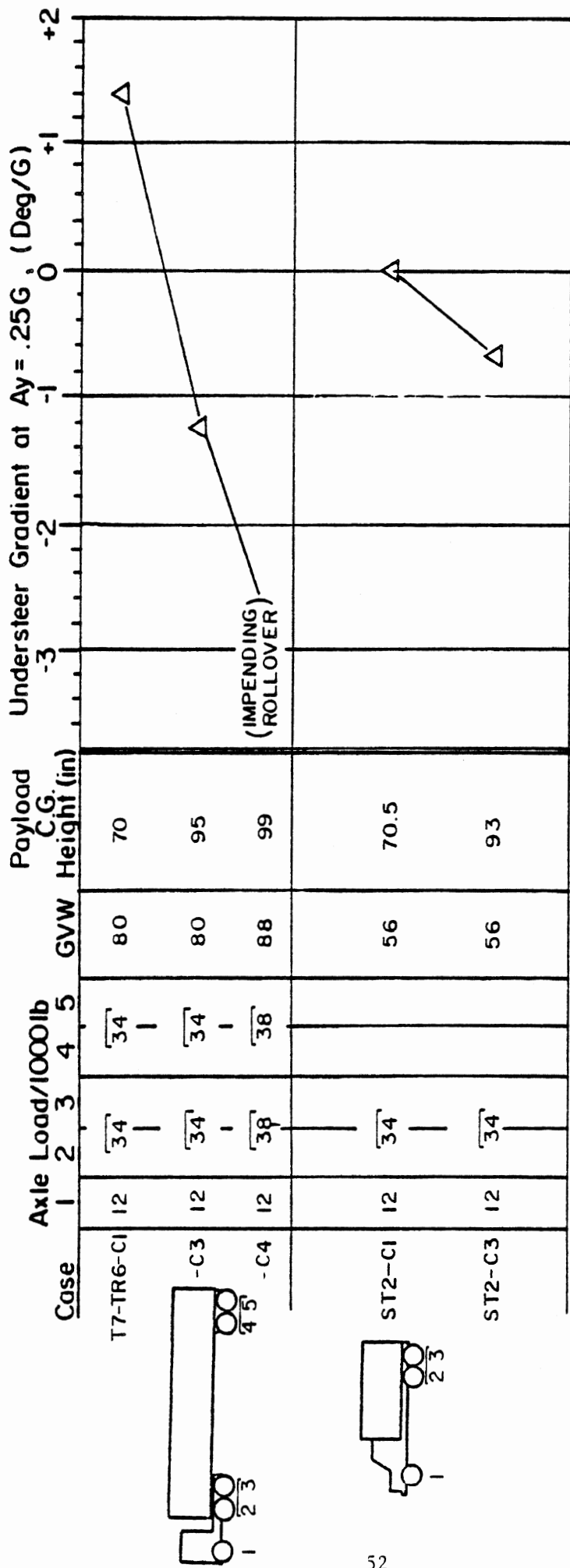


Figure 19. Influence of Payload C.G. Height on Understeer Level

within the nominal range of loading conditions occurring in service every day as a consequence of differences in payload density.

2.2.2.3 Partial unloading. One case of partial unloading was covered in the test matrix. Shown in Figure 21 are test data illustrating the influence on stopping distance of the practice of unloading half of the payload from the rear of a 45-foot (13.7-m) semitrailer in a five-axle tractor-semitrailer combination. The stopping distances are seen to increase due to the reduction in loading of the trailer rear axle. That is, the lighter rear axle load permits lockup of the wheels on the trailer axles at a deceleration level which is less than that achieved before lockup in the baseline case. Of course, the specific level of influence which might be measured on a given vehicle in this type of test will depend entirely upon the distribution of brake torques achieved at the various axles involved. As expounded upon in Volume I, the brake torques generated on heavy trucks vary widely due to differences in design, maintenance, and inherently non-stationary properties. Thus, while the basic nature of the observed result can be explained fairly readily, it must be recognized that a broad range of apparent influences of the "partial unloading" condition could be observed if a large number of vehicles were tested.

2.2.2.4 Types of vehicle combinations. The test program included various types of vehicle combinations, ranging from tractor-semitrailers to triples. Two categories of vehicle maneuvering conditions were examined by means of full-scale tests. The two categories in question involve stopping distance and rearward amplification performance. Although certain of the various vehicles were also subjected to understeer and roll stability evaluations, these tests were not conducted over the whole matrix of vehicles for purposes of distinguishing the influences of vehicle type, per se. Of course, the selection of the test conditions to be covered was based upon hypotheses concerning the performance categories which were likely to have the greatest sensitivity to the type of combination.

For example, the understeer measure was not of general interest in this regard since it describes a response property of the tractor in a combination vehicle. While the attached semitrailer, and particularly its loading, does

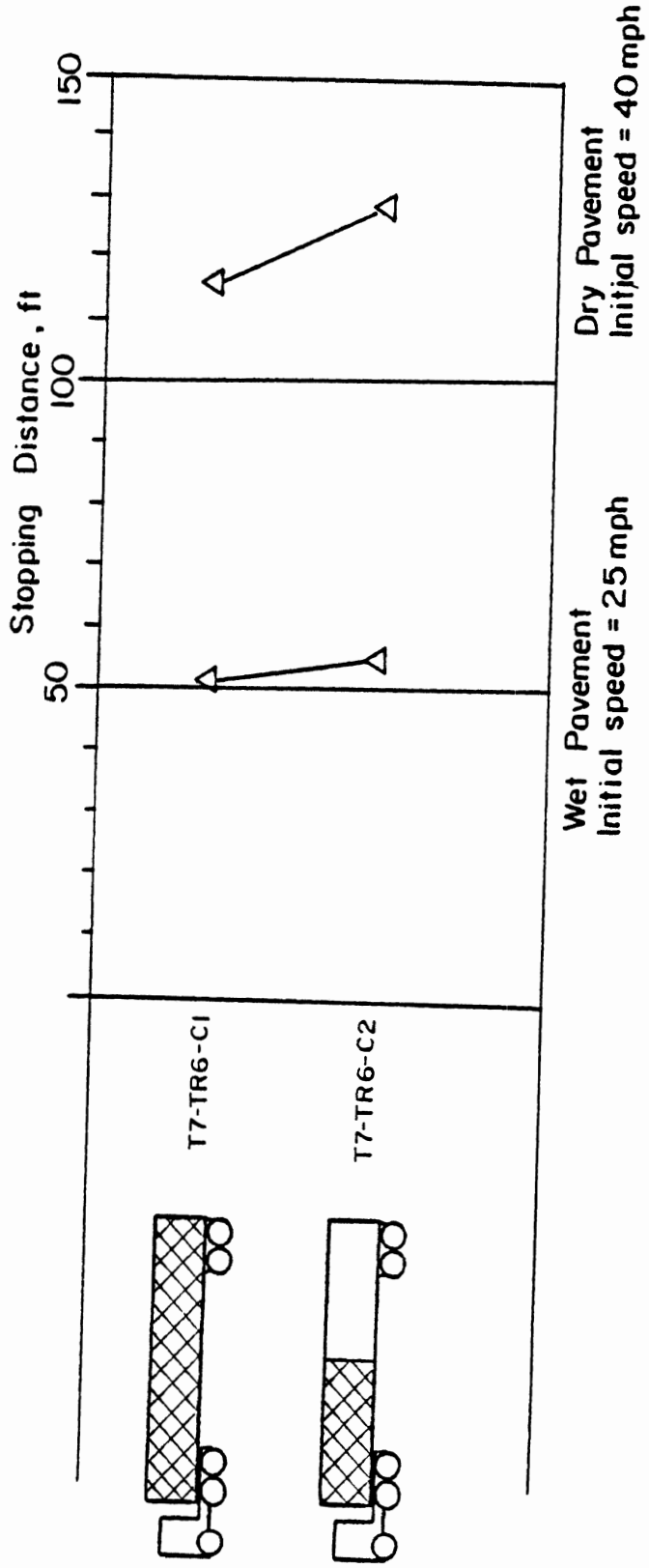


Figure 21. Influence of Partial Loading on Stopping Distance Performance

play a role in determining the tractor's understeer quality, the addition of full trailers to the rear of the first semitrailer is of no consequence to the tractor's yaw behavior. This observation is based upon the well-known principle that the conventional dolly which couples full trailers in multiple-trailer combinations is incapable of transmitting significant levels of either lateral force or roll moment through its attachment at the pintle hitch. Accordingly, the configuration of the combination after the first semitrailer has no influence on either the roll or yaw behavior of the tractor-semitrailer portion of the combination.

Stopping distance. Test data addressing the influence of combination type on the braking performance of differing vehicles are shown in Figure 22. The primary question addressed in these data is "What is the influence of additional trailers on the stopping performance of a vehicle combination?" The test data show differing influences among the vehicle combinations represented.

In the case of the combinations involving the long, 45-foot (13.7-m) trailers, we see that the addition of another trailer to the rear of the five-axle tractor-semitrailer causes the stopping distance to increase markedly. In cases involving the short, 27-foot (8.3-m) trailers, we see stopping distance first decreasing with the addition of one trailer (thereby producing a double) and, subsequently, increasing moderately with the addition of another trailer (so as to constitute a triples combination). Again, since the test data involves such a limited number of samples, the reader is advised to interpret the results cautiously. It is suspected that the test results obtained in both cases are more reflective of the influence of combining particular vehicle specimens than of the generic influence of combining additional trailers to constitute longer combinations.

For example, the case involving the addition of another long trailer to constitute a "turnpike double" configuration adds a tandem axle dolly and a tandem axle semitrailer to the original five-axle combination. No additional experiments were conducted to assess the brake torque levels of either of these additional elements in the combination. Given that such large increases in stopping distance are observed with the addition of the

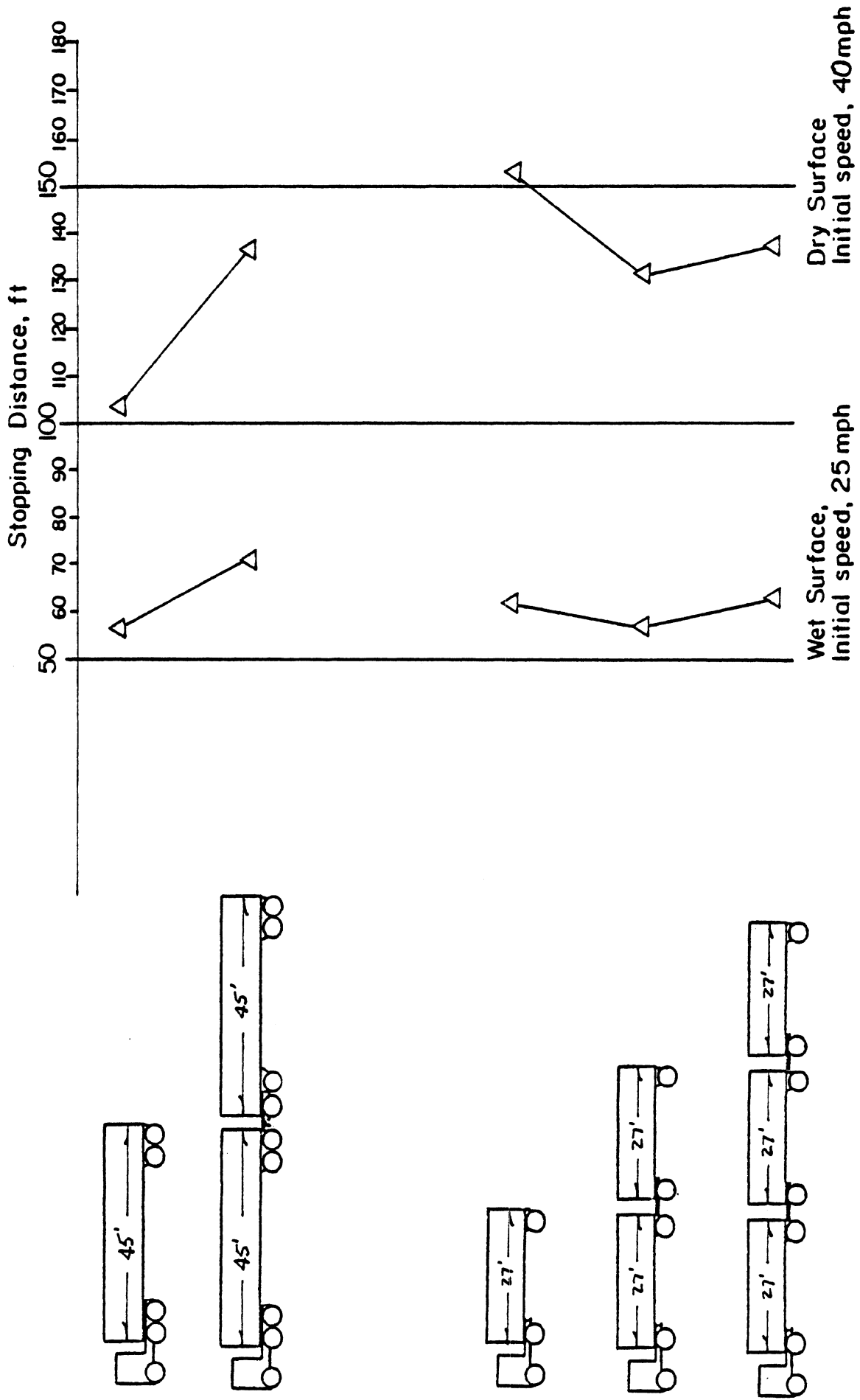


Figure 22. Influence of Combination Type on Stopping Distance

dolly and extra semitrailer, it is suspected that these added units are simply deficient in torque capacity. This supposition is based upon examination of the results presented earlier, in Figure 14, showing that the T3-TR6-C1 configuration (which was the baseline tractor-semitrailer combination from which the turnpike double was assembled) exhibited the shortest stopping distance of all the combination vehicles tested, especially on the dry surface. Thus, since the T3 tractor and TR6 semitrailer were seen to be unusually high in braking capability, when coupled as a "single," it seems reasonable to assume that the lowered level of performance seen in the turnpike double is attributable largely to deficient torque outputs from the added units.

Conversely, the two-axle tractor, T1, is seen as having brakes which are low in torque capacity such that a very long stopping distance is seen in the single semitrailer configuration. Subsequently, when one additional trailer is coupled to form the double, T1-TR1-TR2, stopping distances on the wet and dry surfaces decrease. This result suggests that the nominal "torque deficiency" of the two-axle tractor is being "overcome" with the higher capacity braking systems on the trailer and dolly axles. The moderate increase in the stopping distance of the triple, with respect to that attained by the double, is then indicative of either a "genuine" multi-unit combination effect (such as increased air transmission times) or is due to an anomalously lower torque capacity among the brake systems on the third semitrailer and its dolly.

Moreover, such a large number of axles are involved in the long combinations examined here that a large range of stopping performance levels are thought to be attainable—simply on the basis of the widely-ranging torque output levels of commercial vehicles in service [12,13,14]. The reader should note that the overall issue of the influence of combination type on stopping capability is addressed in Volume I.

Rearward amplification. Shown in Figure 23 are the values of the rearward amplification measure obtained in the sinusoidal steer test with each of six differing vehicle combinations. The figure ranks the vehicles from the lowest amplification level to the highest. Since the amplification phenomenon is strongly sensitive to speed, the levels of response shown

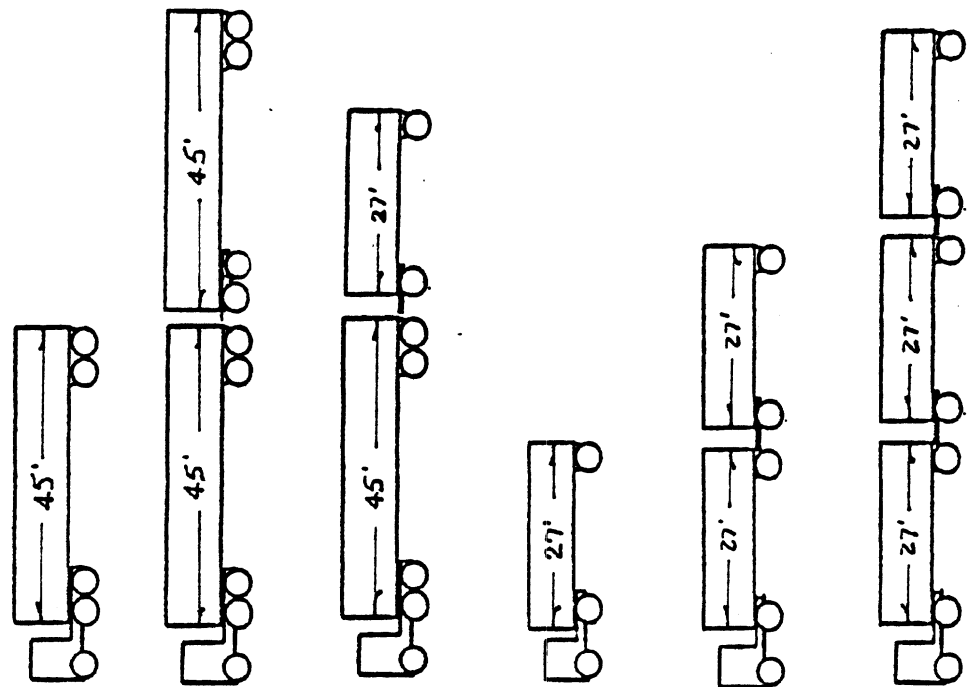
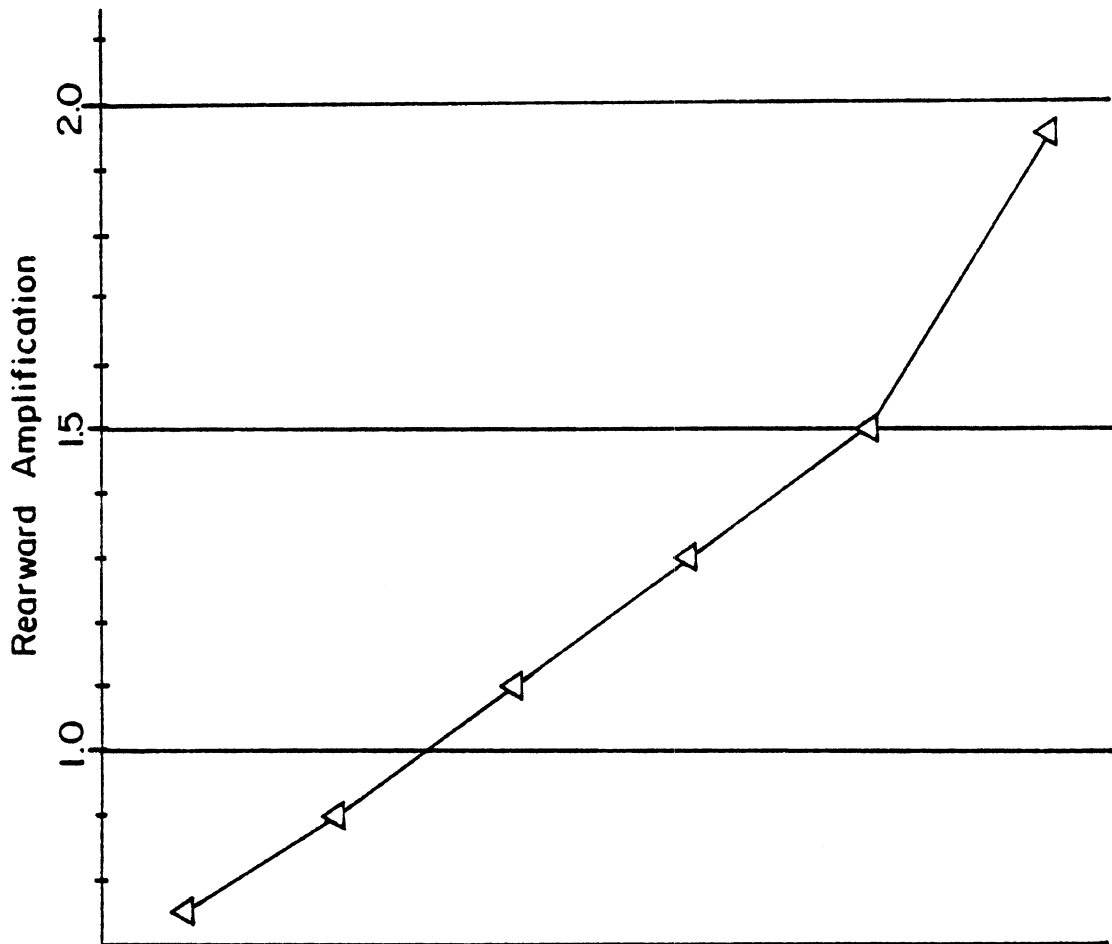


Figure 23a. Influence of Combination Type on Rearward Amplification (at 45mph)

here for a test speed of 45 mph (72 km/h) are substantially lower than the values which would occur in a maneuver at, say, the national speed limit of 55 mph (88 km/h). Nevertheless, the results clearly discriminate among the differing vehicles. Further, these results line up rather well with theoretical considerations which show that amplification level increases as the number of articulation points increase and as the length of trailers decreases [15].

We see that the two top vehicles in the figure actually produce an attenuated lateral acceleration response (i.e., a value less than 1.0) at the rear trailer with respect to the tractor in this test maneuver. The vehicle combinations constituted of the short 27-foot (8.2-m) trailers exhibit the larger levels of amplification and, further, these levels increase strongly with the addition of more trailers.

Moreover, the test results show that the conventional five-axle double and the seven-axle triple exhibit relatively large levels of amplification while the five-axle tractor-semitrailer, turnpike double, and Rocky Mountain double varieties exhibit minor levels of this amplification measure.

2.3 Comparison of Test and Simulation Results

The task of comparing test and simulation results in this study suffers, to a large degree, from the "apples and oranges" syndrome. That is, for a number of reasons, the vehicles, maneuver conditions, and data formats used in connection with full-scale testing do not correspond directly with the vehicles, maneuvers, and data formats adopted in the simulation effort. Nevertheless, there is a sufficient "overlap" in these two respective data sets to enable a meaningful comparison of results. In fact, the level of agreement found upon comparing these sets of results was deemed sufficient to warrant the use of the more comprehensive simulation results as the basis for presenting the study's findings in Volume I. Further, the test and simulation findings were both seen to be broadly supported by the existing state of knowledge in the field of the mechanics of heavy-duty trucks.

Moreover, it was concluded prior to the simulation portion of the study that theoretical understandings had been confirmed by test results to

such an extent that the simulation effort could be designed simply to provide the maximum coverage of the size and weight issues without assuming the costly burden implied by the task of precisely "matching" the test cases. Having organized the simulation study with this objective, it is the purpose of this section to examine the extent of agreement between the basic findings obtained in the test and simulation tasks. It should be noted that this exercise does not constitute a "validation" activity in the classical sense since the precise "matching" of vehicle and condition variables, as mentioned, was not undertaken.

The vehicle part of the "mismatch" derives, in part, from the simple fact that the measurement of the mechanical properties of the test vehicle components constitutes a very large task which was beyond the scope of the study. Thus, the extent of the similarity between the mechanical properties of brakes, suspensions, steering systems, etc., on the test and simulation vehicles is largely unknown. In other respects, certain differences between the respective data sets resulted directly from the design of the test and simulation exercises and thus can be identified. These differences will be discussed in Section 2.3.1, below.

To the extent that the test vehicles and test procedures do overlap with those represented in the simulation effort, performance measures will be compared in Section 2.3.2.

2.3.1 Distinctions in the Vehicles and Operating Conditions. The vehicles examined through test and simulation are known to have differed in the following aspects:

- 1) The brake systems on the test vehicles were generally low in maximum torque capacity relative to the simulated vehicles. The brakes on the test vehicles were thus unable to achieve wheel lockup under the majority of the loading conditions which were of interest. The simulated vehicles, on the other hand, were configured with brakes whose torque capacities were sized and proportioned among differing axles according to a scheme which is seen as reflecting the modern design practices of brake engineers. This scheme is defined in Volume I. These systems were generally capable of achieving wheel lockup under virtually all of the loading conditions examined.

2) As was mentioned in Section 2.2, the test condition involving a mixed installation of radial- and bias-ply tires on the front and rear axles, respectively, of test tractors was disturbed by a tire wear problem. Thus, the difference in effective front and rear cornering stiffnesses accruing under these test cases was less dramatic than planned. The simulated cases in which the tire mix condition was represented, on the other hand, involved not only full-tread tires, but also the selection of rear-placed (bias-ply) tires such that a very low value of cornering stiffness prevailed at the rear. That is, the specific bias-ply tire selected for the rear positions in these special simulation cases involved a lug-type tread design yielding a cornering stiffness level which represents a more extreme, but very real, case among those found in actual service.

Shown in Figure 23 is a plot of the cornering stiffness characteristics of the tested and simulated tires—with an estimation of the range of values for the test-worn bias-ply tires. The estimations are based upon data provided in Reference [10], showing the influence of treadwear on cornering stiffness.

3) The test and simulation cases were distinguished by differing baseline levels of the height of the payload center of gravity. Also, the increment by which the payload c.g. height was elevated upon increasing the gross weight level was different between test and simulated cases. The baseline level of payload c.g. height employed in the test cases was approximately 70 inches (178 cm), while the corresponding simulated value was an average of 83 inches (211 cm). The baseline test condition was limited by the dimensions of available loading racks. The simulated value of the baseline payload c.g. height was selected to provide a reference value of 80 inches (203 cm) for the c.g. height of the composite mass (i.e., the trailer sprung mass plus the payload). The 80-inch value has been identified in other research as a reasonable estimate of the median freight density condition—and a condition which is useful for relating vehicle characteristics to rollover accident data [27].

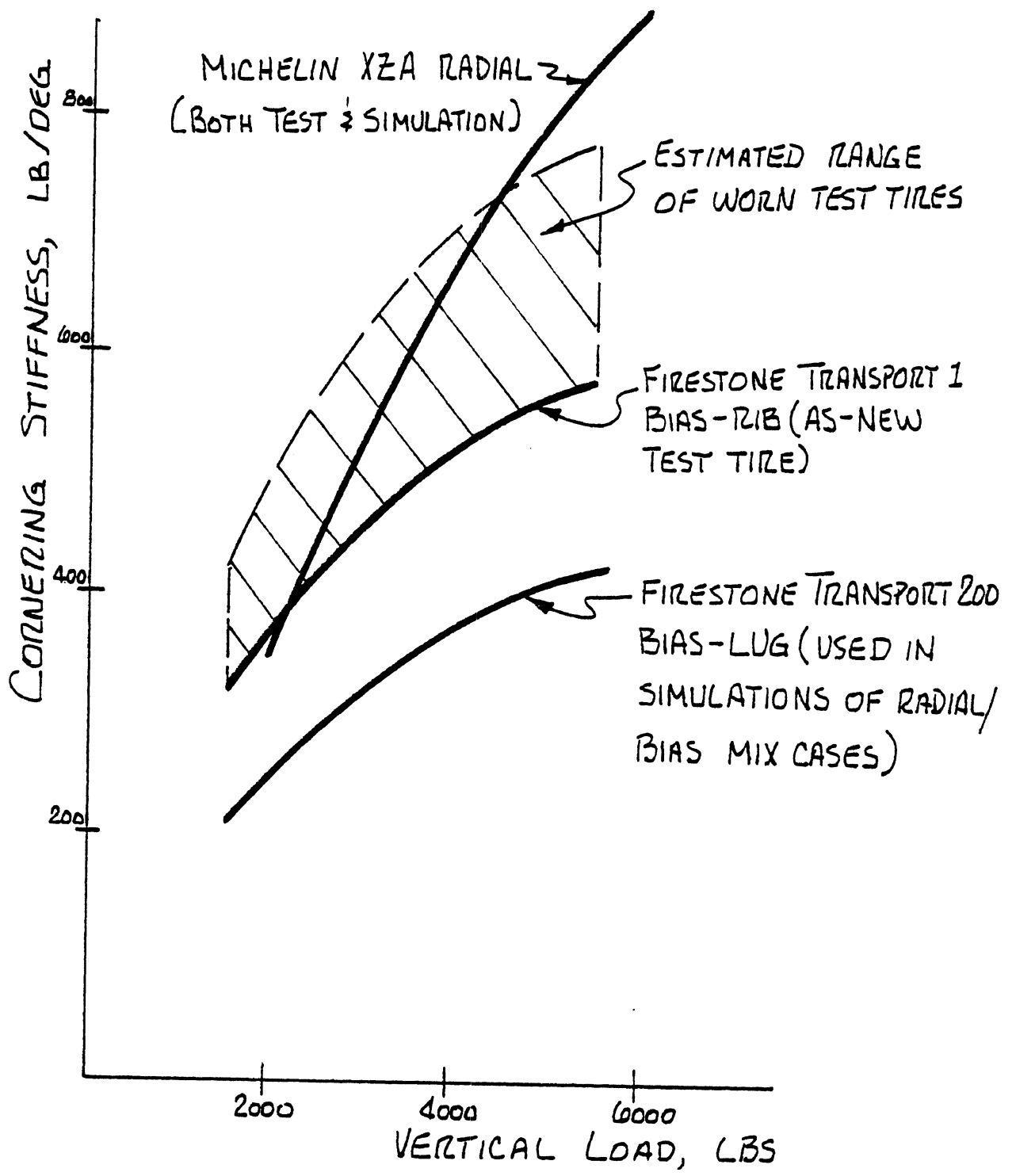


Figure 23b. Cornering stiffness vs. load for tires involved in Test and simulation tasks.

The increment by which the payload mass center was raised upon increasing the gross weight level was determined in the test cases by the physical layout of the water tank assembly. For tractor-semitrailer cases involving 45-foot (13.7-m) trailers, the achievement of a gross weight level of 88,000 lbs (39.9 m tons) resulted in a nominal 9-inch (22.8-cm) rise in the payload center of gravity over the position which prevailed in the baseline case, with a gross weight of 80,000 lbs (36.3 m tons). For the corresponding simulation case, the payload c.g. height was raised by only 5 inches (12.7 cm), according to a scheme by which a constant-density-freight condition is assumed. Thus, while both the test and simulated cases imposed arbitrary constraints upon the baseline and incremental values used in locating the payload center of gravity, the actual freight-loading scenarios which might correspond to the two approaches are significantly different.

In addition to the above items, the tested and simulated vehicles differed in unknown ways with regard to the stiffness, coulomb friction, free-play, and kinematic characteristics of suspensions, the stiffness and kinematics of steering systems (as they influence understeer level), and in the effective torsional stiffnesses of frames and hitch assemblies.

With regard to the operating conditions and control inputs, the test and simulation cases differed as follows:

- 1) The tests were run under two pavement conditions; namely, dry asphalt and wet, coated, asphalt surfaces. While the test and simulation results obtained on the dry surfaces should not differ significantly from one another for reasons of the tire/road traction limits, it is clear that differences in the wet surface conditions were sufficient to cause marked differences in results. The wet surface employed in tests involving straight-line braking and braking in a turn was seen to yield high levels of "peak" traction relative to the levels achieved in the locked-wheel condition. In fact, test data presented in Volume III show that average deceleration levels achieved by trucks stopping on the wetted surface from 25 mph (40 km/h) were very nearly the same as the deceleration levels achieved on the

dry surface from 45 mph (72 km/h). Simulations representing stopping on a low-friction surface, however, produced much lower deceleration levels than those achieved under the simulated "dry," or high-friction surface condition.

2) Test speeds were all lower than simulated speeds. The lower values of test speed were primarily due to the layout of the test facility and the practical inability to accelerate the heavily-loaded test vehicles up to the full level of highway speeds. Thus, all tests on the dry surface were conducted at a nominal speed condition of 45 mph (72 km/h). Test safety considerations led to the selection of 25 mph (40 km/h) as the initial speed for conducting braking tests on the wetted pavement. All simulations, on the other hand, represent vehicle operation at the national speed limit value of 55 mph (88 km/h). The differences in test versus simulated speeds have the obvious effect on the stopping distance measures and also upon the rearward amplification behavior of multiple-unit combinations.

3) Steer input conditions differed substantially in certain cases. The two cases in which differences in the steer input condition are most notable are the trapezoidal and sinusoidal steer test maneuvers. The trapezoidal test provides for an approximately steady-state cornering response, after the initial transient responses have died out. The understeer levels characterized from the resulting steady-state data have been analyzed and are reported as the key measure which speaks to the yaw stability of the various test cases. In the corresponding simulations, an alternative approach was taken in which the steering was applied as a linearly-increasing ramp of steering-wheel angle. This method was chosen for the great improvement in efficiency offered by the "sweep" of steer input level. The resulting understeer measure obtained from simulations, however, is distinctly non-steady state in character, although it can be used very effectively to illustrate the relative influence of changes in vehicle parameters, such as in this study of size and weight variations. The understeer level determined from ramp-steer-type maneuvers is always seen to be higher than the corresponding level observed in a steady-state turn condition [14]. Thus, as will be shown, the simulation-derived understeer values fall well above those obtained from full-scale tests.

The second maneuvering case for which significantly different steer inputs were applied involved the sinusoidal-steer test procedure—in contrast to the closed-loop obstacle-avoidance maneuver conducted by means of simulation. Although the basic time period over which the primary portion of the steer inputs were applied was 2.0 seconds in both cases, the closed-loop maneuver can involve a more complex steering waveform than the test case. Note in the example of Figure 24 that the closed-loop steering input typically involves additional zero-crossings as the simulated "driver" fine-tunes the vehicle's heading to arrive precisely in the target lane. These differences in steer input will have some effect on the rearward amplification behavior of multiple-unit vehicle combinations.

4) As stated earlier, the means of identifying the roll instability point was different in the test and simulation cases. The touchdown of the outrigger constituted the occurrence which identified an approximate roll instability point in the case of the test vehicles. This practice was "approximate" insofar as each vehicle still possessed a certain additional rollover resistance at the touchdown condition since the outrigger was adjusted on each vehicle to touch the ground at a value of trailer angle which resulted in the trailer wheels lifting off of the ground by some 4-8 inches (10-20 cm). In this condition, all of the tractor tires were typically still in contact with the pavement, although the inside set of tires on the tractor drive axle(s) were typically on the verge of liftoff. Clearly, the extent of the consistency of the outrigger touchdown criterion as an indicator of rollover threshold depends upon the differences in the various vehicle properties which influence the tire liftoff sequence. Moreover, this test methodology produces an approximation of the rollover threshold value, in g's of lateral acceleration, which is always somewhat less than the actual rollover threshold level. The simulation, on the other hand, directly measures the peak level of lateral acceleration which the vehicle can tolerate without rolling over.

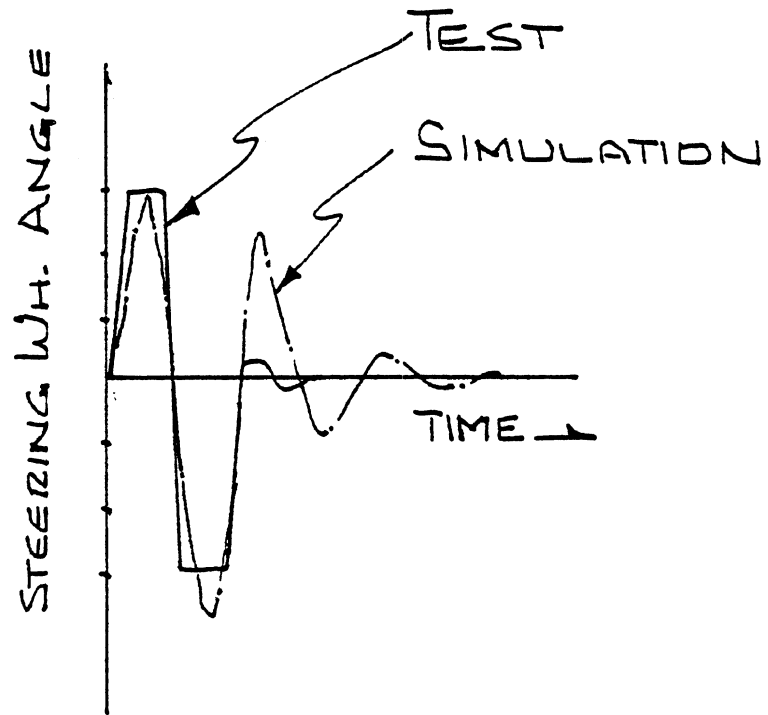


Figure 24. Distinctions between steer input time histories used in test vs. simulated study of emergency lane change-like maneuvers.

2.3.2 Comparison of Results. Test and simulation results can be directly compared in regard to the following categories of size and weight variation:

- Combined variations in axle loading and gross vehicle weight
- Payload c.g. height
- Partial loading
- Type of combination vehicle

Plots showing the corresponding results will be presented below, together with comments on the extent of the agreement indicated.

2.3.2.1 Combined axle and gross weight variations.

Stopping Distance - Shown in Figure 25 are stopping distance values representing test and simulation results for four differing vehicles. Note that for each vehicle, there is one baseline and one increased-load case. The simulation results reflect stopping distances from an initial speed of 55 mph (88 km/h) on both wet and dry pavements. The test data represent stopping distances from (a) 45 mph (72 km/h) on a dry pavement and (b) 25 mph (40 km/h) on a wetted pavement. Since the test conditions differ so greatly, the data are useful only for illustrating the trends (i.e., slopes) in the influence of the loading variables.

As was discussed in Section 2.2 and also in Volume I, the trend of the influence of increased loading on stopping distance can be either positive or negative, depending upon the torque capacities of the brake systems which are involved. The figure shows that essentially opposite trends were present in the simulated and test cases, although both data sets do include examples of both positive and negative slopes in the sensitivities to increased loading.

Moreover, the two data sets certainly do not agree, although the disagreement is seen as traceable to differences in the brake systems of the simulated and tested vehicles. It is known that both "types" of brake systems are realistic and do exist commonly in today's trucks. The

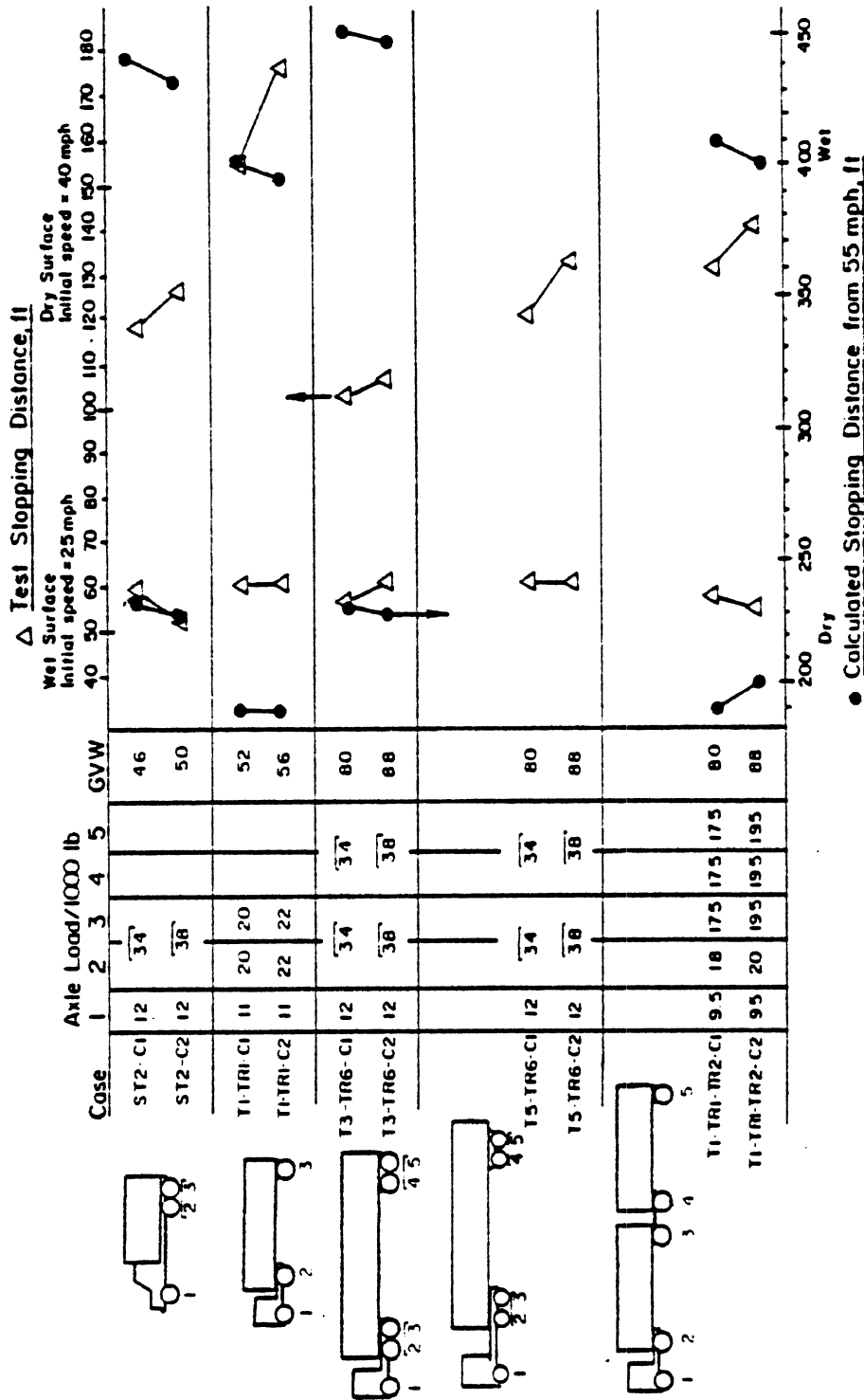


Figure 25. Influence of Variations in Axle Load and Gross Weight on Stopping Distance Performance

determination of which type (involving the proportioning of torques among axles and the overall levels of torque capacity at each axle) is more representative is beyond the scope of this project. One can certainly say that vehicles such as those represented by the test vehicles definitely exist in service and thus would exhibit longer stopping distances when loaded to increased levels of axle load or gross weight allowance. Further, such a result agrees completely with theoretical considerations, for vehicles having such braking systems.

Understeer Level - Shown in Figure 26 is a comparison of test and simulation measures of the influence of loading variables on understeer level. In both cases, the understeer measure is defined for a lateral acceleration level of 0.25 g's. We see, firstly, that the simulation results lie above the values found through testing (that is, at higher values of understeer level). This contrast is in line with the distinction in steering input procedure cited above. The ramp-type input of steering applied in the simulation causes the vehicle to exhibit a higher level of understeer. It is interesting to observe that the straight truck, ST2, shows understeer levels from simulation which are nearer to the test values than are those for the articulated vehicles. This feature is also in line with observations made in Reference [28]; namely, that a primary cause of the difference between the understeer levels obtained with tractor-semitrailers in a ramp-steer versus steady-turn condition derives from the lag in the response of the semitrailer. Since the straight truck includes no such lag mechanism, its ramp-steer and steady-state-derived understeer levels are more nearly the same.

With regard to trends, the influences of load changes on the understeer level are very similar in the test and simulation results. We see that all of the increased-load cases caused understeer level to decline with respect to the baseline condition. Listed below are the nominal decrements in understeer level obtained in the cited test and simulation cases.

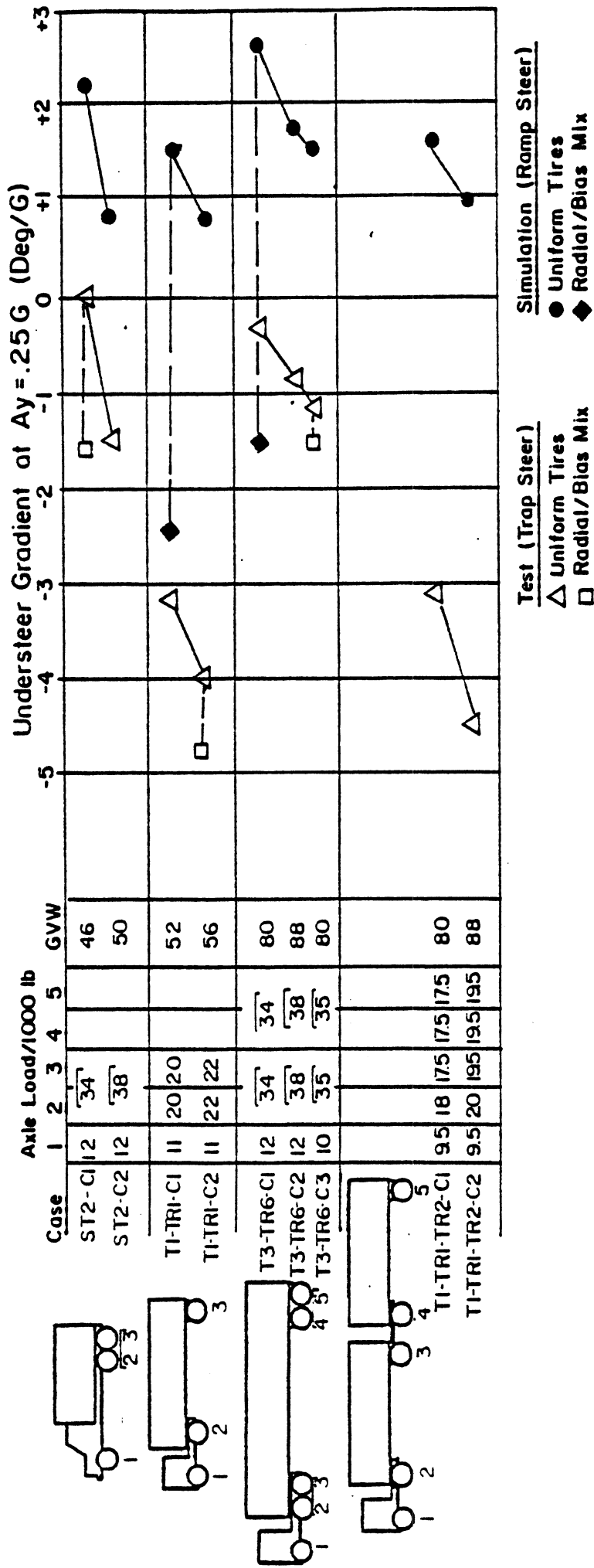


Figure 26. Influence of Variations in Axle Load and Gross Weight on Understeer Level

Vehicle	Condition Codes	Understeer Decrements, deg/g, Due to Increased Loading	
		Test	Simulation
Truck, ST2	C2 - C1	-1.5	-1.4
Tractor-Semi, T1-TR1	C2 - C1	-0.8	-0.7
Tractor-Semi, T3-TR6	C2 - C1	-0.5	-0.9
	C3 - C1	-0.8	-1.1
Double, T1-TR1-TR2	C2 - C1	-1.3	-0.6

The tabulated decrements show a remarkable degree of agreement between test and simulation results. Indeed, given all of the unknown properties of the test vehicles, the extent of this agreement seems rather coincidental. Nevertheless, the test and simulation data quite reasonably confirm that increased loading, and particularly rear-biasing of axle load distribution, cause distinct reductions in the understeer levels of heavy vehicles.

Also in Figure 26 one notes that the decrement in understeer level accompanying the radial/bias tire mix cases are very different in the simulation and test results. The simulated cases are seen to produce decrements on the order of 4 deg/g due to the tire mix condition, while the test cases yield decrements from 0.4 to 1.6 deg/g. As discussed above, this difference in results is attributed to the great difference in the actual tire properties which prevailed in the test and simulated cases. While the simulated tire mix condition involved a large spread in effective cornering stiffnesses on the front and rear axles of the vehicles involved, the test vehicles actually achieved only a small spread in tire properties as a result of test-induced treadwear on the rear-mounted bias-ply tires.

Rollover Threshold - Shown in Figure 27 are the rollover threshold values obtained through simulation and test at various loading conditions. The figure shows that increased loading resulted in a decreased rollover threshold in all test and simulation data. We see also that:

- a) The test values of rollover threshold always lie above the values obtained in simulation—reflecting the substantially

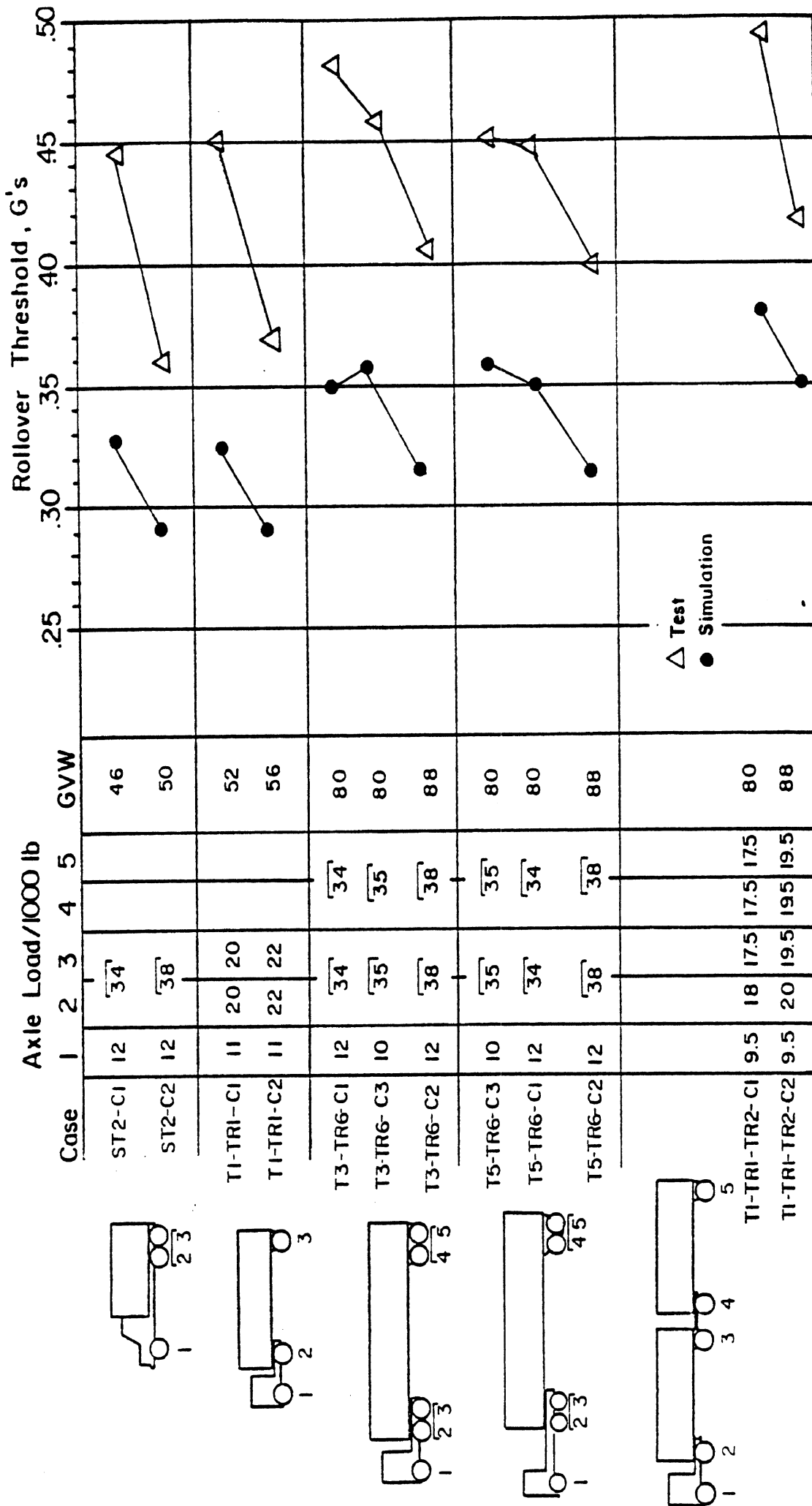


Figure 27. Influence of Variations in Axle Load and Gross Weight on Rollover Threshold

lower values of payload c.g. height employed in the test vehicles, as was discussed above.

- b) The incremental reductions in rollover threshold deriving from the increased load states are generally larger in the test cases than in the simulated results—again reflecting the greater incremental change in payload c.g. height employed in conjunction with the increased load level in the test cases (viz., a 9-inch (23-cm) increase in the test cases versus a 5-inch (13-cm) increase in the simulation).

Listed below are the decrements in rollover threshold observed due to loading in the test and simulated cases.

Vehicle	Cases	Rollover Threshold Decrement Due to Increased Loading, g's	
		Test	Simulation
Truck, ST2	C2 - C1	-.085	-.035
Tractor-Semi, T1-TR1	C2 - C1	-.080	-.035
Tractor-Semi, T3-TR6	C2 - C1	-.075	-.035
	C3 - C1	-.020	+.010
Tractor-Semi, T5-TR6	C2 - C1	-.050	-.035
	C3 - C1	-.010	-.020
Double, T1-TR1-TR2	C2 - C1	-.075	-.035

Over all of the entries above citing changes in loading level, namely, cases C2 - C1, the decrement in rollover threshold measured in full-scale tests is an average of 2.08 times the decrement observed through simulation. These decrements derive primarily from the increase in payload c.g. heights which accompany the increased loading condition. If we ratio the payload c.g. heights prevailing in the C2 versus C1 conditions, we see that the test vehicle payloads increased in height by $9/70 = .13$ while the payload c.g. heights in the simulated vehicles increased by $5/83 = .06$. That is, the

test vehicles experienced increases in payload c.g. height which were greater by a factor of 2.13 than those incurred in the corresponding simulation cases. Accordingly, the observed value of 2.08 which was cited above as the contrast in test versus simulated decrements in rollover threshold is seen to compare very favorably with the 2.13 difference in the corresponding changes in payload c.g. height.

Rearward Amplification - The doubles configuration, T1-TR1-TR2, was tested with gross weight levels of 80,000 and 88,000 lbs (36.3 and 39.9 m tons). In Section 2.2, the rearward amplification level measured in these two test cases was reported to be virtually identical—indicating that a 10% change in the gross weight on such vehicles has a negligible influence on rearward amplification. In Volume I, a set of simulations was reported in which gross weight variations had been made on the same type of conventional double. Amplification ratio was seen to change in these simulation cases by approximately 3% as a result of the gross weight change from 80,000 to 88,000 lbs (36.3 to 39.9 m tons).

Thus, simulation and test data confirm that modest increases in gross weight do not have a significant influence upon the rearward amplification behavior of vehicles of this type. Theoretical considerations suggest that this finding should apply rather broadly to other conventional multiple-trailer configurations, as well.

2.3.2.2 Variations in payload c.g. height. Very limited samples of data are available comparing the influence of payload c.g. height variations on dynamic behavior. Test cases employing c.g. height variations, alone—without accompanying changes in load level—included only one tractor-semitrailer and one straight truck. Simulation cases included only the tractor-semitrailer and the conventional doubles configuration. Thus, the only overlap between test and simulation cases showing the influence of payload c.g. height are those involving tractor-semitrailer combinations.

Stopping Distance - Shown in Figure 28 are the stopping distances obtained in the test and simulation cases for 70 and 95 inches (178 and 241 cm) values of payload c.g. height. Both of these cases were examined at the payload weight condition yielding a gross weight level of 80,000 lbs (36.3 m tons). Again, note that the very different pavement and speed conditions involved result in gross differences in the absolute level of stopping distances achieved. We see that stopping distances increase in both the test and simulation cases with increased height of the payload center of gravity. Of course, as stated earlier, the different nature of the respective braking systems on the test and simulated vehicles makes quantitative comparison unwarranted. Nevertheless, since the test vehicle was capable of locking the trailer wheels on the wet surface in the "low c.g." condition, it was certainly expected that stopping distance would increase when the payload c.g. is raised—as the simulated cases also indicate.

Understeer Level - Shown in Figure 29 are test and simulation results showing the influence of payload c.g. height on the understeer level. We see that the elevated c.g. case causes a decline in understeer level in both cases, although the reduction is approximately three times as great in the case of the test results (at a gross weight level of 80,000 lbs (36.3 m tons)). Since a large number of steering, suspension, and tire properties can influence this particular sensitivity function, the minimal definition of the test vehicle's parameters leaves little basis for commenting upon the difference observed here.

Rollover Threshold - Shown in Figure 30 are values of rollover threshold obtained in three cases of test and simulated response. The same two cases cited above are augmented with another case involving an elevated payload which gives a gross weight level of 88,000 lbs (39.9 m tons). (This latter condition was also examined for understeer behavior but was discarded because the understeer measure was invalidated by the impending rollover condition accruing in the vicinity of the 0.25 g level of lateral acceleration at which the understeer measure is defined.)

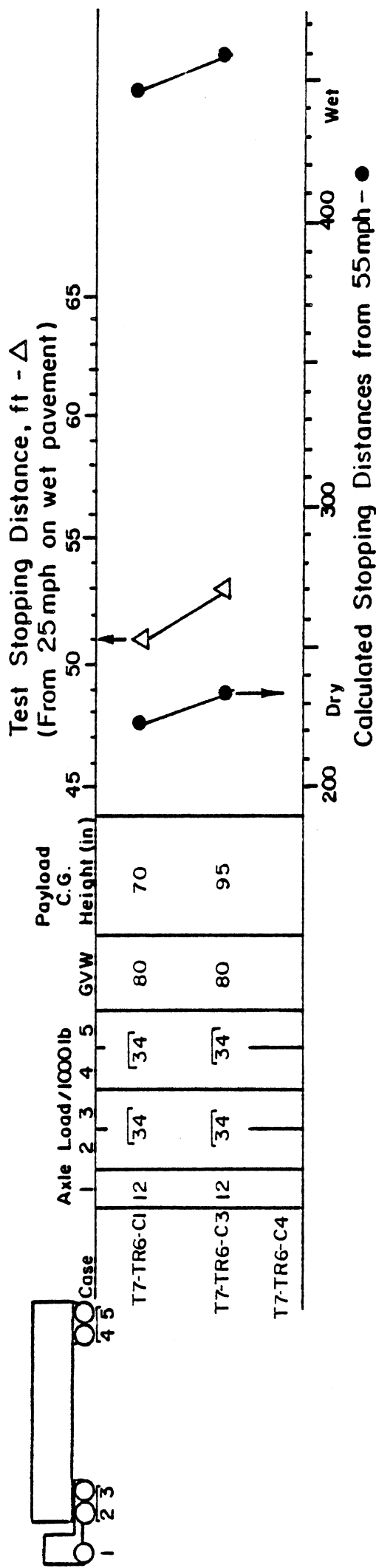


Figure 28. Influence of Payload C.G. Height on Stopping Distance

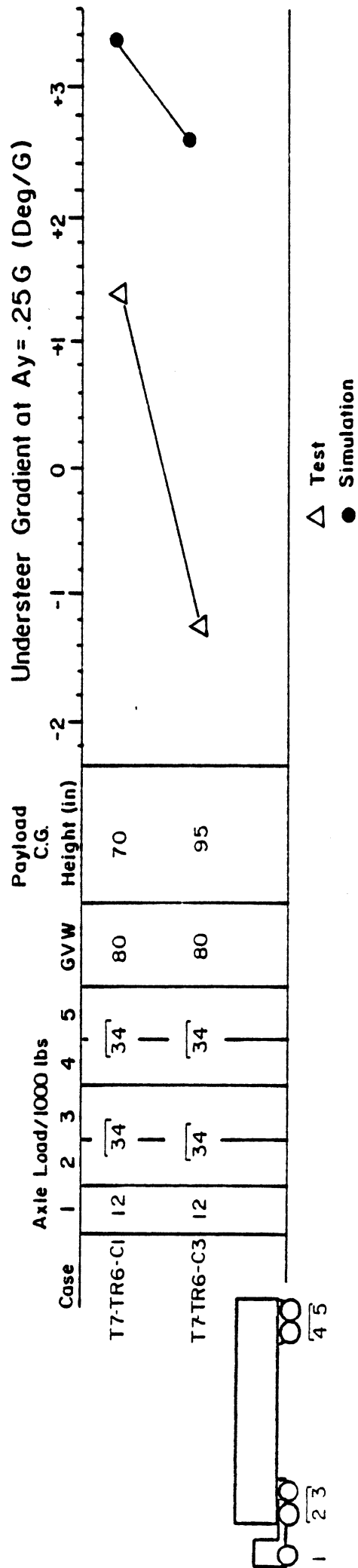
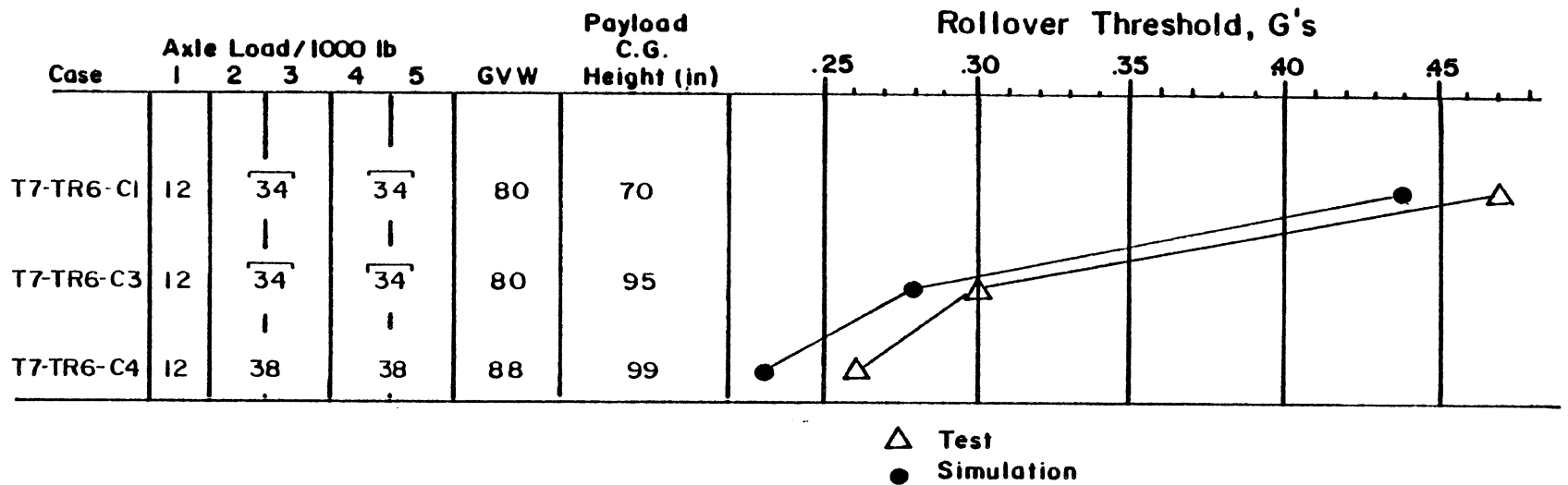
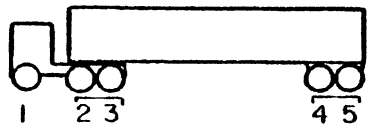


Figure 29. Influence of Payload C.G. Height on Understeer Level



08

Figure 30. Influence of Payload C.G. Height on Rollover Threshold

We see that very good agreement is obtained between the test and simulation results—suggesting that when identical payload c.g. placements and loading values are considered, the T7-TR6 test vehicle and the simulated five-axle tractor-semitrailer behave very similarly in their roll response. This result depends upon a reasonable match in the roll-related properties of the respective suspensions, especially those installed at the rear of the tractor and on the semitrailer axles.

2.3.2.3 Partial loading. Only one set of corresponding test and simulation data are available which speak to the influence of partial loading on vehicle response. Shown in Figure 31 are results presenting the influence of the examined partial load case on stopping distance. Again, the differences in absolute value stem from distinctions in speed and surface conditions. The figure shows that the removal of half of the payload from the rear of the semitrailer causes the stopping distances to increase in all cases, although the simulated vehicle exhibited a much greater sensitivity to this loading change than did the test vehicle. The differences in sensitivity can certainly be attributed in part to the more aggressive brake systems involved in the simulated cases, by which the more lightly loaded trailer axles are prematurely locked in the partial load case. Nevertheless, the very low level of sensitivity seen in the test data was not anticipated and cannot be explained in any deterministic way. Apparently, the brakes on the crucial trailer axle locations produced sufficiently low levels of brake torque that the half-load case did not incite wheel locking at the much lower level of deceleration that was expected.

2.3.2.4 Type of multiple-trailer combinations. Differing types of multiple-trailer combinations were of interest in the test matrix primarily in terms of the rearward amplification behavior exhibited. Although braking test data were also presented in Section 2.2, the corresponding simulations were not produced.

Shown in Figure 32 are rearward amplification values obtained through test and simulation. The figure shows three sets of rearward amplification values for each of six vehicle combinations. The vehicles are ranked on the

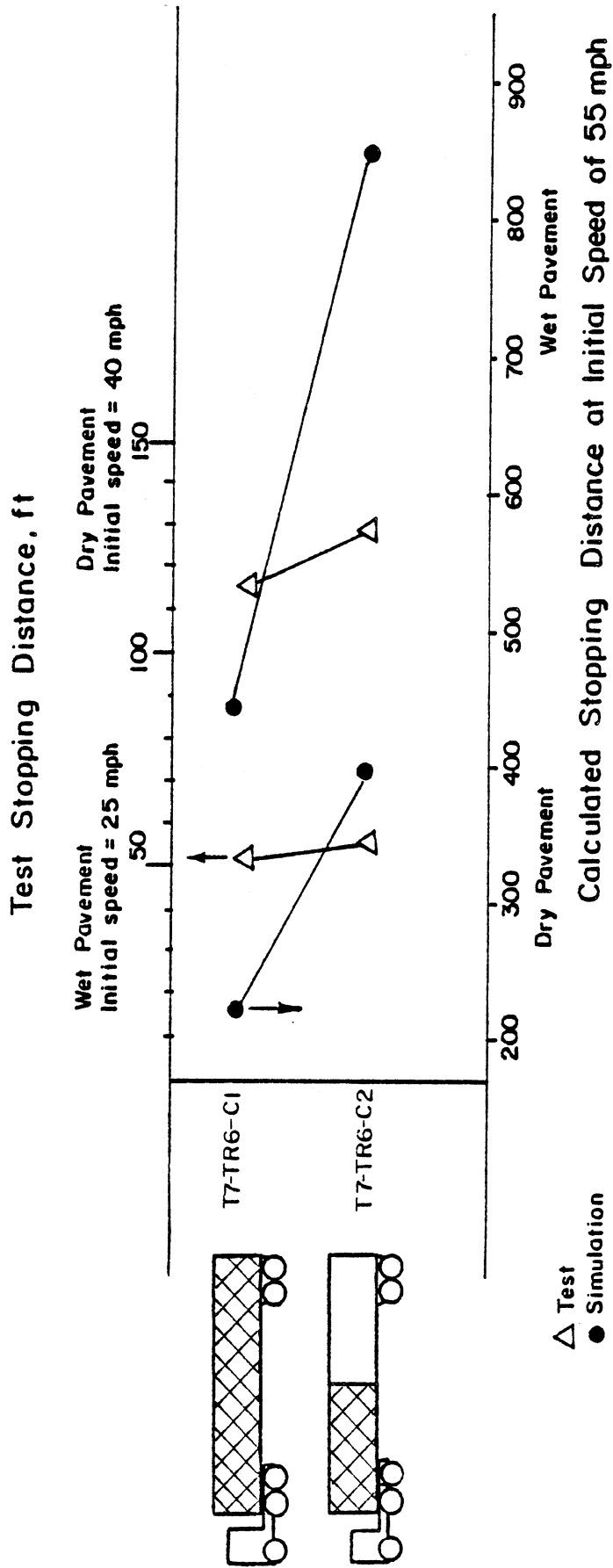


Figure 31. Influence of Partial Loading on Stopping Distance Performance

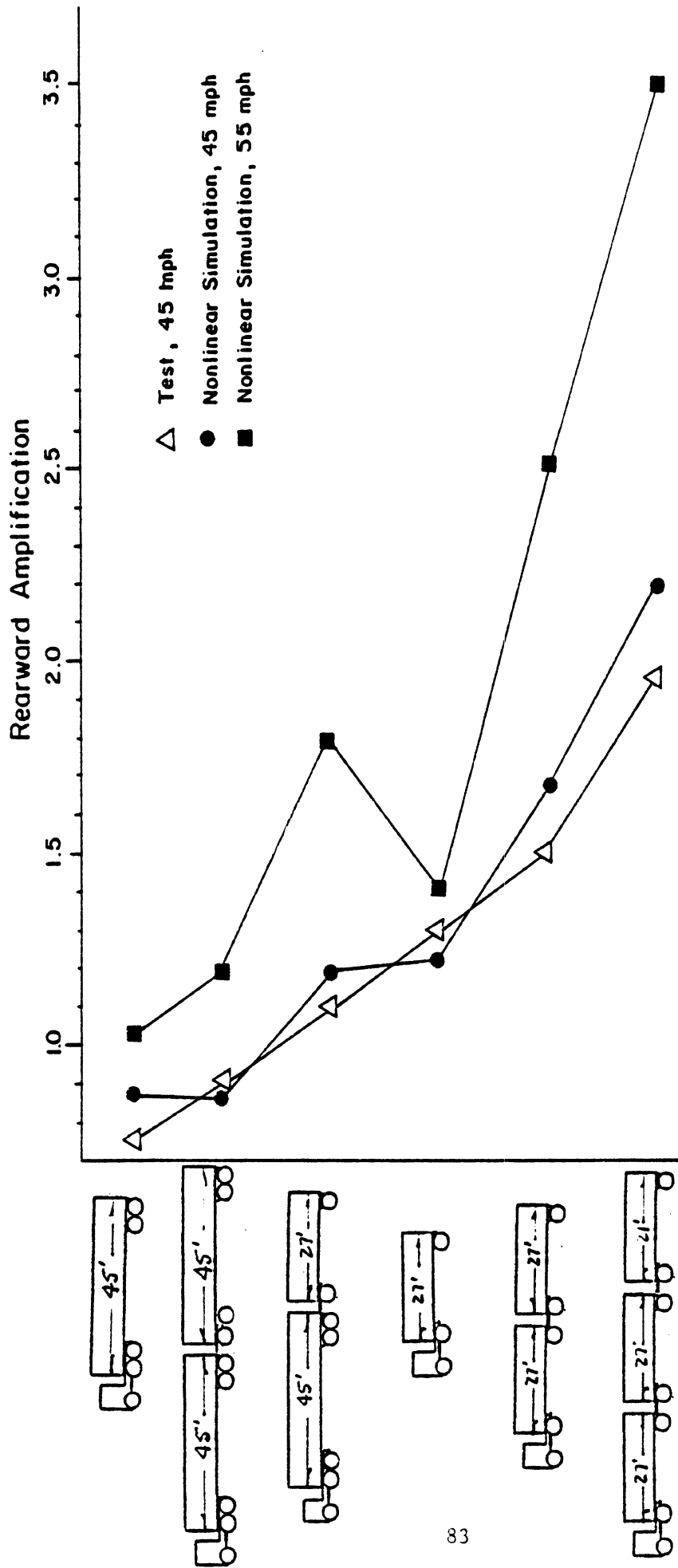


Figure 32. Influence of Combination Type on Rearward Amplification (at 45 mph)

figure from the lowest to highest level of rearward amplification measured in full-scale tests. The test procedure which was employed in producing these amplification values involved one cycle of a steering waveform approximating a sine wave, with the vehicle traveling at 45 mph (72 km/h). The simulation results exhibiting the highest values of amplification ratio were obtained in an obstacle-avoidance maneuver which was run at a simulated speed of 55 mph (88 km/h). These basic maneuver conditions were discussed earlier.

We see that the amplification ratios obtained from these calculations register considerably higher than the values measured in the similar test runs made at 45 mph (72 km/h). The distinctions shown in the figure between the test data at 45 mph (72 km/h) and the simulated results at 55 mph (88 km/h) are not surprising, however. In fact, the basic observation that amplification ratio goes up dramatically with vehicle speed is well known and has been documented by various researchers (e.g., [5,37]). In order to more easily assess the agreement between the test and simulation methods in regard to this measure, however, an additional set of simulations was run using a speed condition which matched the test speed of 45 mph (72 km/h). This extra simulation effort which attempted to match the test conditions was thought to be warranted here because it is known that the rearward amplification behavior is primarily sensitive to length parameters which could be accurately matched between test and simulated cases.

The simulation results obtained at a speed of 45 mph (72 km/h) are seen to agree rather well with the test results. In the case of the triple, the actual agreement is slightly better than indicated since the test runs on this vehicle were conducted at a speed of approximately 43 mph (69 km/h) rather than the target value of 45 mph (72 km/h) as a result of an inability to reach the target speed in the distances available.

Moreover, the simulation results are seen to be reasonably confirmed by the test measurements which were made on the six vehicle combinations shown.

CHAPTER 3

ANALYTICAL METHODS

In Volume I of this report, a broad set of findings concerning the influence of size and weight variables on the stability and control of heavy vehicles was presented. These findings were based essentially upon the results of simulation activities conducted during the project. A variety of simulation models were employed in conducting these analyses. In this chapter, these simulation models will be identified and the basic schemes for representing the vehicle will be discussed. In the cases in which the simulation model existed prior to its application in this research effort, the model is only briefly introduced and the reader is referred to published documents for a more complete presentation of the basic formulation. Simplified models which were developed in the course of this study are outlined in more detail.

The models will each be discussed in turn, beginning with those which had been developed previously.

3.1 Previously-Developed Models

The study made use of four simulation models which had been developed at The University of Michigan's Transportation Research Institute for the analysis of the dynamic behavior of heavy vehicles. These models are the following:

- Linear Yaw Plane Model (documented in Reference [16])
- Static Roll Model (documented in Reference [17])
- Yaw/Roll Model (documented in Reference [18])
- Comprehensive Braking and Handling Model - Phase IV (documented in Reference [19])

Each model was employed to perform a different portion of the investigation. The respective tasks performed with each model will be identified below, together with a brief outline of the features of the mathematical formulation.

3.1.1 Linear Yaw Plane Model. This model was employed for evaluating the rearward amplification of multiple-unit vehicle combinations in those cases in which a load bias existed such that the front- and rear-located tires were not being loaded uniformly. In general, the model provides for evaluation of the dynamic yaw response of vehicle combinations having up to four individual units, such as in a conventional doubles configuration. The model has the following features and assumptions:

- 1) The model represents the vehicle by a system of linear equations representing the directional dynamics of articulated vehicles which are assumed to behave as rigid bodies in the horizontal plane.
- 2) The degrees of freedom are limited to the lateral velocity and yaw rate of the tractor, and the articulation motions in the horizontal plane of each of the various elements of the vehicle combination.
- 3) The cornering forces and aligning moments generated at the tire-road interface are assumed to be linear functions of the sideslip angle of the tire.
- 4) Articulation angles are small such that small-angle approximations apply.
- 5) The surface is assumed to have uniform frictional properties.
- 6) Braking and tractive forces of the tire are assumed to be negligible.
- 7) Pitch and roll motions of the sprung mass are neglected.
- 8) All joints are assumed to be frictionless and articulation of these joints takes place about vertical axes.

- 9) Steering input is assumed to be applied directly to the front wheels, with no "steering system" interaction.
- 10) Gyroscopic forces due to rotating wheels are neglected.

The model was employed in this study at a fixed value of forward velocity, with a sinusoidal steering input applied in an examination of the relative amplitudes of the lateral acceleration responses at the tractor and at each of the vehicle's elements along the combination. The results represent first-order estimates of rearward amplification behavior. The principal shortcomings of the model arise when the maneuver severity causes tire slip angles to become large (say, greater than 3-4 degrees) and when the lateral acceleration condition causes large changes in the vertical loads being borne on left- and right-side tires.

3.1.2 Static Roll Model. The static roll model provides for a nonlinear treatment of the rolling motion of a vehicle comprised of a maximum of three "lumped" suspension systems. In its basic formulation, the model was constructed to represent the roll behavior of tractor-semitrailers in which the tractor steering axle, the tractor rear axle(s), and the trailer axle(s) constituted the three lumped suspension assemblies. The model is employed to evaluate the static rollover threshold—that is, the value of steady lateral acceleration beyond which the vehicle suffers a divergent roll response.

In this model, the vehicle is assumed to constitute rigid bodies except that the tractor is split into two rigid elements connected by a torsional spring which represents the central section of the vehicle's frame. This centrally-located frame section is assigned a torsional spring rate and provides for a roll moment to be transmitted between the cab section of the tractor and the fifth wheel and rear suspension section. Also, a torsional compliance parameter reflecting the combined compliance of the fifth wheel connection and the attached semitrailer is represented.

Additional features and assumptions of this model are as follows:

- 1) The articulation angles are small so that the effect of articulation angle on the rollover threshold can be neglected.

2) The relative roll motion between the sprung mass and the axles is assumed to take place about roll centers which are at fixed distances beneath the sprung mass. The suspension springs are assumed to remain perpendicular to the axle centers and to transmit only compressive or tensile forces. Further, all axle forces which act along the axle centerline are assumed to act through the roll center.

3) Suspension nonlinearities such as backlash and progressively hardening suspension springs are represented by a tabular load-deflection input format. The suspension forces and the spring rates at any given deflection are then compared by linear interpolation.

4) The total vertical load carried by each composite axle is assumed to remain constant during the rollover process. In order to accommodate any pitching motion that might take place during rollover, the sprung mass is permitted to take up different vertical deflections at each of the three axle locations.

5) The vertical load carried by the tires is assumed to act through the midpoint of the tread width. The effect of camber angle and the effect of the lateral compliance of the tire tend to have opposing effects on the lateral translation of the centroid of the normal pressure distribution at the tire-road interface. Since these effects are small and tend to cancel out, the lateral translation of the normal load reaction in the tire is neglected.

6) The roll angles of the sprung mass and the axles are small, such that the small angle assumptions apply. In this study, all rollover threshold values were calculated using the static roll model except for those cases involving laterally-offset payloads.

3.1.3 Yaw/Roll Model. The Yaw/Roll Model is a time-domain mathematical simulation capable of simulating the yaw/roll response of multiple-articulated vehicles. The model was formulated for the purpose of analyzing the combined directional and roll behavior of trucks, tractor-semitrailers, and doubles combinations during dynamic maneuvers which approach the rollover limit. The model is limited to a maximum of four vehicle units and 11 axles,

and the axles can be distributed as desired among the vehicle units. Vehicles equipped with a variety of hitching mechanisms can also be studied by making simple modifications to the computer code.

The equations of motion of the vehicle are formulated by treating each of the sprung masses as a rigid body with five degrees of freedom, namely: lateral, vertical, yaw, roll, and pitch. The longitudinal degree of freedom is not included, since the forward velocity of the lead unit (or tractor) is assumed to remain constant during the maneuver. The axles are treated as beam axles which can roll and bounce with respect to the sprung masses to which they are attached. The total number of degrees of freedom, N_d , of a multiple-articulated vehicle with N_s sprung masses and N_a axles is therefore given by the expression: $N_d = 5N_s + 2N_a$.

The simplifying assumptions made in the process of deriving the equations and the essential features of the model are given below:

- 1) The vehicle is assumed to travel on a horizontal surface with uniform friction characteristics.
- 2) The pitch motion of the sprung masses are assumed to be small such that the small angle approximations hold true.
- 3) The relative roll angle between the sprung masses and the axles are assumed to be small so that the same approximations may be applied to the roll deflections between the sprung and unsprung masses.
- 4) The relative roll motion between the sprung and unsprung masses is assumed to take place about a roll center which is at a fixed height beneath the sprung mass. In order to simplify the equations, the suspension springs are assumed to remain perpendicular to the axle centers and to transmit only compressive or tensile forces. Further, all axle forces which act along the axle centerline are assumed to act through the roll center. When a relative roll motion takes place between the sprung mass and the axles of a leaf-spring-type suspension, the leaf springs tend to be twisted in the roll plane and hence produce an additional roll-resisting moment. This effect is represented in the model by an auxiliary roll stiffness parameter.

5) Suspension nonlinearities such as backlash are represented by using a tabular load-deflection input format.

6) The model permits the simulation of vehicles equipped with a wide variety of hitching mechanisms. The equations are formulated such that the equations of motion are independent of the constraint equations. Hence, the vehicles equipped with any given hitching mechanism can be analyzed by simply altering the constraint equations.

7) The nonlinear cornering force and aligning torque characteristics of the tires are represented as tabular functions. The tire forces and moments are computed by a double table look-up for the given vertical load and sideslip angle.

8) The forces acting on each axle are treated independently, i.e., no interaxle load transfer effects are incorporated in the model.

9) Simulations can be performed in the closed-loop or open-loop modes. In the open-loop mode, the time history of the steering input is provided as input to the model. In the closed-loop mode, the trajectory to be followed by the vehicle is specified and the "driver model" computes the steering input that is necessary to accomplish the maneuver. In this study, the model was used in the open-loop mode to study vehicle response to trapezoidal steering input and in the closed-loop mode to examine rearward amplification occurring when the "driver" steered the vehicle to clear a fixed-width obstacle.

3.1.4 Comprehensive Braking and Handling Model (Phase IV). The Phase IV program is a time-domain mathematical simulation of a truck/tractor, a semitrailer, and up to two full trailers. The vehicles are represented by differential equations derived from Newtonian mechanics that are solved for successive time increments by digital integration.

The program is written in a generalized fashion to allow simulation of a large number of vehicle configurations. The first vehicle is the power unit and may be a truck or tractor, both of which may carry payload. As a single unit with no payload, the vehicle is equivalent to an empty truck or bobtail tractor. With payload, it is a truck, which, with a semitrailer as well,

simulates a car hauler, dromedary tractor, etc. The second unit is always a semitrailer (i.e., the current version of this model does not include a truck with full trailer). The third and fourth units are full trailers consisting of semitrailers on either a fixed or converter dolly. Separate payload may be specified for each trailer.

The truck/tractor unit is distinguished by the fact that it can have only a single front axle with single tires, and can be arbitrarily steered. All other axles on the vehicle combination can be represented as single or tandem axles with single or dual wheel sets.

The mathematical model incorporates up to 71 degrees of freedom. The number of degrees of freedom are dependent on the vehicle configuration and derive from the following:

- Six degrees of freedom (three translational and three rotational) for the truck/tractor sprung mass
- Three degrees of freedom for the semitrailer (the three other degrees of freedom of the semitrailer are effectively eliminated by dynamic constraints at the hitch)
- Five degrees of freedom for each of the two full trailers allowed
- Two degrees of freedom (vertical and roll) for each of the 13 axles allowed
- A wheel rotational degree of freedom for each of the 26 wheels allowed.

The motion of each of the sprung masses is determined from the summation of forces and moments upon it arising from the tires (acting through the unsprung mass of the axle and suspension), gravity, and the hitch point constraints. Small angle assumptions are made in the implementation of the mathematical equations so that the simulation can be validly applied up to a maneuver limit at which wheel lift-off occurs.

The Phase IV model includes the basic features of the so-called T3DRS:V1 model which was reported to the Federal Highway Administration in Reference [20]. Perhaps the comprehensiveness of the Phase IV model can be best described by outlining the types of vehicles and performance characteristics which can be studied. The model can be used, for example, to simulate the following vehicle configurations:

Straight truck, empty and loaded

Bobtail tractor

Tractor-semitrailer (3 to 5 axles), empty and loaded

Tractor-semitrailer-full trailer (5 to 9 axles), empty and loaded

Tractor-semitrailer-full trailer-full trailer (7 to 13 axles), empty and loaded

For simulation of braking performance, the program incorporates state-of-the-art representation of truck air brake systems, antilock wheel control systems, and tire-road friction models. Typical examples of braking studies for which it can be or has been used are:

- 1) Stopping distance performance
- 2) Effects of brake timing
- 3) Dynamic behavior in braking
- 4) Comparisons of antilock wheel control logic
- 5) Influence of tire-road friction coupling
- 6) Split friction surfaces
- 7) Brake proportioning
- 8) Tandem-axle effects on braking limits

For simulation of cornering performance behavior, the program incorporates state-of-the-art representations of truck tire lateral force characteristics (with roll-off effects during combined braking), and vehicle suspension properties of significance to cornering behavior. Typical examples of studies involving cornering are as follows:

- 1) Understeer/oversteer properties of commercial vehicles
- 2) Determining cornering limits
- 3) Assessing tandem-axle effects on cornering
- 4) Jackknife prediction
- 5) Effects of suspension properties on cornering and cornering limits
- 6) Accident simulation

In addition to the above, the program can be operated open-loop (defined steer angle inputs) or closed-loop (defined path input), and on roads of specified grade or cross-slope.

The Phase IV program is uniquely applicable in directional response studies in which the influence of the following items are to be considered in detail:

- 1) Spring force/deflection characteristics (hysteresis and free-play)
- 2) Brake "fade"—brake temperature
- 3) Brake hysteresis
- 4) Load-leveler action in tandem suspensions
- 5) Brake proportioning algorithms
- 6) Steering system compliance (inputs at the steering wheel)
- 7) Frame torsional stiffness

In this study, the Phase IV program was employed only in a limited capacity. The one special application involved evaluation of the dynamics of tractor jackknife during braking in a turn.

3.2 Simplified Method of Analyzing Vehicle Braking Performance

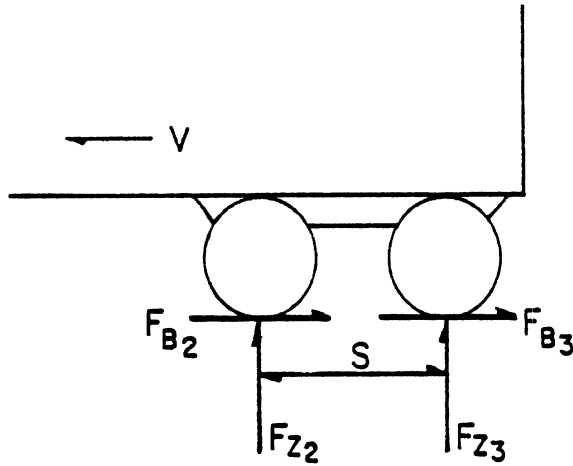
A simplified method of calculating braking performance was derived in order to provide a means of obtaining a first-order estimate of the stopping distance behavior of a great number of vehicles under differing size and weight constraints. This method for analyzing braking performance assumes that the vehicle is making a constant deceleration stop. The input to the calculation is the level of braking, F_{Bi} , occurring at each axle of the vehicle. In this study fixed proportioning, typical of that employed in current vehicles, has been used. For fixed proportioning, the braking forces, F_{Bi} , are calculated for pressures ranging from 10 to 100 psi in increments of 10 psi.

The response to the applied braking forces is described in terms of the longitudinal deceleration, \ddot{X} , and the vertical loads, F_{zi} , carried by each axle. These quantities are found by solving the equations of motion pertaining to each unit of the combination vehicle during a constant deceleration stop.

In this simplified analysis, the influence of vertical load on tire-road friction is not considered. Further, for each level of braking input, the "minimum" value of friction needed to avoid wheel lockup is determined. Under the assumptions of this analysis, the wheels on the axle with the largest ratio of F_{Bi} to F_{zi} will lock up first. That is, the maximum ratio of F_{Bi}/F_{zi} represents the friction coefficient, μ_p , required to perform a wheels-unlocked stop at the calculated level of deceleration, \ddot{X} .

The formulation of the equations of motion is a straightforward process except for the treatment of tandem suspensions having inter-axle load transfer. The method used to represent inter-axle load transfer depends upon a special parameter, $P_{i+1,i}$, that is used to describe the load transfer between the i^{th} and $i+1^{\text{st}}$ axles in a tandem pair (see Figure 33). This parameter not only describes the amount of load transfer, but also the pitch moment reacted by the sprung mass (see Figure 33).

Having adapted a means for treating tandem suspensions, the same general approach is used in formulating the equations of motion for all of



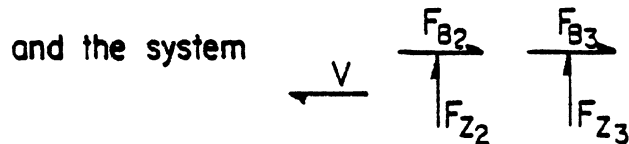
Notes:

- 1) For a walking beam the load on the front is increased, ie. $P_{i+1,i} > 0$.
- 2) For a 4 spring: $P_{i+1,i} < 0$.

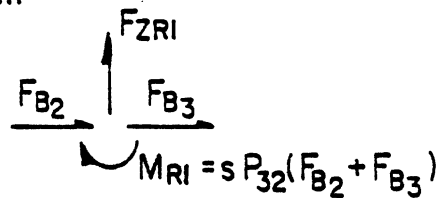
$$F_{Z2} = \frac{F_{ZRI}}{2} + P_{32}(F_{B2} + F_{B3})$$

$$F_{Z3} = \frac{F_{ZRI}}{2} - P_{32}(F_{B2} + F_{B3})$$

where $F_{ZRI} = F_{Z2} + F_{Z3}$



is replaced by this system



The term $sP_{32}(F_{B2} + F_{B3})$ needs to be added to the appropriate pitch moment equation.

Figure 33. Approximate Representation of Interaxle Load Transfer.

the combination vehicles studied in this project. The general approach will be illustrated here by developing the equations of motion for a five-axle tractor-semitrailer. The parameters and variables used in the equations are presented in Figure 34. Free-body diagrams for the tractor and semitrailer are developed as shown in the figure. First, the longitudinal acceleration of the total vehicle is determined (see Eq. (1)). Then longitudinal, pitch, and vertical equations describing a constant deceleration stop are formulated for the last unit (in this case, the semitrailer). See Equations (2) through (4). Then the pitch and vertical equations ((5) and (6)) are written for the tractor. Finally, expressions ((7)-(10)) for inter-axle load transfer are included. Note that Equations (1) through (10) are a simultaneous set of linear algebraic equations that can be solved sequentially (using the results from the previous equation to solve the next one).

Equations (1) through (10) may be expressed in vector matrix notation as follows:

$$[A] \vec{X} = [B] \vec{F} + \vec{C} = \vec{D} \quad (11)$$

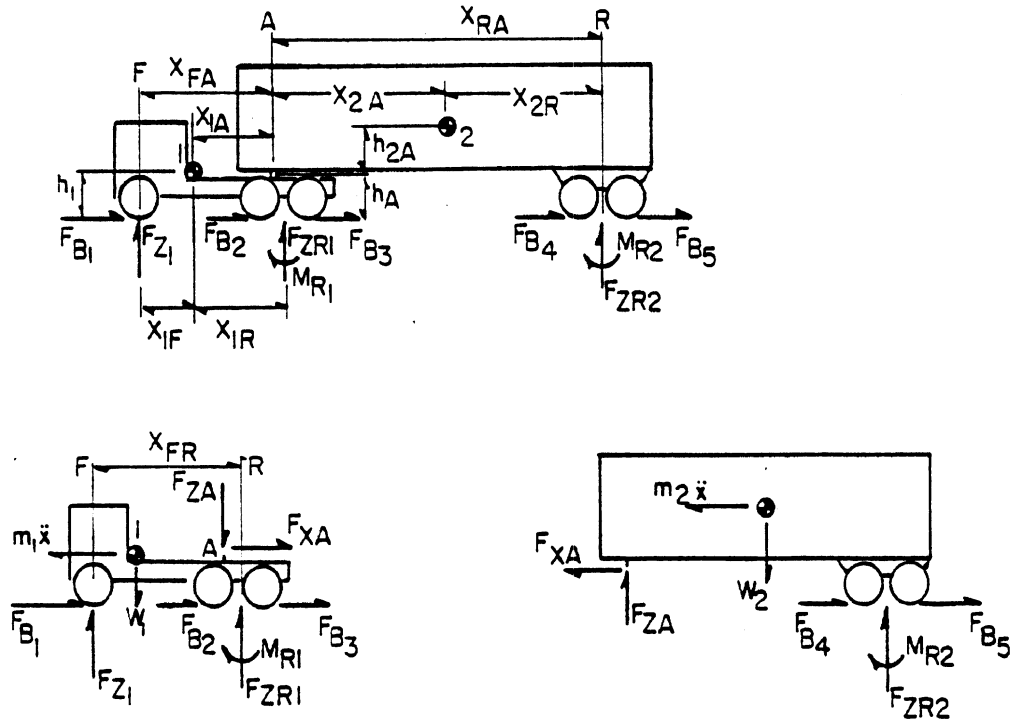
where

$$\left. \begin{array}{l} [A] = \\ \vec{X} = \\ [B] = \\ \vec{F} = \\ \vec{C} = \end{array} \right\} \begin{array}{l} \text{This equation is shown in} \\ \text{complete form in Figure 35} \end{array}$$

The solution to (11) is

$$\vec{X} = [A]^{-1} \vec{D} \quad (12)$$

In this study, the arrays [A], [B], and \vec{C} were entered into a digital computer program that solves for \vec{X} . Then the quantities F_{Bi}/F_{zi} are calculated and printed out along with \vec{X} (XDD) for various levels of pressure. (see Table 3).



A) Longitudinal equations

$$(m_1 + m_2) \ddot{x} = F_{B1} + F_{B2} + F_{B3} + F_{B4} + F_{B5} \quad (1)$$

$$m_2 \ddot{x} + F_{XA} = F_{B4} + F_{B5} \quad (2)$$

B) Semitrailer pitch about the 5th wheel and vertical equations

$$m_2 \ddot{x} h_{2A} + F_{ZR2} X_{RA} + h_A (F_{B4} + F_{B5}) - X_{2A} W_2 - M_{R2} = 0 \quad (3)$$

$$F_{ZA} + F_{ZR2} = W_2 \quad (= s_{54} P_{54} (F_{B4} + F_{B5})) \quad (4)$$

C) Tractor pitch about front tire/road contact and vertical equations

$$m_1 \ddot{x} h_1 + F_{ZR1} X_{FR} - F_{ZA} X_{FA} - F_{XA} h_A - W_1 X_{IF} - M_{R1} = 0 \quad (5)$$

$$F_{Z1} - W_1 + F_{ZR1} - F_{ZA} = 0 \quad (= s_{32} P_{32} (F_{B2} + F_{B3})) \quad (6)$$

D) Interaxle load transfer

$$F_{Z2} = \frac{F_{ZR1}}{2} + P_{32} (F_{B2} + F_{B3}) \quad (7)$$

$$F_{Z3} = \frac{F_{ZR1}}{2} - P_{32} (F_{B2} + F_{B3}) \quad (8)$$

$$F_{Z4} = \frac{F_{ZR2}}{2} + P_{54} (F_{B4} + F_{B5}) \quad (9)$$

$$F_{Z5} = \frac{F_{ZR2}}{2} - P_{54} (F_{B4} + F_{B5}) \quad (10)$$

Figure 34. Example: 5-Axle Semi, 2 Tandem Sets

STRAIGHT BRAKE PROGRAM - 5 AXLE TRACTOR-SEMITRAILER

TEST : TEST RUN - GVM:A6

TRACTOR GVM : 15500.00 STATIC LOADS : 12000.00 18000.00 18000.00
 TRAILER GVM : 68500.00 STATIC LOADS : 18000.00 18000.00 18000.00

BRAKE PRES	XDD (G)	FB1/FZ1	FB2/FZ2	FB3/FZ3	FB4/FZ4	FB5/FZ5
10.00	0.0286	0.0280	0.0268	0.0268	0.0307	0.0307
20.00	0.1241	0.1089	0.1177	0.1177	0.1366	0.1366
30.00	0.2195	0.1750	0.2113	0.2113	0.2479	0.2479
40.00	0.3150	0.2300	0.3078	0.3078	0.3651	0.3651
50.00	0.4104	0.2764	0.4072	0.4072	0.4888	0.4888
60.00	0.5059	0.3161	0.5097	0.5097	0.6194	0.6194
70.00	0.6013	0.3505	0.6155	0.6155	0.7576	0.7576
80.00	0.6968	0.3805	0.7246	0.7246	0.9040	0.9040
90.00	0.7922	0.4070	0.8373	0.8373	1.0595	1.0595
100.00	0.8877	0.4305	0.9538	0.9538	1.2247	1.2247

Table 3. Example Printout of Results from Simplified Braking Program.

Using the process described above, comparable models were developed for the following vehicles:

- two-axle straight truck
- three-axle straight truck
- three-axle tractor-semitrailer (2-S1)
- four-axle tractor-semitrailer (2-S2)
- five-axle tractor-semitrailer (3-S2)
- five-axle double (2-S1-2)
- seven-axle triple (2-S1-2-2)

In all of the cases involving full trailers, the dollies were converted dollies. The equations for these dollies are similar to those for a semitrailer.

3.3 Simplified Method for Analyzing Rearward Amplification Level

Frequency response methods have been applied in this study to develop an understanding of the influence of size and weight parameters on the directional performance of combination vehicles employing full trailers. Transfer functions have been used to calculate the contributions of full trailers, trucks, and tractor-semitrailers to the rearward amplification between the lateral accelerations of the towing and last units in truck-full trailers, doubles, and triples combinations. These transfer functions show how (a) the frequency content of the steering input, (b) the forward velocity of the vehicle, (c) the distances between pintle connections and center of gravity locations, and (d) tire cornering coefficients influence rearward amplification.

The equations used in making these calculations were derived in SAE Paper No. 821259 [15]. The primary simplifying assumptions used in that analysis are (1) the lateral forces at pintle hitch connections on full trailers are small compared to tire side forces, (2) tire side forces may be represented as linear functions of their slip angles, (3) the vehicle is traveling at a constant forward velocity, and (4) full trailers have approximately equally loaded axles and similar tires all around the unit. The

overall rearward amplification of lateral acceleration between the leading and trailing units of a combination vehicle may be estimated by calculating the product of the amplification factors (transfer functions) for each of the units comprising the vehicle. Figures 36 through 39 define and illustrate the symbols used in the analytical expressions describing rearward amplification. Tables 4 through 7 summarize the transfer functions employed in determining the frequency dependence of the amplification factors corresponding to the various types of vehicle units examined in this study.

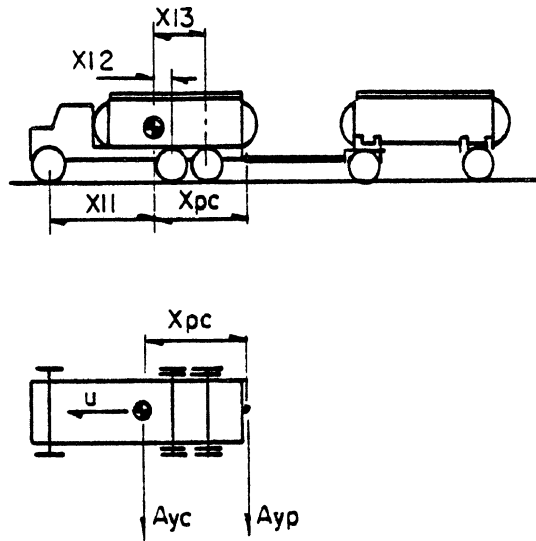
3.4 Low-Speed Offtracking Calculation

A computerized calculation method was developed for assessing the offtracking path of any vehicle configuration in a realistic, non-steady-state, low-speed maneuver.

A transient offtracking maneuver was defined by which a point on the steering axle of the towing vehicle was caused to follow a specific "input" trajectory. The offtracking response would then be defined in terms of the path traced by some second fixed point located on the centerline of the rearmost axle group in the combination. Of course it was necessary that the specific path layout to be used as the input for the steering axle of the towing vehicle could, in fact, be followed by all of the vehicle combinations to be studied. The following are the main physical parameters selected as constraints for the model:

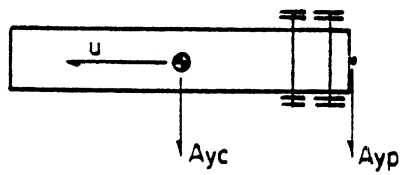
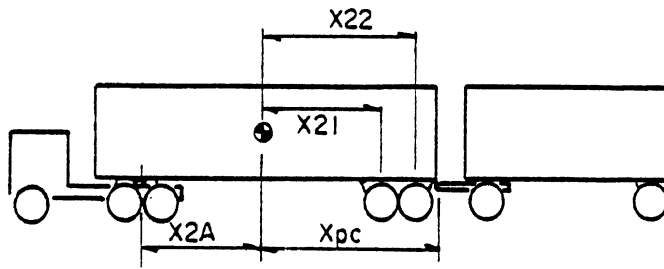
- a) The longest wheelbase of the lead vehicle was chosen to be 30 feet (9.15 m).
- b) The overall width of all units was 8 feet (2.44 m).
- c) The maximum front-wheel steering angle was limited to -45 degrees (inside lock).
- d) No tire mechanics or vehicle dynamics are accounted for, so that only pure Ackerman steering kinematics apply throughout the maneuver.

The maneuver itself was chosen to be a constant radius 90-degree turn, with straight entry and exit input trajectories tangent to the ends of the



- u = forward velocity
- X_{pc} = distance from c.g. to pintle hitch
- X_{li} = distance from the c.g. to the i^{th} axle
- C_{li} = total cornering stiffness of all tires on the i^{th} axle
- ΣC_{α} = sum of the cornering stiffnesses for all axles = $\Sigma_i C_{li}$
- $\Sigma x_{li}^2 C_{li}$ = damping in yaw = $\Sigma_i x_{li}^2 C_{li}$
- m = mass of the truck
- I = yaw moment of inertia
- A_{yc} = lateral acceleration of the c.g.
- A_{yp} = lateral acceleration of the pintle hitch

Figure 36. Symbols Describing a Straight Truck (Towing Unit)



u = forward velocity

X_{pc} = distance from c.g. to pintle hitch

X_{2i} = distance from c.g. to i^{th} axle

X_{2A} = distance from c.g. to the fifth wheel

m_2 = mass of the semitrailer

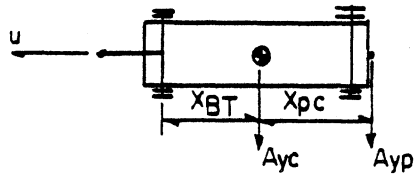
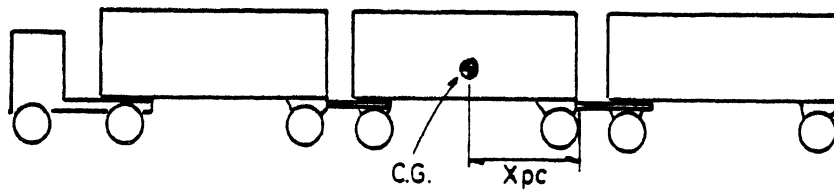
I_2 = yaw moment of inertia

$C_{\alpha 2i}$ = total cornering stiffness for all tires on the i^{th} axle

A_{yc} = lateral acceleration of the c.g.

A_{yp} = lateral acceleration of the pintle hitch

Figure 37. Symbols Describing a Semitrailer (Towing Unit)



u = forward velocity

X_{pc} = distance from c.g. to pintle hitch

X_{BT} = distance from c.g. to turntable or fifth wheel

ΣC_{α} = summation of the cornering stiffnesses of all tires mounted on the trailer

$\Sigma x^2 C_{\alpha}$ = damping in yaw = $\Sigma x_i^2 C_{\alpha i}$ for i axles

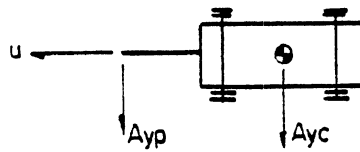
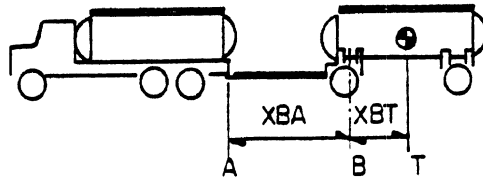
m_T = mass of the trailer

I_T = yaw moment of inertia

A_{yc} = lateral acceleration of the c.g.

A_{yp} = lateral acceleration of the pintle hitch

Figure 38. Symbols Describing a Full Trailer (Towing Unit)



$\dot{X}_A = u =$ forward velocity

X_{BA} = dolly tongue length, distance from pintle hitch to turntable or fifth wheel

X_{BT} = distance from c.g. to turntable or fifth wheel

$\sum C_\alpha = \sum_i C_{\alpha i}$ = sum of the cornering stiffnesses of all the tires mounted on the trailer

m_T = mass of the trailer

A_{yc} = lateral acceleration of the c.g.

A_{yp} = lateral acceleration of the pintle hitch

Figure 39. Symbols Describing a Full Trailer (Towed Unit)

TABLE 4

Towing Unit: Straight Truck

Rearward amplification between the c.g. of a straight truck and its pintle hitch.

$$\frac{A_{yp}}{A_{yc}} = (1 + \Delta A)$$

where

$$\Delta A = \left[\frac{-\frac{x_{pc}}{u} j\omega \left(\frac{m_1 u}{\Sigma C_\alpha} j\omega + 1 \right)}{1 - \frac{I_1}{x_{11} \Sigma C_\alpha} \omega^2 + \frac{j\omega \Sigma x^2 C_\alpha}{x_{11} u \Sigma C_\alpha}} \right]$$

$$j = \sqrt{-1}$$

ω = frequency, rad/sec

TABLE 5

Towing Unit: Tractor-Semitrailer

- a. Rearward amplification between the c.g. of a semitrailer and its pintle hitch connection to the unit being towed.

$$\frac{A_{yp}}{A_{yc}} = (1 + \Delta A)$$

where

$$\Delta A = \left[\frac{-\frac{x_{pc} j\omega}{u} \left(\frac{u m_2 j\omega x_{2A}}{\sum (x_{2i} + x_{2A}) c_{a2i}} + 1 \right)}{1 - \left(\frac{I_2 \omega^2}{\sum (x_{2i} + x_{2A}) c_{a2i}} \right) + j\omega \left(\frac{\sum x_{2i} (x_{2i} + x_{2A}) c_{a2i}}{u (\sum (x_{2i} + x_{2A}) c_{a2i})} \right)} \right]$$

$$j = \sqrt{-1}$$

ω = frequency , rad/sec

- b. Note that for typical tractor-semitrailers, the rearward amplification between the c.g. of the tractor and the c.g. of the semitrailer may range from a maximum of approximately 1.2 to a minimum of approximately 0.8 in the frequency range from 0 to 3.5 rad/sec. Vehicles with short semitrailers tend to have maximum amplification factors greater than 1.0 at frequencies in the range from 1 to 4 rad/sec. Vehicles with longer semitrailers tend to have amplification factors of 1.0 at low frequencies with their amplification factors falling off to approximately 0.8 in the neighborhood of 3 rad/sec. For first-order estimates of overall rearward amplification, a reasonable compromise is to assign an amplification factor of 1.0 between the c.g. of the tractor and the c.g. of the semitrailer if this amplification factor is not known from prior work.

TABLE 6

Towing Unit: Full Trailer

Rearward amplification between the c.g. of a full trailer and the pintle hitch connection to the unit it is towing.

$$\frac{A_{yp}}{A_{yc}} = (1 + \Delta A)$$

where

$$\Delta A = \left[\frac{-\frac{x_{pc}}{u} j\omega \left(\frac{m_{T^u}}{\sum C_a} j\omega + 1 \right)}{\left(1 - \frac{I_T}{x_{BT} \sum C_a} \omega^2 \right) + \frac{j\omega \sum x^2 C_a}{x_{BT^u} \sum C_a}} \right]$$

$$j = \sqrt{-1}$$

ω = frequency, rad/sec

(The amplification factor for a towed full trailer is given next in Table 7.)

TABLE 7

Towed Unit: Full Trailer

Rearward amplification between the pintle hitch connection to the towing unit and the c.g. of the full trailer.

$$\frac{A_{yc}}{A_{yp}}(j\omega) = \frac{1}{1 - \left(\frac{\omega}{\omega_{nc}}\right)^2 + j2\zeta_c \frac{\omega}{\omega_{nc}}}$$

where

$$\omega_{nc} = \sqrt{\frac{\sum C\alpha}{m_T} \frac{1}{X_{BT} + X_{BA}}}$$

$$\zeta_c = \frac{1}{2\dot{x}_A} \sqrt{\frac{\sum C\alpha}{m_T} (X_{BT} + X_{BA})}$$

90-degree arc. This composite trajectory was to be traced by the outermost point on the outside front tire. A constant radius of 35 feet (10.7 m) was determined to be the smallest value of circular radius to comply with the above constraints.

3.4.1 Mathematical Model and Solution Method. As shown in Figure 40, the input trajectory is represented on the x-y plane as an arc of radius $R = 35$ feet (10.7 m), whose center is located at point (35,35), followed by the tangent path lying along the y axis. This trajectory is seen to start at point (35,0), with the whole combination aligned with its left edge on the x axis, and headed towards the origin. The input trajectory thus follows the indicated arc, and, from point (0,35), the positive y axis.

The output trajectory will then be some quasi-hyperbolic-shaped curve, asymptotically approaching the y axis at increasing y (see Fig. 41). Each vehicle unit of the combination is defined by virtue of its separate yaw degree of freedom, such that, for example, a full trailer dolly is considered as one unit, and the "remaining" semitrailer as a separate unit. As shown in Figure 42, each unit "i" is represented on the x-y plane as a straight segment comprising the longitudinal centerline, with points (F_i, R_i, F_{i+1}) denoting axle positions and hitch (or articulation) points. Note that an articulation point may consist of either a fifth wheel, a dolly turntable, or a pintle hook. An articulation joint can be located within the wheelbase or behind the rear axle of the unit.

The point, I, on the towing vehicle which follows the input trajectory is defined in the model as a fixed point on the front axle centerline, four feet (1.22 m) to the left of the unit's longitudinal centerline. The point inscribing the extreme offtracked trajectory (Z) is defined as a fixed point on the centerline of the rearmost axle group of the combination—four feet (1.22 m) to the right of the last unit's longitudinal centerline, following the arbitrarily-adopted "turn to the right" case.

The turning process is simulated by means of a geometric construction which identifies instantaneous turning centers (see Fig. 43). The essence of this approach is as follows:

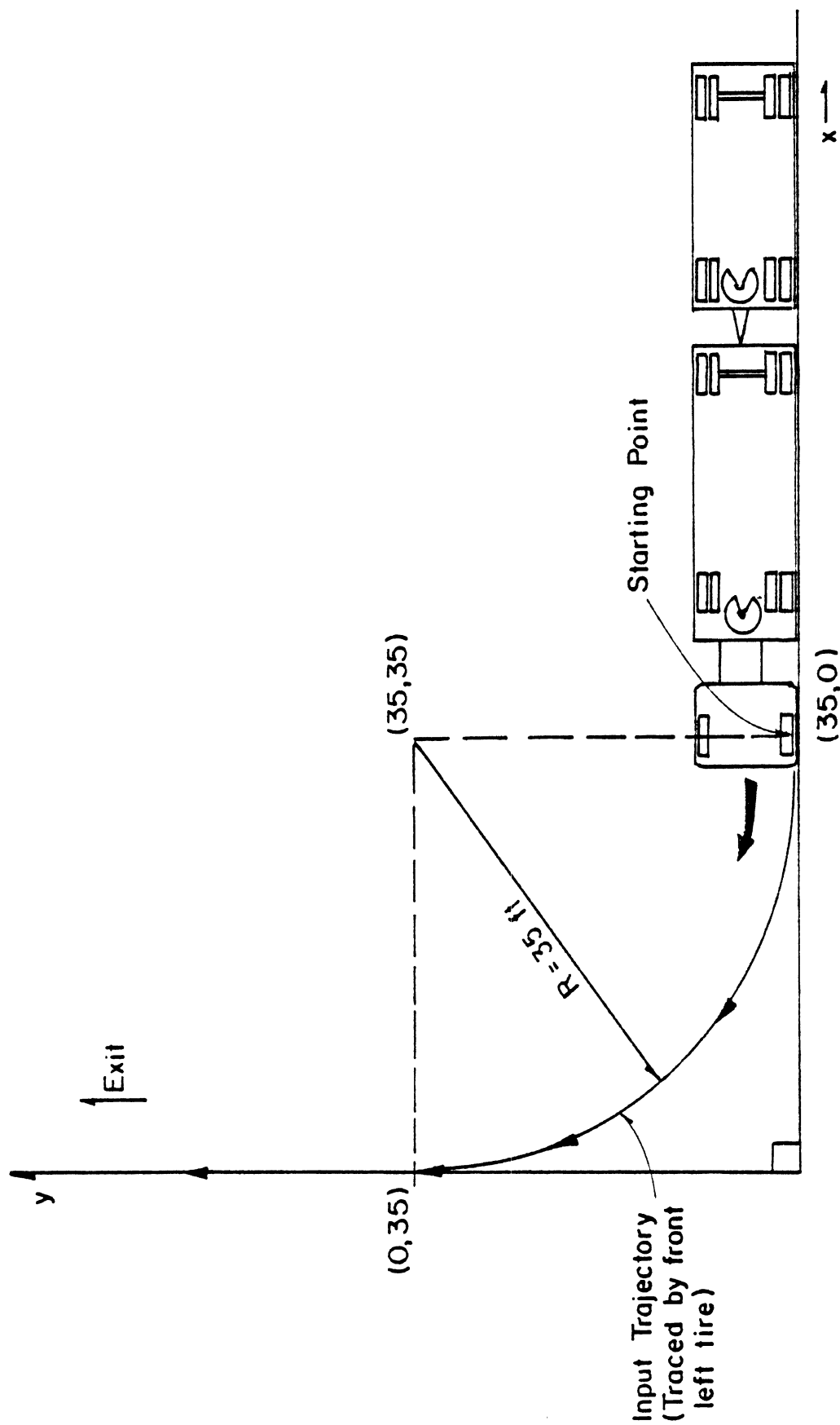


Figure 40. Maneuver Definition

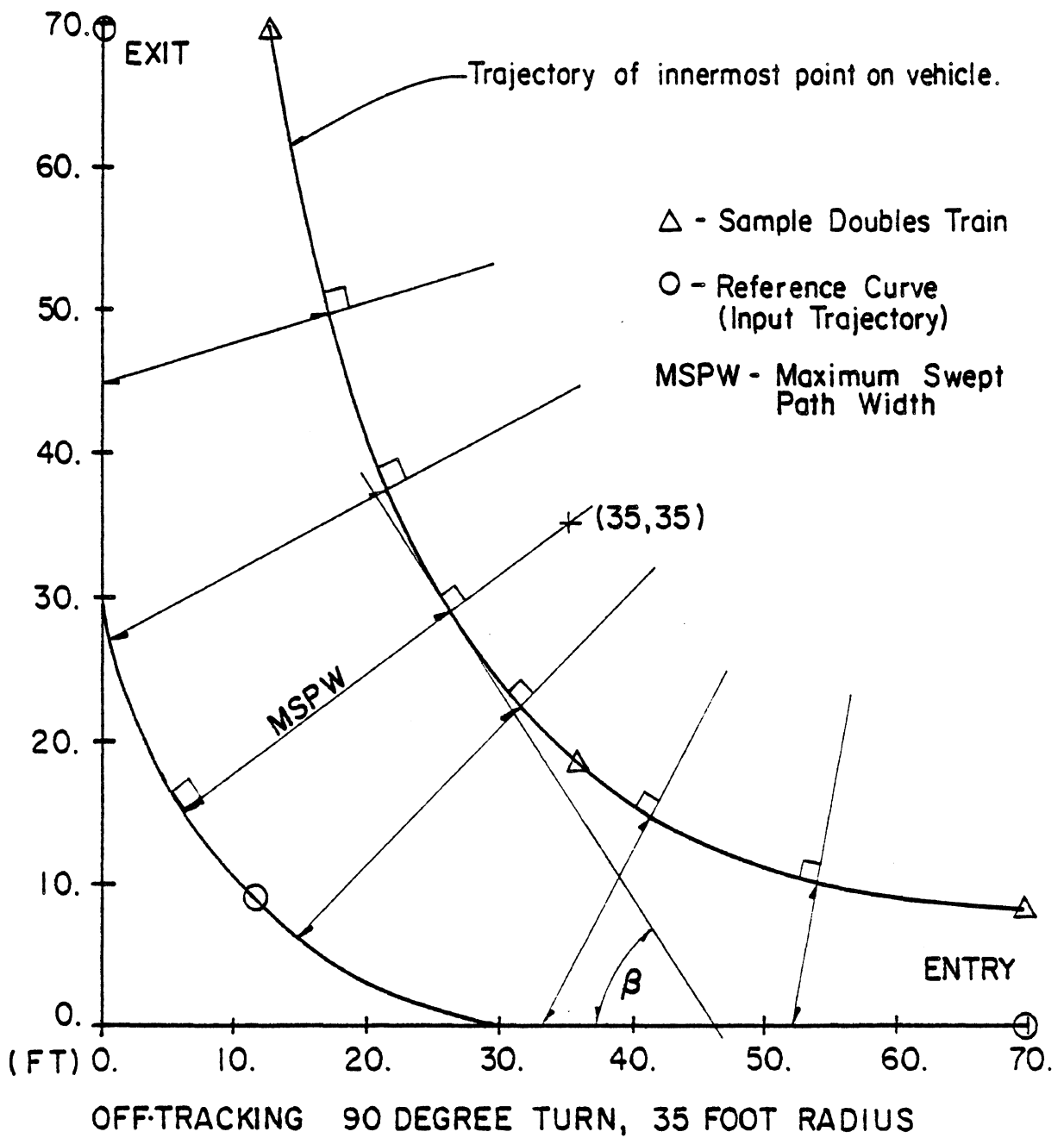


Figure 41. Definition of Maximum Swept Path Width, as Compared to Some Local Swept Path Widths

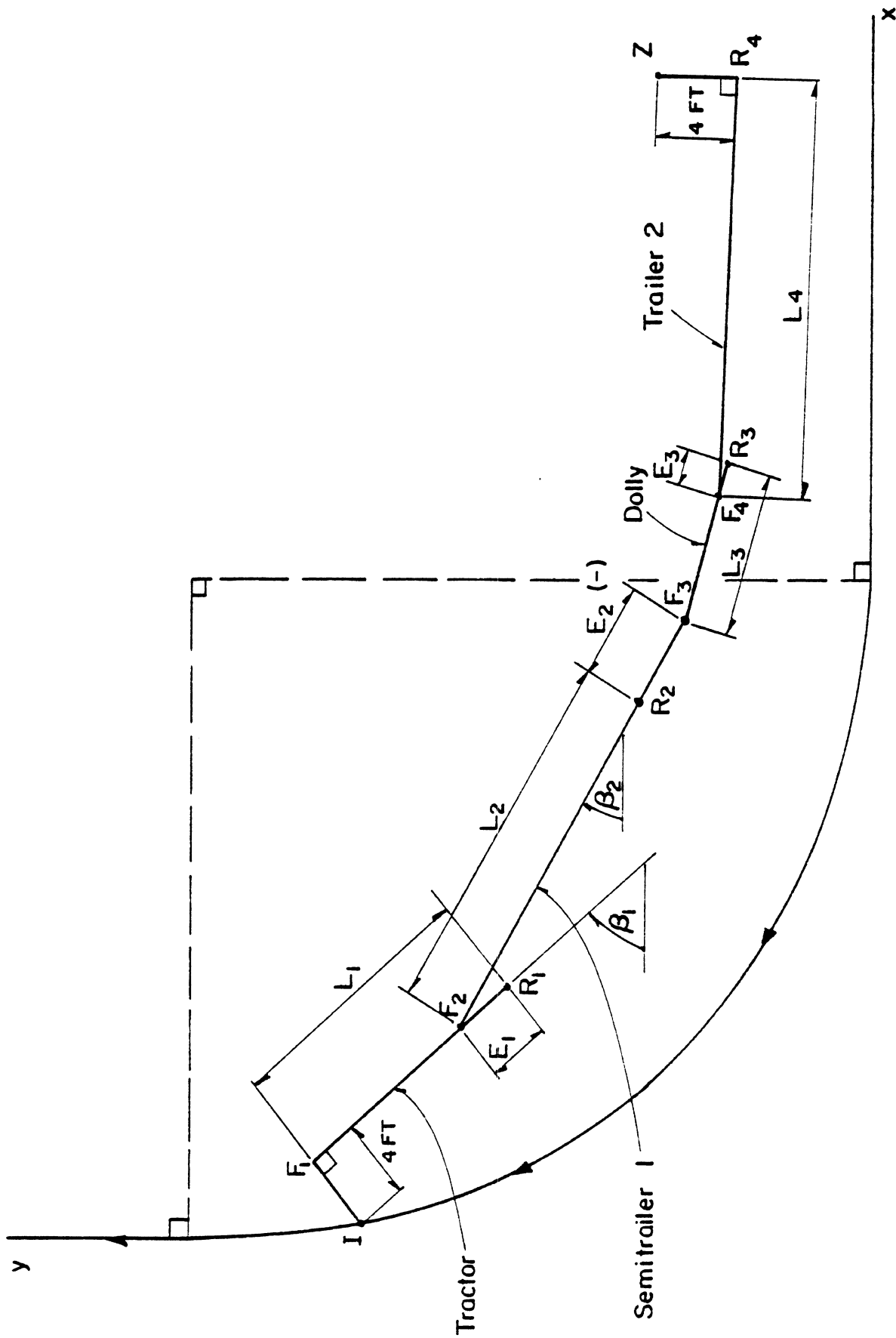


Figure 42. The Mathematical Model, Demonstrated for a "Doubles" Combination.

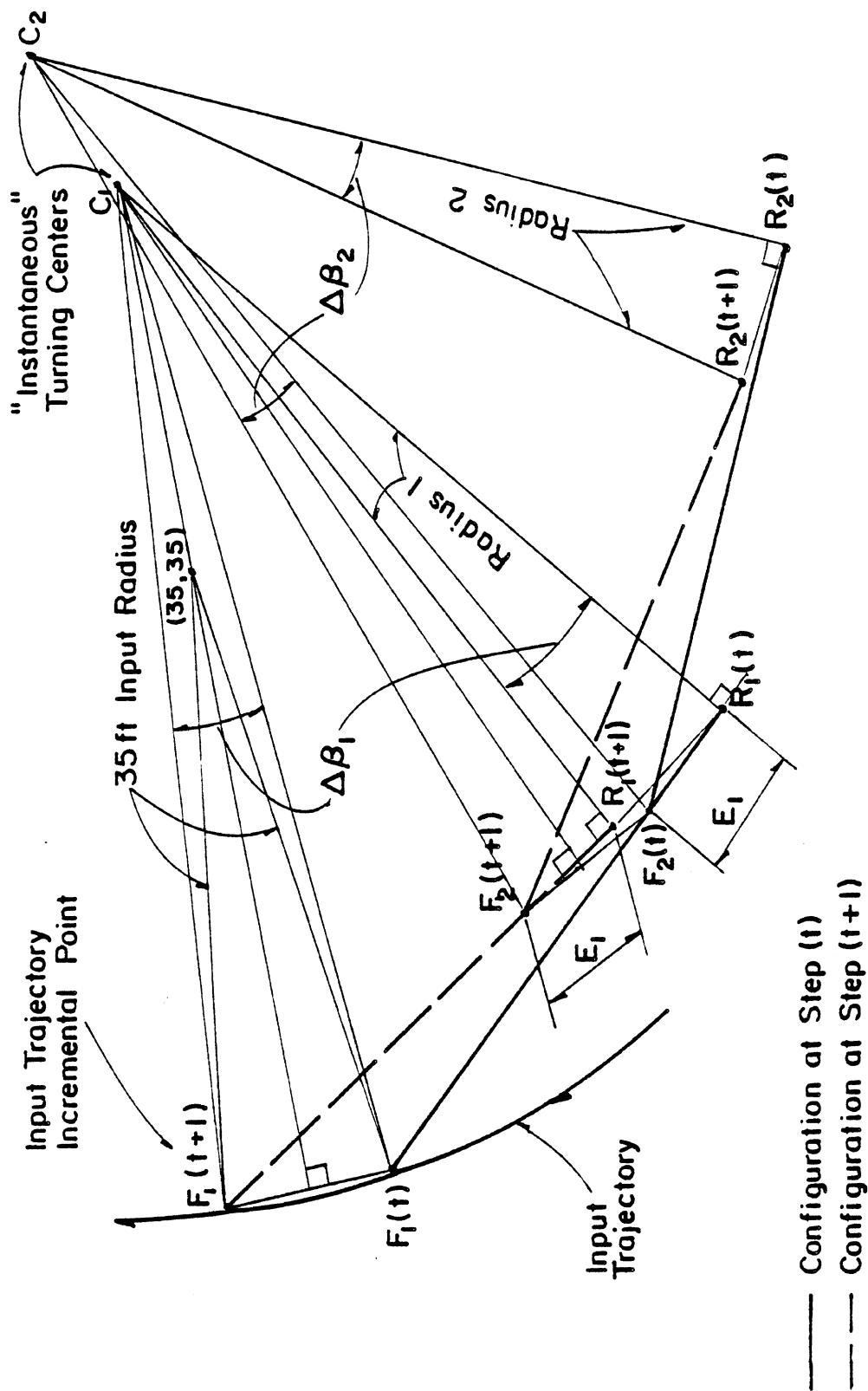


Figure 43. Solution Method Demonstrated for a Simplified 2 Unit Combination
 - Vehicle Width Effect (Points I, Z) Ignored for Clarity

The input trajectory is broken down into a finite number of small, incremental steps, each one being defined in terms of points lying along the trajectory. Assuming some given position of the whole combination at the end of step (i), the position of each unit at the end of step (i+1) will be uniquely determined by the position of its leading articulation joint after step (i+1). The position of this point is, in turn, determined by the position of the preceding vehicle unit at the end of step (i+1), and so on.

Hence, the incremental position of the leading unit has to be computed first by calculating the "instantaneous turning radius" and its center point, which are assumed to be particular to each incremental step and to remain fixed "throughout" the step. The method of computing the instantaneous turning centers and radii after step (i) for the first and second units of a combination is demonstrated in Figure 43 representing the operations of the towing vehicle on the circular radius segment of the maneuver. In Figure 44, the straight exit segment of the input trajectory is illustrated, considering the first unit only.

3.4.2 Offtracking Quantification. Unlike the simpler case of steady-state offtracking, offtracking in a 90-degree turn cannot be characterized by the difference between the innermost and outermost (or minimum and maximum) path radii inscribed by the combination since at no point do these trajectories share a common turn center. Rather, the whole input trajectory, along both its curved and straight parts, actually produces continuously-varying response trajectories for the towing and trailing units.

Thus, the offtracking performance was quantified here by means of a measure called "the maximum swept path width," defined as shown in Figure 41, and described as follows:

If a perpendicular to the tangent of the offtracked trajectory is constructed at every point on that trajectory, then the local swept path width will be defined as the distance measured along this perpendicular between the input and offtracked trajectories. The greatest value of the swept path width dimension is defined as the maximum swept path width.

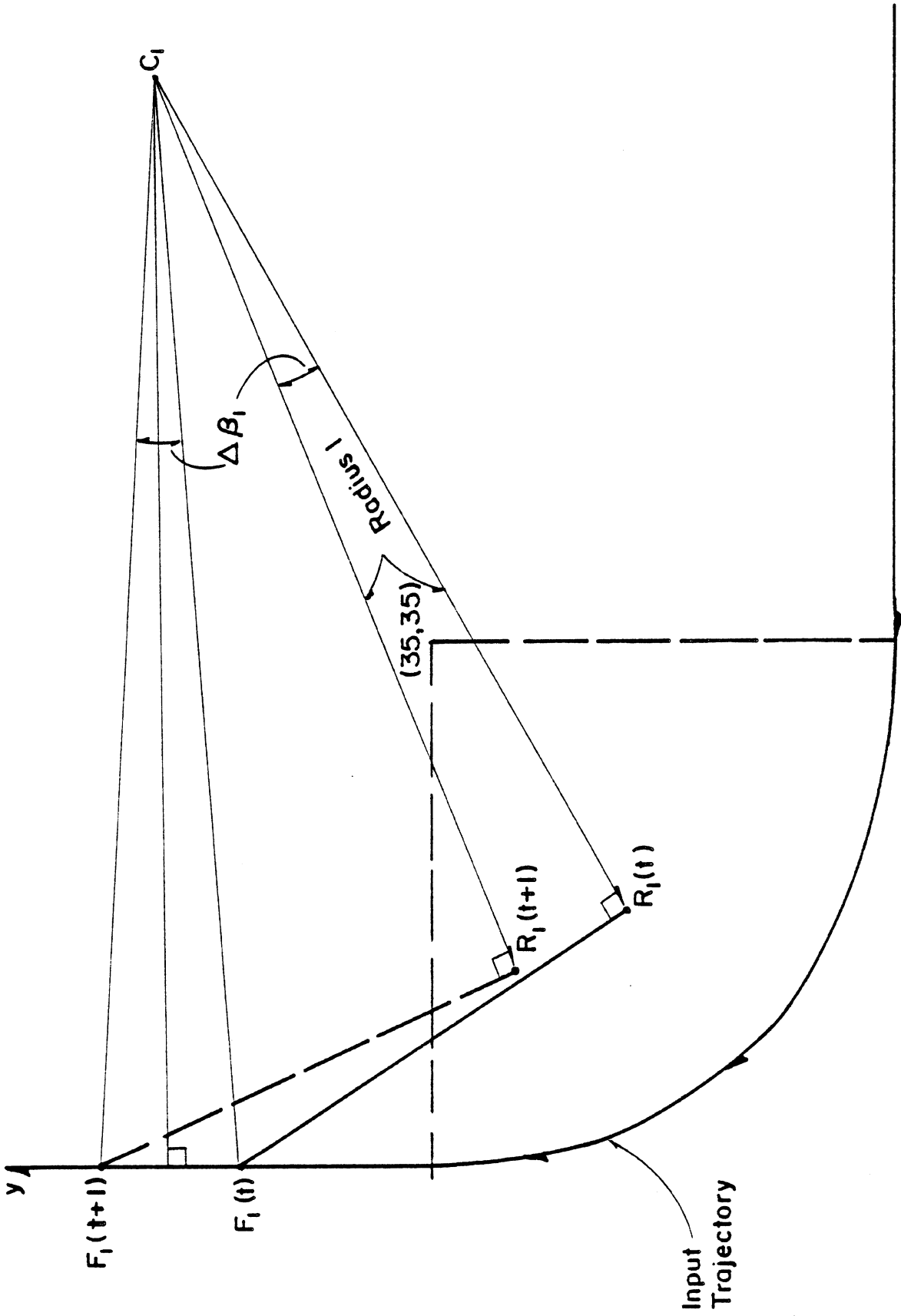


Figure 44. Solution Method Demonstrated for a Simplified Single Unit with Vehicle Width Effect Ignored for Clarity.

It can be proven geometrically that the perpendicular containing the "maximum swept path width" will occur at one unique point at which this perpendicular line segment is also perpendicular to the tangent of the input trajectory. This point will thus identify the only perpendicular to the "offtracked" trajectory which passes through the center of the input trajectory arc (point 35,35). These properties are used in the actual computation of the maximum swept path width from a known offtracked trajectory. In simple terms, this measure will directly reflect the extent to which a combination will cut to the inside of the negotiated corner.

The actual method of computation used to generate the offtracked trajectory and to calculate the maximum swept path width is direct numerical incrementation, followed at each step by the calculation of the local swept path width and its comparison to the previous value. The generated off-tracked trajectory is stored as a sequence of x-y coordinates sampled once every fixed number of steps, so as to create plotting data of reasonably limited size, without degrading the computational accuracy of the method. After some experimenting with different "window" sizes, the final window for plotting the simulated offtracked trajectory was set to be $2R_1 \times 2R_1$ ($0 \leq x, y \leq 70$ feet). The leading vehicle unit keeps incrementing along the input trajectory (the y axis) until the point Z on the last unit inscribing the offtracked trajectory clears the window ($y_E > 70$).

3.5 High-Speed Offtracking Calculation

The high-speed offtracking characteristic of vehicles was examined by means of a simplified analysis of the kinematics of the steady-turn condition. The analysis was based upon a linear derivation given in Reference [26] for a vehicle unit which trails behind a point which is tracking a circular curve of specified radius, R. This analysis assumes a linear relationship between tire lateral force and slip angle and further applies to curved paths in which the radius of curvature greatly exceeds the wheel-base of the vehicle unit. It also assumes that tire aligning moment effects are negligible and that zero roll steer is present.

The unit vehicle is treated as developing a certain level of tire slip in achieving the centripetal acceleration level which is associated with the defined values of turn radius and velocity. The magnitude of the lateral slip result is, of course, dependent upon the cornering stiffness level of the installed tires, given the prevailing tire loads. Given the vehicle's wheelbase, this slip condition determines the outboard offtracking dimension, X, of the axle center point, A, as seen in Figure 45. This offtracking dimension is given in Reference [26] by the relation:

$$X = L/R \left(\frac{U^2}{\bar{C}_\alpha g} - L/2 \right)$$

where

L = the wheelbase of the vehicle unit (measured to the center of the single axle or to the geometric center of a tandem)

U = velocity

R = path radius

g = acceleration of gravity

\bar{C}_α = total cornering coefficient for the axle set on the unit, defined by:

$$\bar{C}_\alpha = \frac{\Sigma C_\alpha}{\Sigma F_z}$$

with

ΣC_α = sum of the cornering stiffness levels of the tires installed on the axle set and,

ΣF_z = total load borne on the axle set in question

To determine the total offtracking of a multi-unit vehicle combination, one must determine the offtracking achieved at each of the coupling points. The total high-speed offtracking of the combination is then defined as the sum of the offtracking dimensions achieved at the hitch points connecting

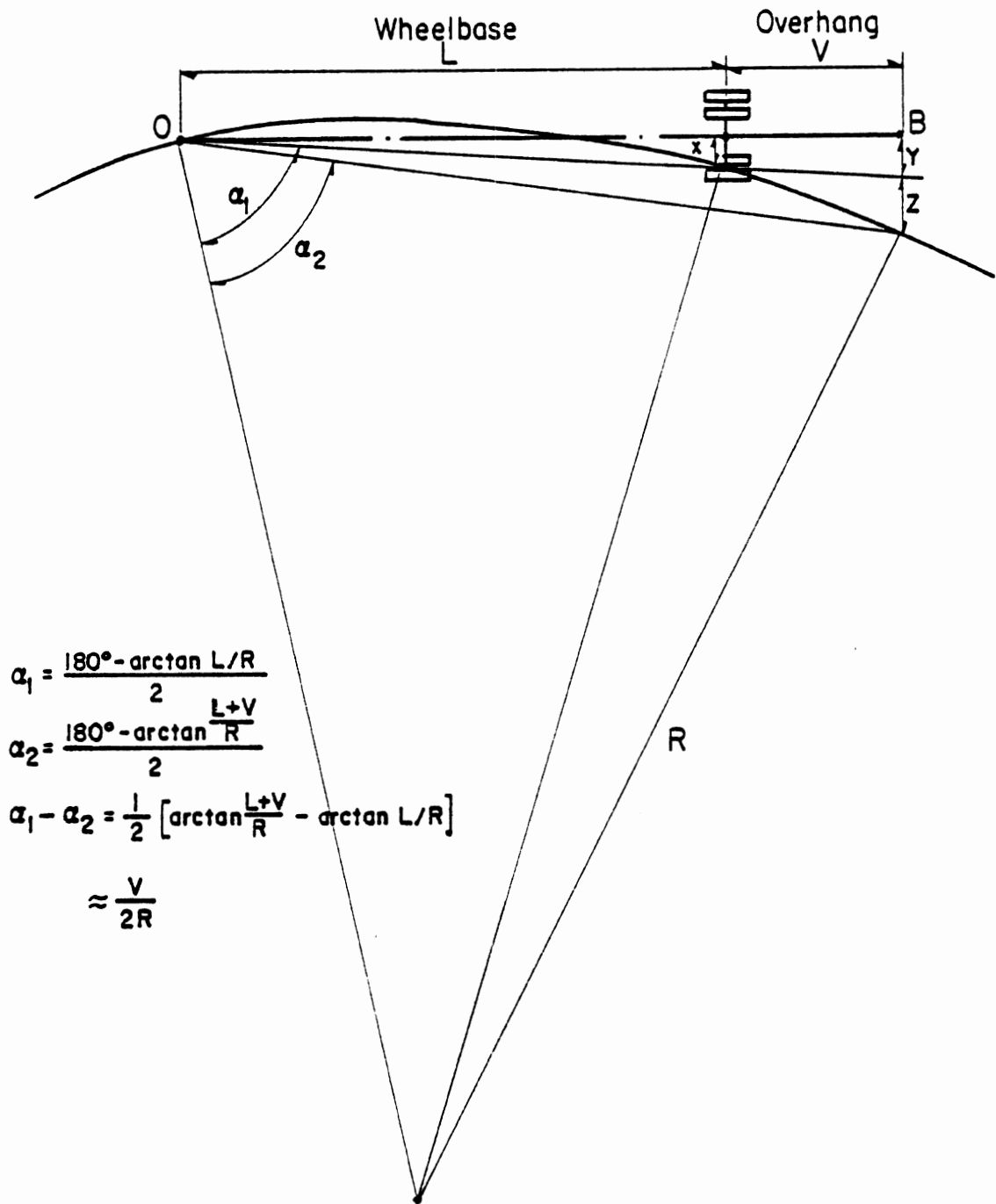


Figure 45. Layout of High Speed Offtracking Geometry for a Single Trailing Unit.

intermediate vehicles plus the offtracking achieved at the rear axle center of the rearmost element in the vehicle train. Looking again at Figure 45, we see that the offtracking of a hitch point located at the overhang dimension, V, aft of the rear axle of any trailing unit derives from two contributions, Y and Z. The Y dimension is simply defined by the relation:

$$Y = X(L + V)/L$$

The Z dimension defines the additional distance to the reference path, itself, by the relation:

$$Z = \frac{V(L+V)}{2R}$$

The offtracking of the hitch point, B, with respect to the path being followed by the forward hitch point, O, is thus given by the sum of (Y + Z).

For the multiple-unit combination, the forward hitch point on each trailing unit is assumed to track on the outboard path established by the rear hitch point of the preceding unit. Nevertheless, the path radius, R, is considered to be so large relative to the offtracking values that it is presumed to be held fixed in the calculation of the X offtracking dimension (above) for each trailing unit.

In this study, the high-speed offtracking of various vehicle combinations was calculated for a path radius of 600 feet (183 m) and a vehicle velocity of 55 mph (88 km/h). All vehicles were assumed to employ radial-ply tires having a cornering stiffness level of 650 lb/deg (2951 N/deg) at a load level of 4250 lbs/tire (1.93 m tons/tire).

3.6 Conventions for Fixing Typical Vehicle Parameters

This section defines the principal baseline parameters used to describe the vehicles examined within the computer simulation study. Equivalent parameters used in the simplified model studies were derived from the baseline parameters listed here. Also included in this section are the major "rules of thumb" used to modify each parameter whenever variations away from baseline values were required. References [11, 21, 22, 23, 24, 25] have been used as primary sources for many of the parameter values appearing in this section.

Tires - The standard tire used on each vehicle was a relatively stiff radial (XZZ Michelin) taken from Reference [11]. Tire cornering stiffnesses for loads greater than 6,000 lbs (26,700 N) were based on the radial tire measurements shown in Figure 3.1 of Reference [21]. Tire data used for representing the lug tire variation was also taken from Reference [11]. The selected tire was a Firestone Transport 200, representing the low end of the range of cornering stiffnesses.

Masses and Inertias - The following mass and inertia values were assumed for the baseline vehicles:

Tractor front axle unsprung weight	1200 lb (544 kg)
Tractor rear axle unsprung weight	2300 lb (1043 kg)
Trailer front/rear axle unsprung weight	1500 lb (680 kg)
Tractor sprung weight	9700 lb (4400 kg)
27-foot (8.2-m) trailer sprung weight (empty)	4500 lb (2041 kg)
45-foot (13.7-m) trailer sprung weight (empty)	9000 lb (4082 kg)

For any trailer of length (ft), x , ($27 < x < 45$), the assumed empty weight (lbs) of the trailer sprung mass varied linearly as given by the following formula:

$$\text{weight} = 4500 + (x-27) \left[\frac{4500}{(45-27)} \right]$$

Single axle dolly weight	1000 lb (454 kg)
Tandem axle dolly weight	1500 lb (680 kg)

Whenever variations in vehicle mass and length were required, pitch and yaw moments of inertia were increased (decreased) by the factor

$$(m_1 L_1^2) / (m_0 L_0^2)$$

The variables appearing in the above expression are defined to be

- m_0 - the baseline vehicle mass value
- L_0 - the baseline vehicle (trailer body) length
- m_1 - the "new" (modified) vehicle mass value
- L_1 - the "new" (modified) vehicle (trailer body) length value

Roll moments of inertia were varied in direct proportion to vehicle mass changes.

Dimensions - The following standard dimensions were assigned to the baseline vehicle configurations:

Two-axle tractor wheelbase	121 in (307 cm)
Three-axle tractor wheelbase	144 in (366 cm)
27-foot trailer wheelbase	252 in (640 cm)
45-foot trailer wheelbase	432 in (1097 cm)
Tractor sprung mass c.g. height above ground	44 in (112 cm)
Trailer sprung mass (body) c.g. height above ground	60 in (152 cm)
Trailer sprung mass (body + payload) height above ground	80 in (203 cm)
Trailer loading bed height above ground	54 in (137 cm)

Tractor front axle track	80 in (203 cm)
Tractor rear/trailer track	72 in (183 cm)
Tractor front axle spring spacing	32 in (81 cm)
Tractor rear/trailer spring spacing	38 in (97 cm)
Axle height above ground	19.5 in (50 cm)
Tractor front suspension roll center height	23 in (58 cm)
Tractor rear/trailer roll center height above ground	29 in (74 cm)
Tractor rear suspension lash	1 in (2.59 cm)
Trailer suspension lash	1.5 in (3.8 cm)
Steering gear ratio	28:1

Payloads - Payloads were assumed to be distributed uniformly over the length of the trailer body. The height of the standard payload was determined by the requirement to fix the composite c.g. (body + payload) height above ground at 80 inches (203 cm) for the baseline vehicle. Depending upon the vehicle and its GW, the payload weight would typically be located in the 81-83 inch (206-211 cm) range. For load variations away from the baseline configuration, material of the same density was assumed to have been added to or removed from the top layer of the baseline payload.

Suspensions - Suspension vertical rate data were obtained primarily from Reference [22]. Front axle suspension characteristics were assumed to behave as shown in Figure A-1 of Reference [22], whereas rear suspension properties were assumed equal to "scaled-up" (stiffer) suspensions defined qualitatively by the force-deflection characteristics seen in Figures A-5, A-6 of [22]. The nominal vertical spring rates (local slope of the force-deflection table) under static (full gross weight) load conditions are:

Tractor front axle	1200 lb/in/spring (2102 N/cm/spring)
Two-axle tractor, rear suspension	8000 lb/in/spring (14016 N/cm/spring)
Three-axle tractor, rear suspension	6000 lb/in/spring (10512 N/cm/spring)
Single axle trailer	10000 lb/in/spring (17520 N/cm/spring)
Tandem axle trailer	9000 lb/in/spring (15768 N/cm/spring)
Tire vertical spring rate	4500 lb/in/tire (7884 N/cm/tire)

Auxiliary roll stiffness at each axle was assumed equal to 10% of the roll stiffness deriving from the springs alone.

CHAPTER 4

DYNAMIC WHEEL LOAD

Use of the public road system by heavy commercial vehicles is known to accelerate deterioration of the roadway structure as a result of the greater wheel loads imposed. The understanding of the loading aspects of road/vehicle interactions is a prerequisite for developing sound practices in both the engineering and use of highways. This portion of the report documents a limited experimental study of the actual wheel loads produced by commercial vehicles on typical roads.

The load experienced between tire and road is the sum of two components: the static load, as measured when the truck is placed on a weight scale; and a dynamic load, caused by the interaction between road roughness and the dynamic properties of the vehicle as it travels at normal speeds. Pioneering research on this subject in Australia [29] and England [30] has indicated that the dynamic component of instantaneous loading produced by commercial vehicles varies as a function of their design and operating conditions. Further, the dynamic components are high enough in certain cases to suggest the need to recognize these vehicle differences in evaluation of pavement damage. The Australian study, reported by P. Sweatman, covered the following variables: tandem and triple suspension design; operating speed; road roughness (as measured on the Australian roughness scale); axle static load; and tire inflation pressure. Suspension type, roughness, and speed were the outstanding factors in determining the magnitude of dynamic loading. The tandem suspension found to be the "worst," from the viewpoint of pavement loading, was the "walking-beam" type, used primarily for drive axles on tractors, popular in the United States for its durability. The "best" design was a torsion-bar suspension with hydraulic shock absorbers. The popular four-leaf trailer suspension was found to have performance lying somewhere in the middle.

A similar study was undertaken in this project to measure and analyze the dynamic wheel loads produced by a loaded tractor-semitrailer vehicle, covering the extremely good and poor combinations identified by Sweatman. While the experimental scope of the study was more limited than that of the Australian one, more extensive analyses were applied in order to better explain the observed results. For the experimental measurements, a wheel-force transducer built for FHWA by Maritime Dynamics, Inc., was used along with a digital data acquisition system built for FHWA by Systems Technology, Inc. Intending to provide a "quick look" at the problem of dynamic wheel loads imposed by commercial vehicles, the study had the objectives:

1. to calibrate the wheel-force transducer owned by FHWA and determine its ability to measure dynamic wheel load, and
2. to corroborate the major points in Sweatman's findings.

After performing a number of laboratory and parking-lot tests of the equipment, three tractor-semitrailer vehicles were tested on three roads, at two test speeds. In each vehicle test configuration, the wheel-force transducer was mounted on the leading axle of a tandem suspension on the driver's side of the vehicle. The wheel-force transducer, which includes a dual wheel assembly, was equipped with two Michelin XZA 10R20 tires for the calibration and all tests. One suspension installed at the drive axles of a tractor was a Hendrickson "walking beam." This suspension incorporated multi-leaf springs and was comparable to the unit measured by Sweatman and identified by him as the "worst" type. The second was a Fruehauf four-spring on a trailer tandem axle, similar to the one considered "typical" by Sweatman. The third as a Kenworth torsion-bar suspension mounted on a tractor drive axle, identified by Sweatman as the "best." The three road sites had roughness levels nominally equivalent to smooth, moderate, and rough.

4.1 Measurement of Dynamic Wheel Load

The dynamic wheel-load transducer built by Maritime Dynamics is a strain-gauged structure which bolts directly to a hub meant for mounting disc-type wheels. The transducer, itself, supports tire/rim assemblies such as conventionally employed on cast-spoke wheels. The transducer is instrumented for measurement of vertical, lateral, and longitudinal forces,

designated as A, B, and T. The orientations of the A and B sensors rotate with the wheel, such that these sensors actually measure a force vector rotating through the vertical and the longitudinal directions. The instantaneous A and B signals are therefore functions of the wheel rotational position as well as the vertical and longitudinal force components. The T (transverse) signal is intended to represent the lateral force transmitted between tire and road.

Preliminary check-outs of the wheel-load transducer by its manufacturer indicated that a significant cross-coupling could occur between the vertical load input and resulting bending of the transducer. This finding suggested that the calibration methods should be performed under realistic loading conditions. For this purpose, the tire/transducer/wheel assembly was mounted on a truck tire test machine at UMTRI which allowed calibration with controlled loads input through the tires. The setup is shown in Figure 46. The calibration consisted of measuring the gains and cross-talk effects of the two rotating load cell channels (designated A and B) under the same loading conditions that occur on the road.

The wheel-force transducer includes a sin/cos potentiometer (pot) and an electronic force resolver, that resolve the signals from the A and B load cells into vertical and longitudinal forces. Initial tests indicated many potential areas in which errors were anticipated such as: limitations in the accuracy and linearity of the analog multiplier; inaccurate SIN and COS waveforms produced by the sin/cos pot; a tendency of the load cell signals to drift; and a requirement that the sin/cos pot be accurately positioned to maintain the correct phase relationship between the SIN and COS signals, relative to the A and B signals. All of these factors can be evaluated and to some extent controlled, yet because later analyses were to be performed with a digital computer, it was more straightforward to simply record the raw transducer signals and resolve the vertical and longitudinal forces later with the computer. This approach of performing all possible data processing digitally results in greater accuracy and much less critical setup for testing. Based on the experience gained, the methodology used can be recommended for future work in this field.

Figure 47 shows that the "raw" A and B signals have significant offsets. These were found to change slowly with time as the electronic

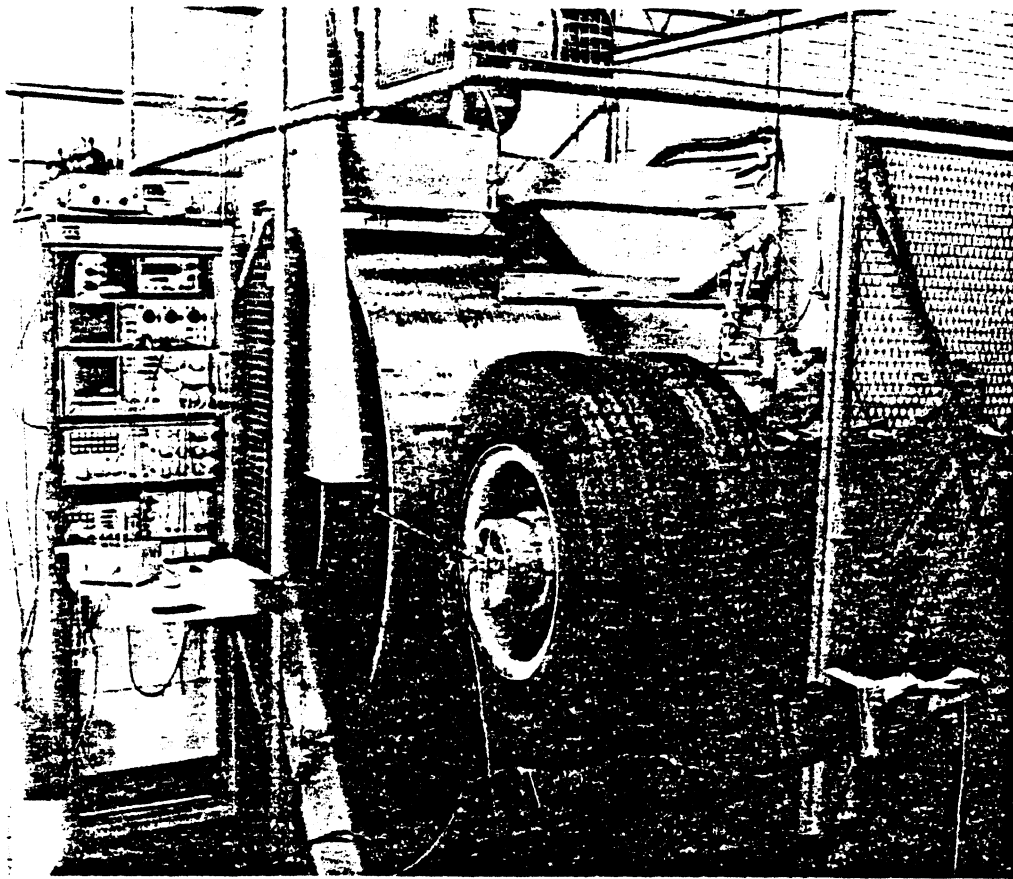


Figure 46. Laboratory calibration of wheel-force transducer.

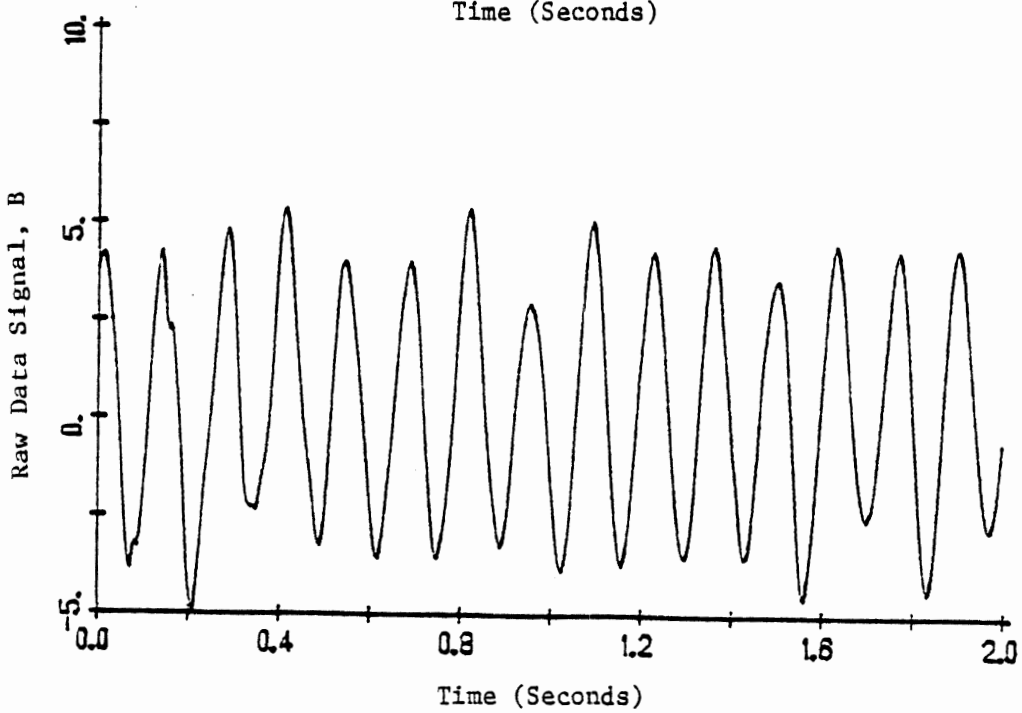
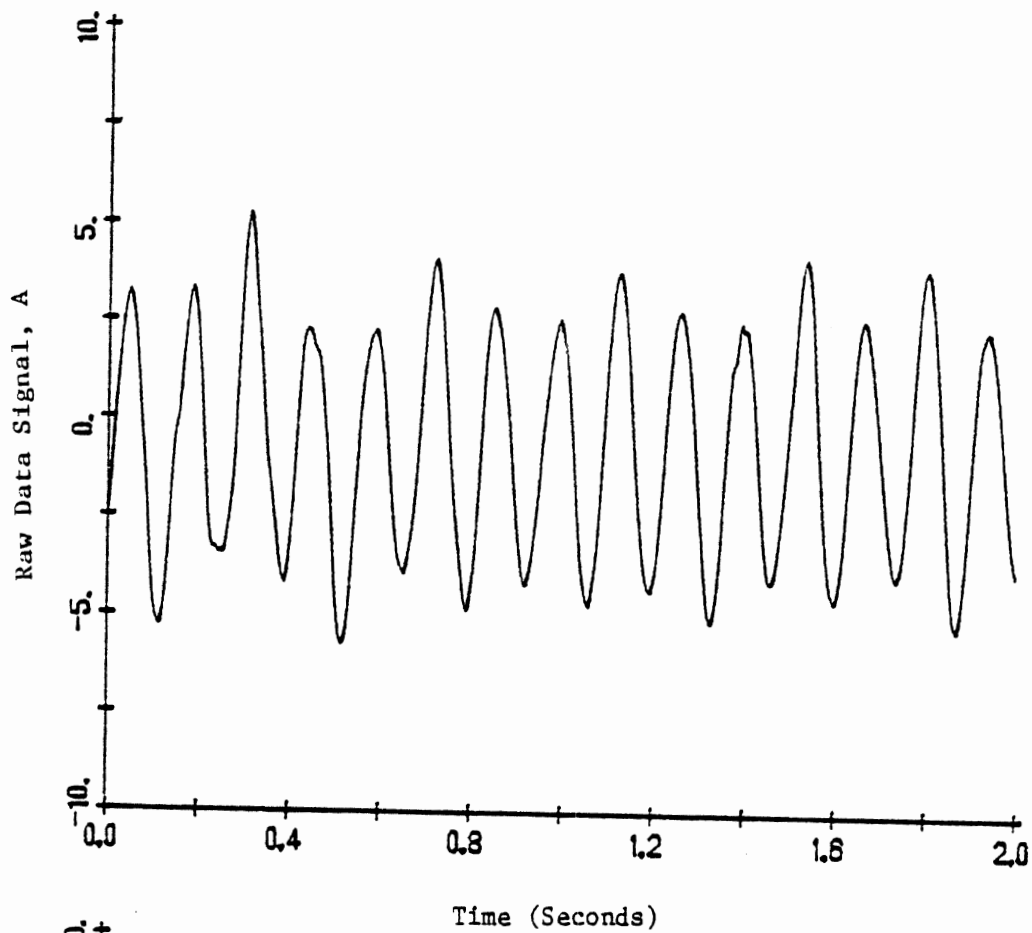


Figure 47. Example on-road measurements from wheel-force transducer.

amplifiers "drift." Thus, the first step in processing the data by computer to resolve the A and B signals into vertical and longitudinal forces is subtraction of the offsets which otherwise would produce major errors in the process of the sin/cos transformation. These errors occur because any offset in the A and B channels is multiplied by a sine function, thus yielding a false sinusoidal force variation proportional to the offset. (Note that this error source is a major impediment to use of the analog resolving system provided with the transducer.) Next, the computer performs a "calibration," using Fourier transforms of the signals, to determine the phase relationship between the A channel and the SIN signal from the sin/cos pot. An error in phase angle between the signals and the computed sine and cosine functions will introduce both sinusoidal variations and an offset into the calculated FZ and FX signals. In practice, it is very difficult to control this phase angle, mechanically, from one test sample to the next, due to the nature of heavy truck suspensions. That is, the "stator" element of the transducer cannot be held precisely fixed in space—thus permitting some shift in the zero-reference needed in establishing the subject phase angles. The described method of analysis compensates for any change in the relative angular position of the pot between test samples and eliminates the need for manual alignment. Essentially, the computer program searches for the maximum static force, defining it as "down." The A and B signals are then combined, with sin and cos values computed digitally using the positive zero crossings of the SIN signal as reference points. Figure 48 shows the lateral force signal, LCT, as well as the vertical and longitudinal force signals, designated "FZ" and "FX," respectively, which are calculated from the "raw" A and B signals shown earlier in Figure 47.

Even with these data processing methods, the errors are significant for the FX computation because the computation process requires the subtraction of two large numbers to obtain a small one. A small relative error in the large numbers can cause a large relative error in the result. For the same reasons, FZ measurements are not accurate at the wheel rotation frequency, which means the wheel-force transducer should not be used to try to discern force variations caused by tire/wheel nonuniformities from those caused by road roughness. (This limitation has almost no effect on measurement of dynamic loading, except for very smooth roads and very nonuniform tire/wheel assemblies.)

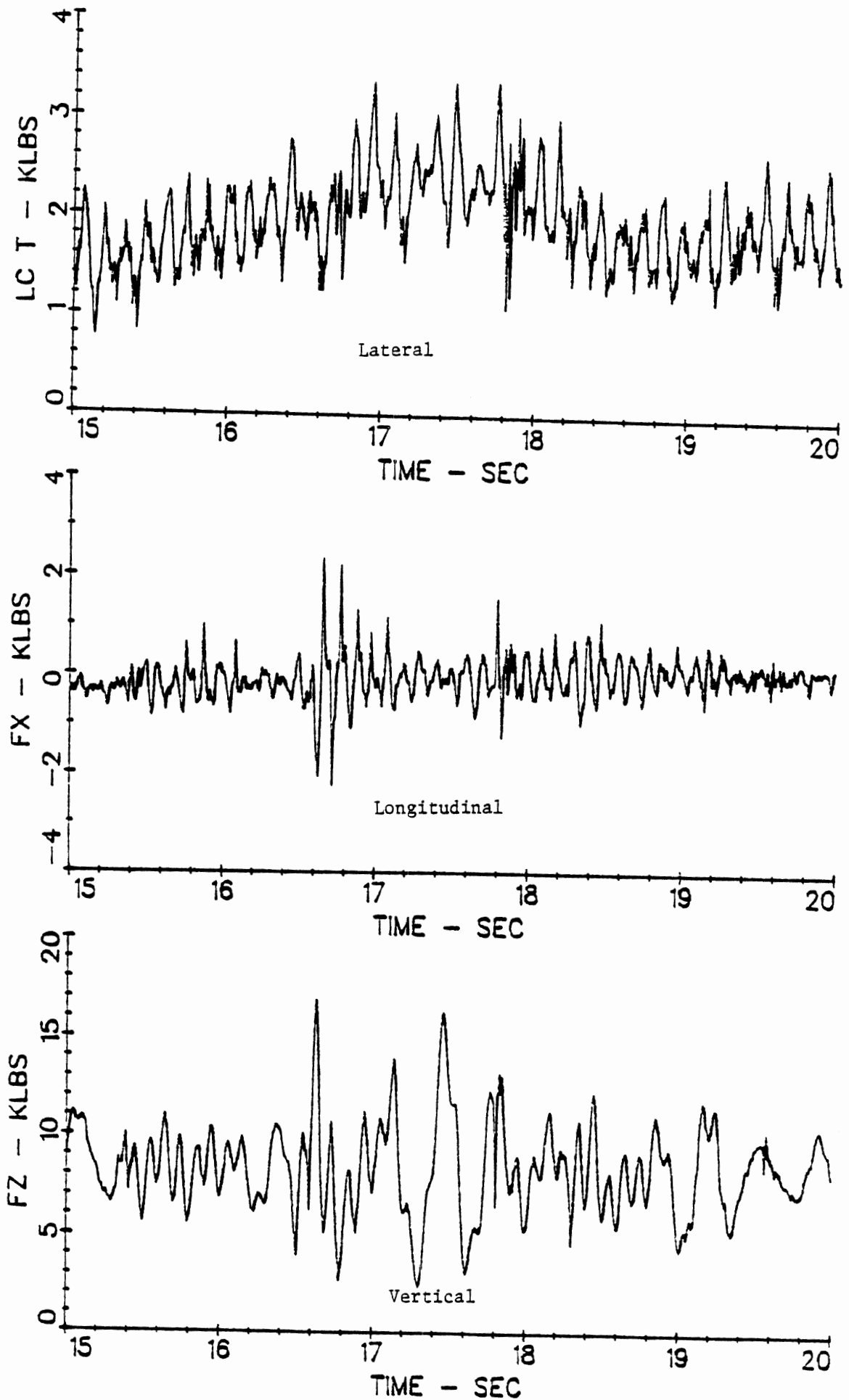


Figure 48. Example of three calibrated force signals from FHWA transducer.

Also note that the T signal in Figure 48 shows a lateral force rapidly oscillating with an amplitude of more than 1000 lbs (4540 N). From knowledge of truck tire/wheel force variation obtained in other research, it is believed that this force magnitude is unrealistically high. The error is most likely caused by cross-talk (mechanical and/or electronic), and could perhaps be removed by a more complete calibration procedure. Inasmuch as this force direction was not of primary interest in the experimental study, no effort was made to identify the cross-talk source or to correct the data. For now we can only state that "as is," the wheel-force transducer should not be considered as a proven means for measuring dynamic variations in lateral force.

Overall, the wheel-force transducer can be considered suitable for measuring the random portion of the dynamic vertical (FZ) forces as well as the static vertical forces. The accuracy of the lateral and longitudinal force measurements, and of cyclic (or wheel-rotation-synchronous) force variations in either of the X and Z directions is less certain. If accurate measures of these small variations were needed from this type of transducer, further development of testing and data processing procedures might be warranted.

Actual forces transferred between vehicle and road must be measured at the tire/road interface to accurately reflect the instantaneous load. In the Maritime Dynamics design, the wheel-force transducer attempts to approach this ideal by minimizing the mass between the sensor and the road. Yet because the mass of the tires and outer portion of the transducer still lies between the load sensors and the road, not all of the pavement force is transmitted to the transducer. Instead, some of the force is absorbed in acceleration of this mass, which is about 500 lbs (227 kg). When available, accelerometer measurements on the axle were obtained so that the data could be corrected for this error. Figure 49 shows the axle acceleration for the example test, along with the "corrected" vertical force, designated as FZ+. The peak-to-peak acceleration levels of ± 5 g's translate to forces of $\pm 2,500$ lbs (11,350 N) "missed" by the wheel-force transducer.

Most of the test results reported by others have been reduced to some sort of "normalized" statistic, such as the Dynamic Index (standard deviation of force divided by mean force). The FHWA wheel-force transducer,

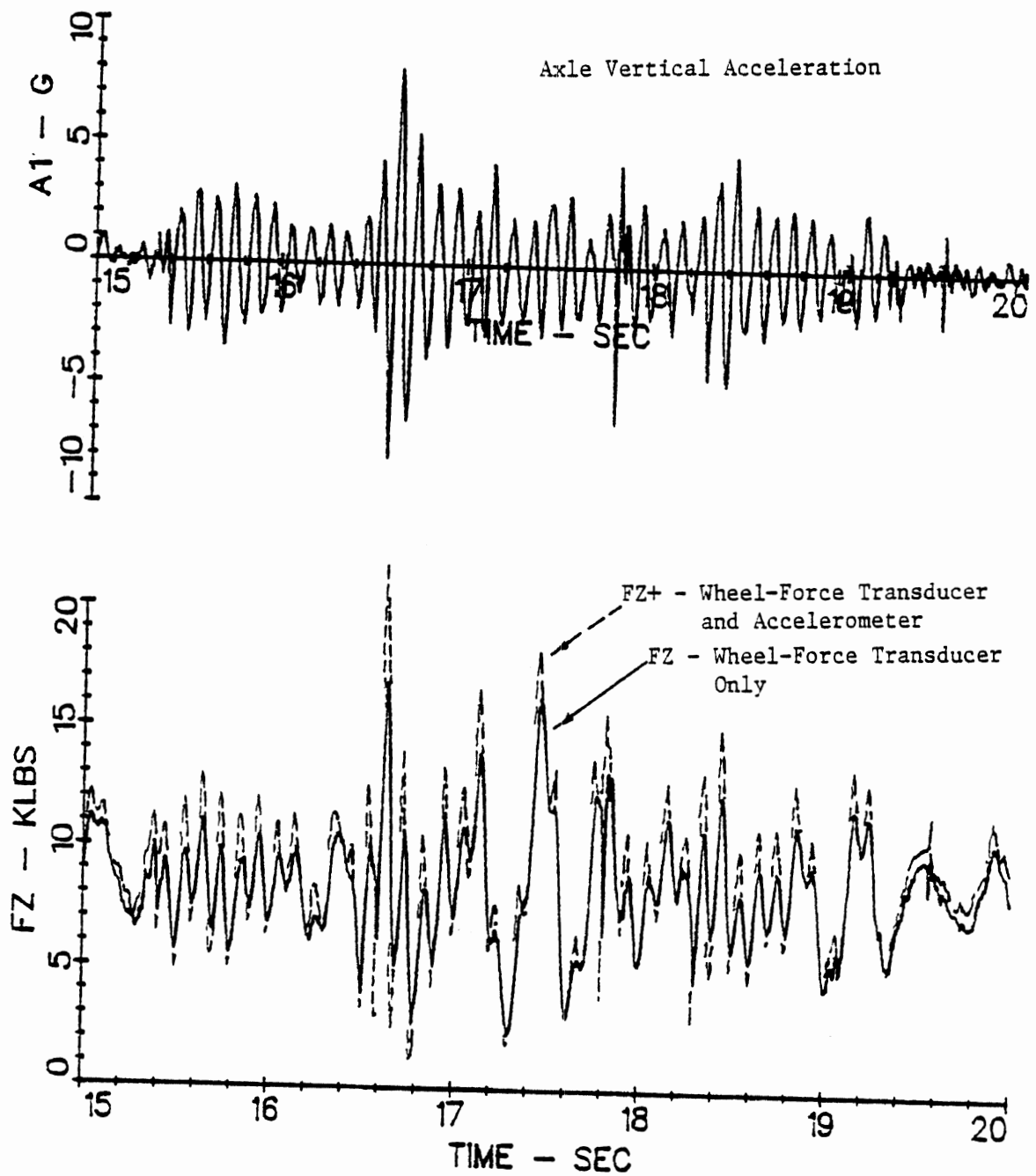


Figure 49. Example of load error with walking-beam suspension.

by itself, produces a static load measure that is too low by an amount equal to the weight between the sensor and the road. If the data were not corrected for this static load difference, the normalized dynamic force (the dynamic index) would be in error on the high side. Similarly, failure to take the mass/acceleration mechanism into account will yield a measured dynamic component which is too low, as shown for the example test in Figures 47-49. Since the error in the dynamic component may be much greater than in the static component, the resulting dynamic index is likely to be in error on the low side. In general, the two errors tend to compensate for each other on vehicles dominated by "low-frequency" dynamic behavior, while the dynamic index will be underestimated on vehicles with dynamic load fluctuations which are dominated by "high-frequency" vibrations. (In this study, the latter category was associated with the greatest dynamic load variations, meaning that this measurement error, if uncorrected, is greatest for the conditions of most interest.)

Of the three suspensions tested, two were instrumented to obtain the axle acceleration. The "walking-beam" type experienced actual normalized dynamic loads, when corrected, that were 5-33% larger than measured directly with the wheel-force transducer. On the other hand, the four-leaf type experienced normalized dynamic loads ranging from 7% smaller to only 2% bigger. Figure 50 compares the corrected and uncorrected force measurements for the same test conditions used in the previous examples. The torsion-bar suspension was not instrumented for measurement of accelerations, but was seen to experience vibrations qualitatively similar to those seen for the four-leaf. Thus the normalized forces reported here for the torsion-bar suspension can be assumed to be marginally higher than their true value.

4.2 Road Test Sites

Tests were conducted at three sites, whose roughness properties are summarized in Figure 51. In an earlier project for FHWA [31], the longitudinal profiles of both wheel tracks were measured with an inertial profilometer. These profiles were processed through a quarter-car simulation

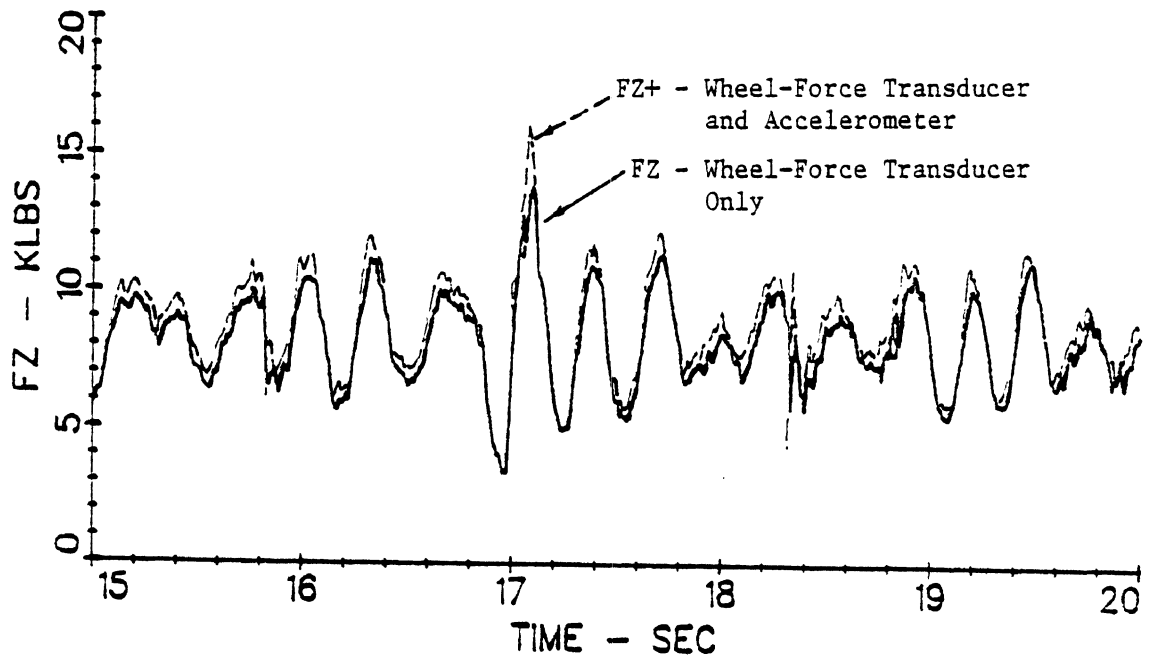
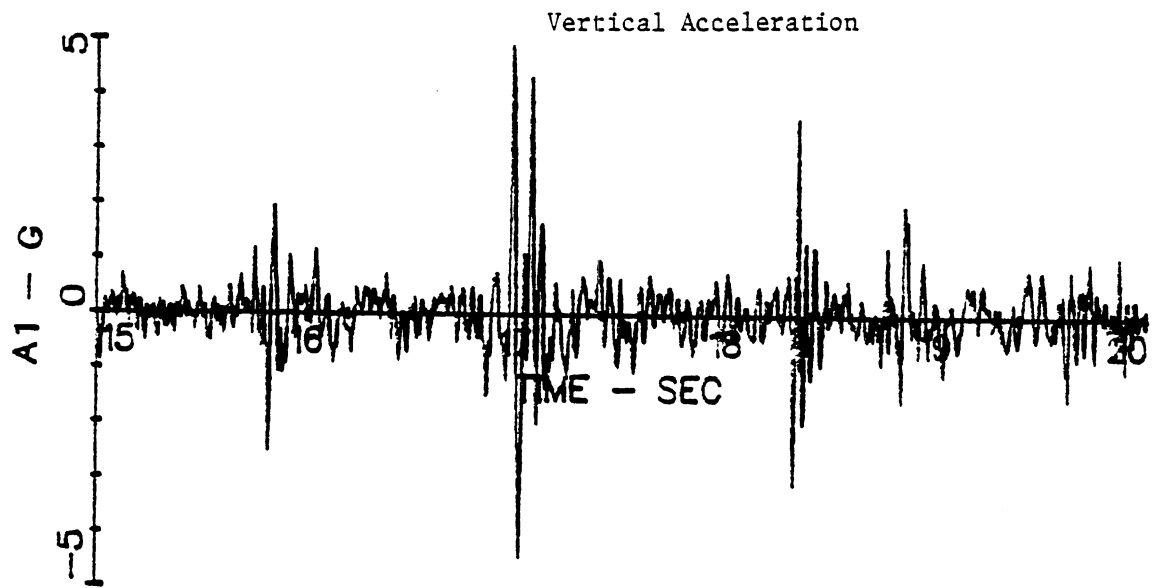


Figure 50. Example of load error with four-leaf suspension.

to evaluate the road's effective "roughness" as would be perceived by a traversing passenger car. The simulation represents a "Reference" Response-Type Road Roughness Measurement System (RTRRMS) as is commonly used for roughness measurement worldwide [32,33]. The roughness is quantified by the RARV (equivalent to the Average Rectified Velocity of the suspension motions for the Reference vehicle) which is closely related to the vibration levels produced in road-using vehicles [31,32]. Because the effective roughness of a road varies with the travel speed, the quarter-car simulation was performed at each speed used by the test vehicles to determine the effective roughness for each speed. The roughness values obtained for each site are shown in the figure for the test speeds of 45 and 55 mph (72 and 88 km/h) used in this experiment.

Along with the roughness numerics, Figure 51 presents plots of the spectral content of that roughness in the form of Power Spectral Densities (PSDs) of slope profile for each site. The smoothest (Site #1) and roughest (Site #2) reveal almost uniform strength over the mid-portion of the wave number range (wave number = 1/wavelength), which is the primary source of vibration excitation to traversing vehicles. Because of this uniformity in roughness content, the frequency distribution of the axle load variations that will be seen on the test vehicles can be attributed solely to the dynamic response properties of the vehicles involved. Site #3—selected because some trucks have been observed to "tune in" and vibrate excessively on this surface—also shows an overall roughness that is evenly distributed, along with specific "peaks" occurring at wave numbers that are harmonics of 0.075 cycle/ft (0.075, 0.15, 0.225, ...). Peaks such as these indicate a periodic element within the otherwise random profile, with the period corresponding to the first harmonic (0.075 cycle/ft = wavelength of approximately 13 feet (4 m)).

4.3 Results

The results of the measurements of dynamic wheel load are summarized in Figures 52-54 for Sites #1, #2, and #3, respectively. For each of the test conditions, the following information is provided:

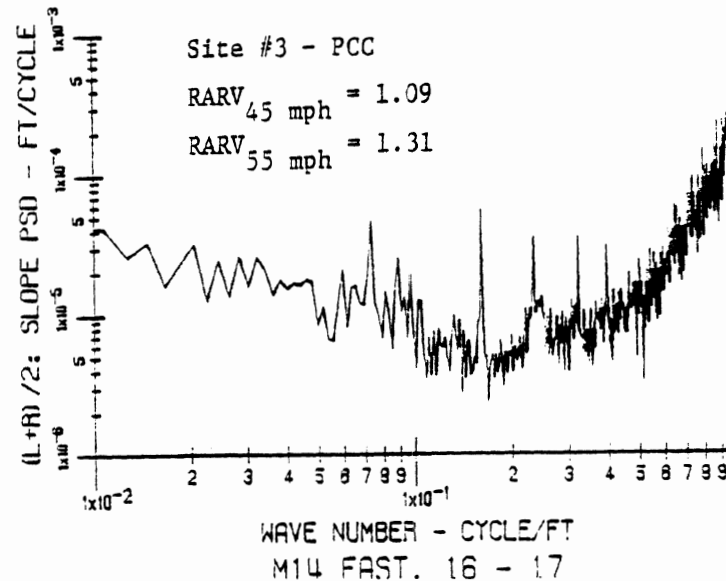
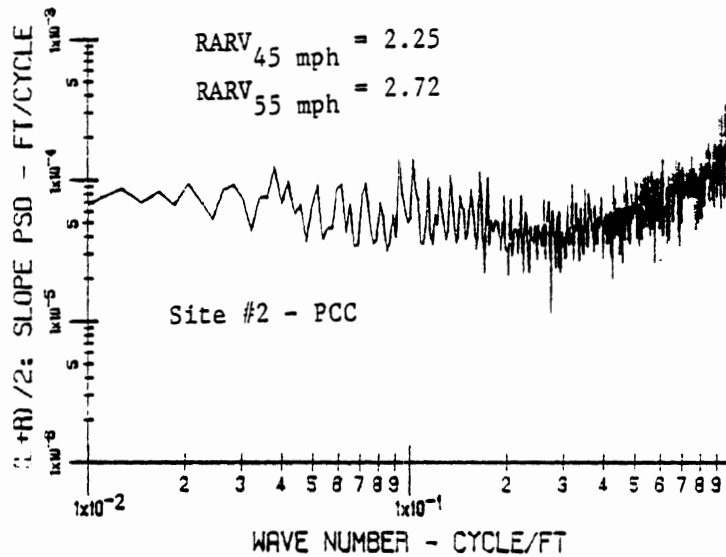
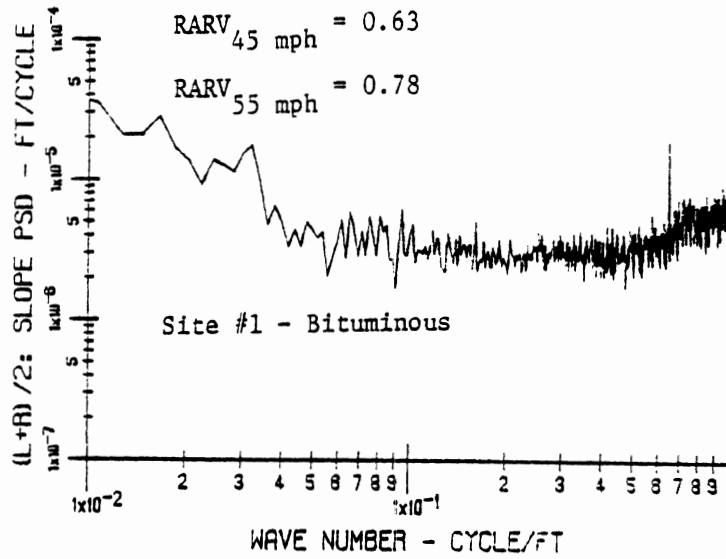


Figure 51. Summary of the roughness properties of three test sites.

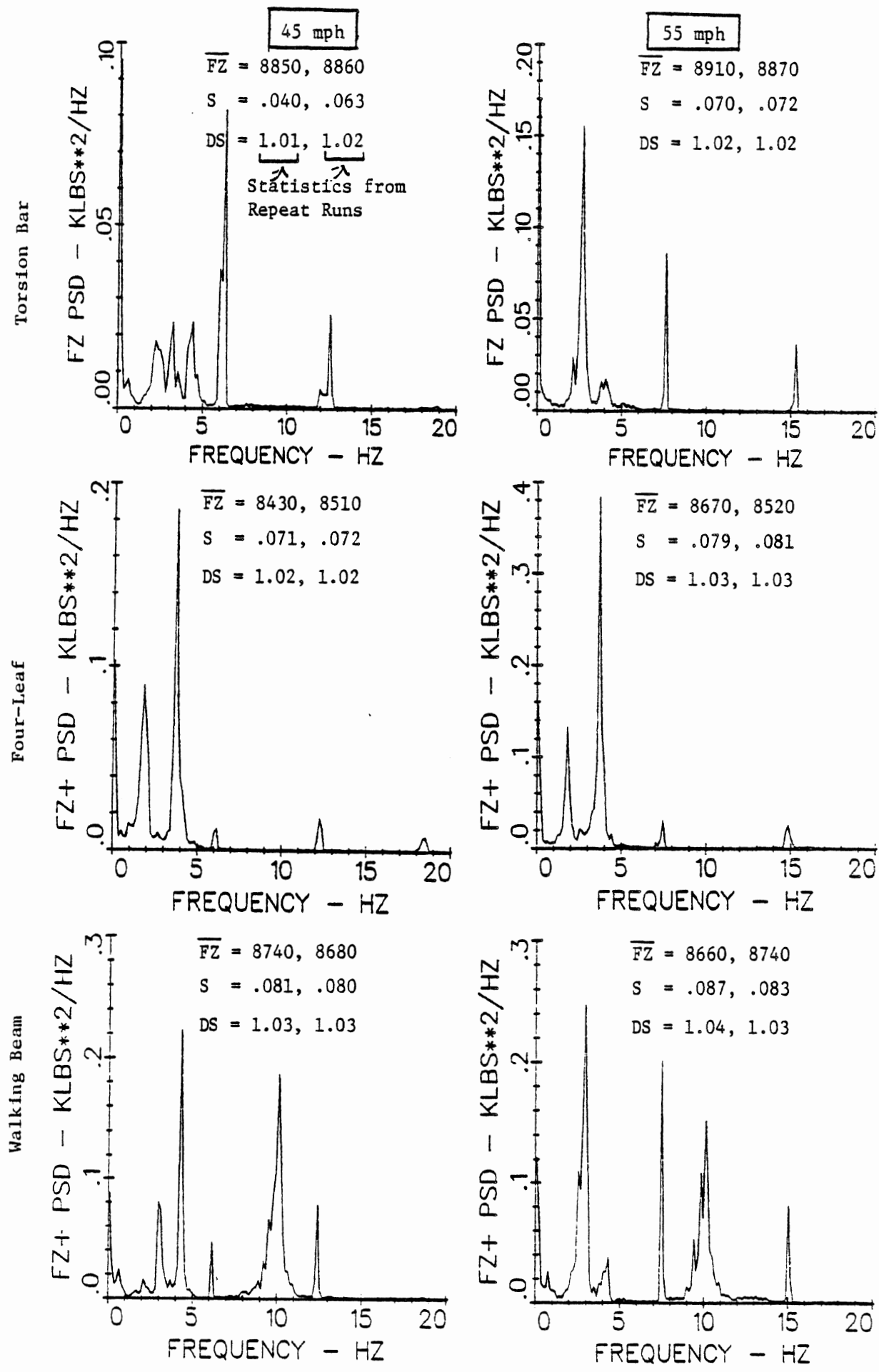


Figure 52. Response of vehicles on a smooth bituminous roadway (Site #1).

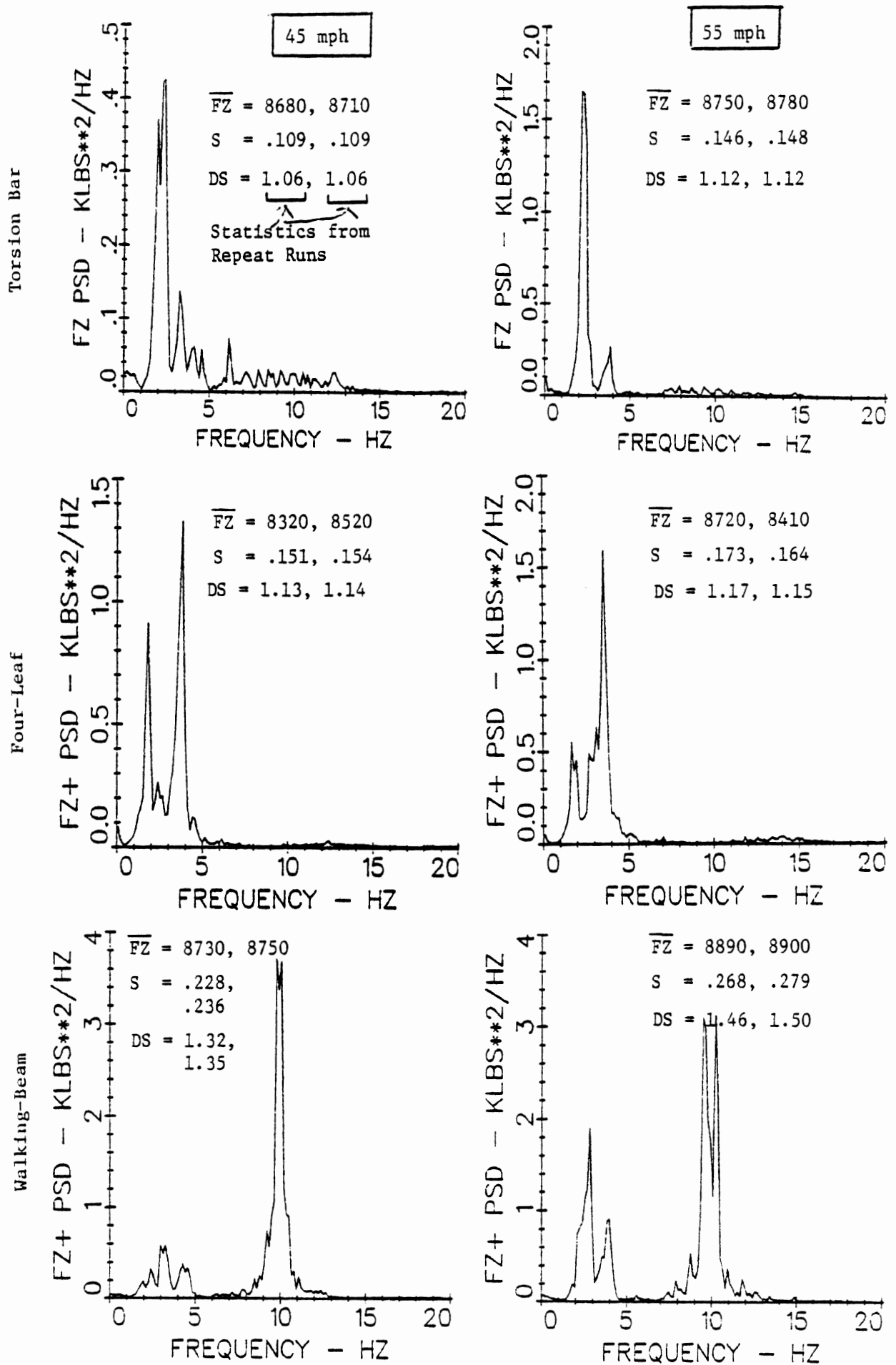


Figure 53. Response of vehicles on aged Portland cement concrete roadway with considerable faulting, cracking, and patching (Site #2).

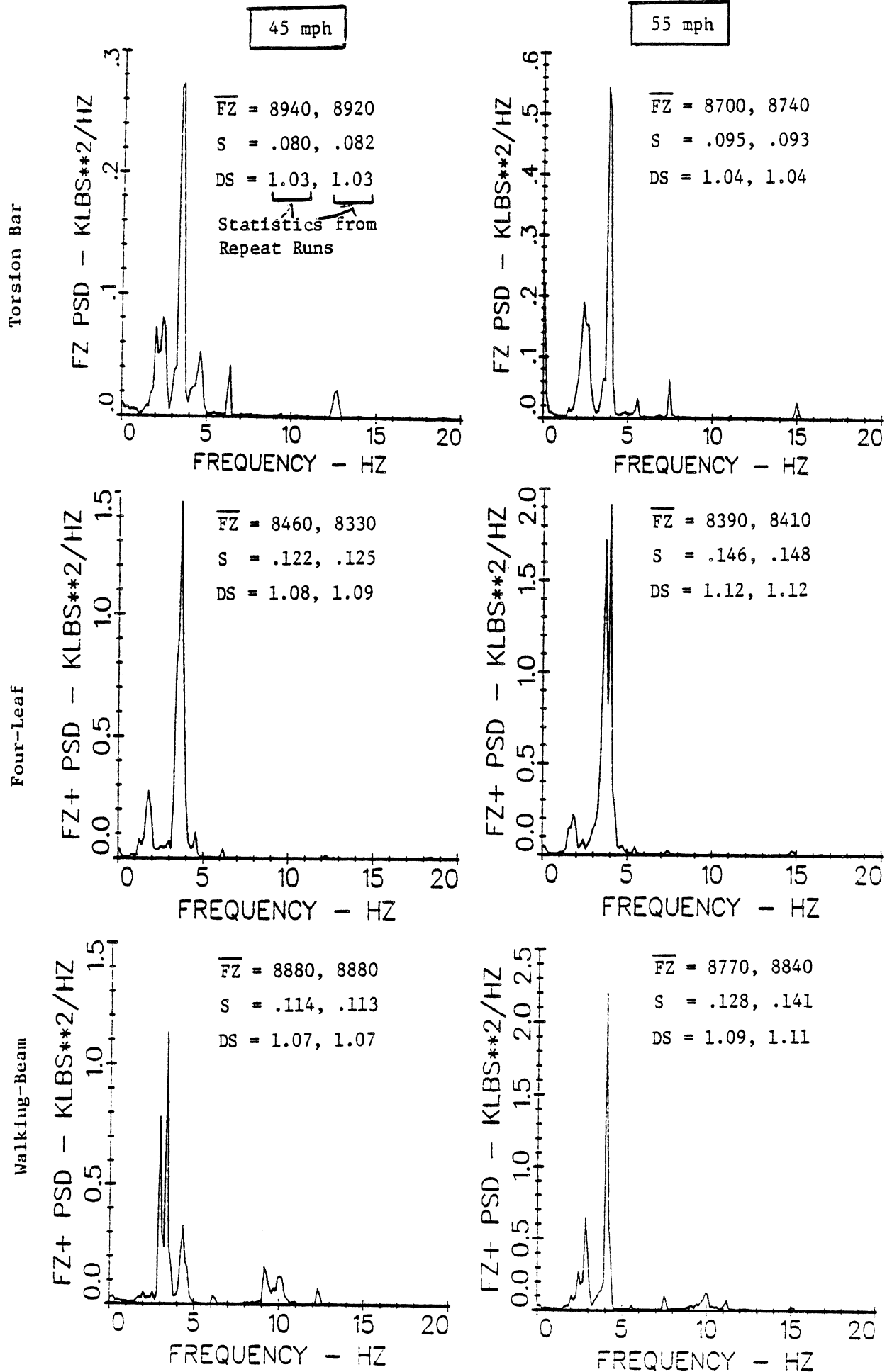


Figure 54. Response of vehicles on new Portland cement concrete roadway (Site #3)

1. The Power Spectral Density (PSD) of the axle load.
2. The mean (static) vertical load.
3. s - Dynamic Index (the standard deviation of the load normalized by its mean value).
4. DS - Dynamic Pavement Stress Factor (the average value of the instantaneous load to the fourth power, divided by the fourth power of the mean load). Based on the rule that pavement damage is proportional to the fourth power of the applied load, this parameter is then the ratio of actual damage to that predicted on the basis of static axle load. If the loads are random with a Gaussian (normal) distribution, DS can also be calculated as:

$$DS = 1 + 6 * s^2 + 3 * s^4$$

The values obtained by the two calculation methods were usually similar, indicating that the loads are approximately Gaussian in their distribution, as was also found in England [30].

Inasmuch as all experimental tests were replicated, two values are shown for each statistic, giving the reader an indication of the degree of repeatability obtained in the testing.

The PSD's show the distribution of the dynamic wheel loads in the frequency spectrum. They are characterized by a number of "peaks" representing different modes of vehicle vibration that contribute to the overall dynamic load. Plotted as they are, in linear-linear format, the total area under the PSD is equal to the mean square dynamic force (after the static load is subtracted). The height of any peak is not especially significant, as it will vary with the data processing methods used. However, the relative area under any peak does provide an accurate picture of how much that vibration mode contributes to the overall dynamic loads produced by that vehicle. For example, Figure 53 shows that most of the dynamic wheel loads imposed on this site by the torsion-bar suspension occur near 2 Hz (as a result of rigid-body bounce modes). On the other hand, the much larger dynamic load

variations with the walking-beam suspension are concentrated in the 10 Hz resonance range (associated with axle mode vibrations). Thus this vibration mode is primarily responsible for the pavement damage caused on this site by dynamic loading from this vehicle.

4.4 Corroboration with Sweatman's Findings

By and large, the results obtained in this study support Sweatman's findings in Australia when the test conditions were repeated. (Note, however, that this study did not cover the wide range of vehicle types studied by Sweatman, nor the effects of tire inflation pressure and vehicle loading.) Close numerical comparison of the results is not possible because the Australian measure of road roughness is not internationally transferable at this time. (Comparison of the dynamic indices reported here and by Sweatman would indicate that "rough" in this report is nominally equivalent to "medium-rough" in Australia.) Specific comments follow, made in the context of Sweatman's previously reported findings.

4.4.1 Effect of Road Roughness on Dynamic Index. The data from this experiment are summarized in Figure 55, showing Dynamic Index, s , as a function of roughness. (Approximate levels of the Present Serviceability Index (PSI)—an older measure less precise than RARV—are also indicated because the PSI scale is more familiar to many highway engineers.) Two of the vehicles show simple relationships between roughness and s , although the third (four-leaf suspension) shows little difference in response to the "medium" site #2 and "rough" site #3.

The dynamic index is not simply proportional to roughness, for even when the roughness is nearly zero (obtained by conducting tests on a smooth road at a speed less than 5 mph (8 km/h), the dynamic index is about the same as found on site #1.

Qualitatively, these results agree with those of Sweatman. The overall magnitudes of dynamic index are also supported by the TRRL research in England involving single-axle suspensions. The nonlinear relationship between roughness and dynamic loads has also been predicted analytically [34,35].

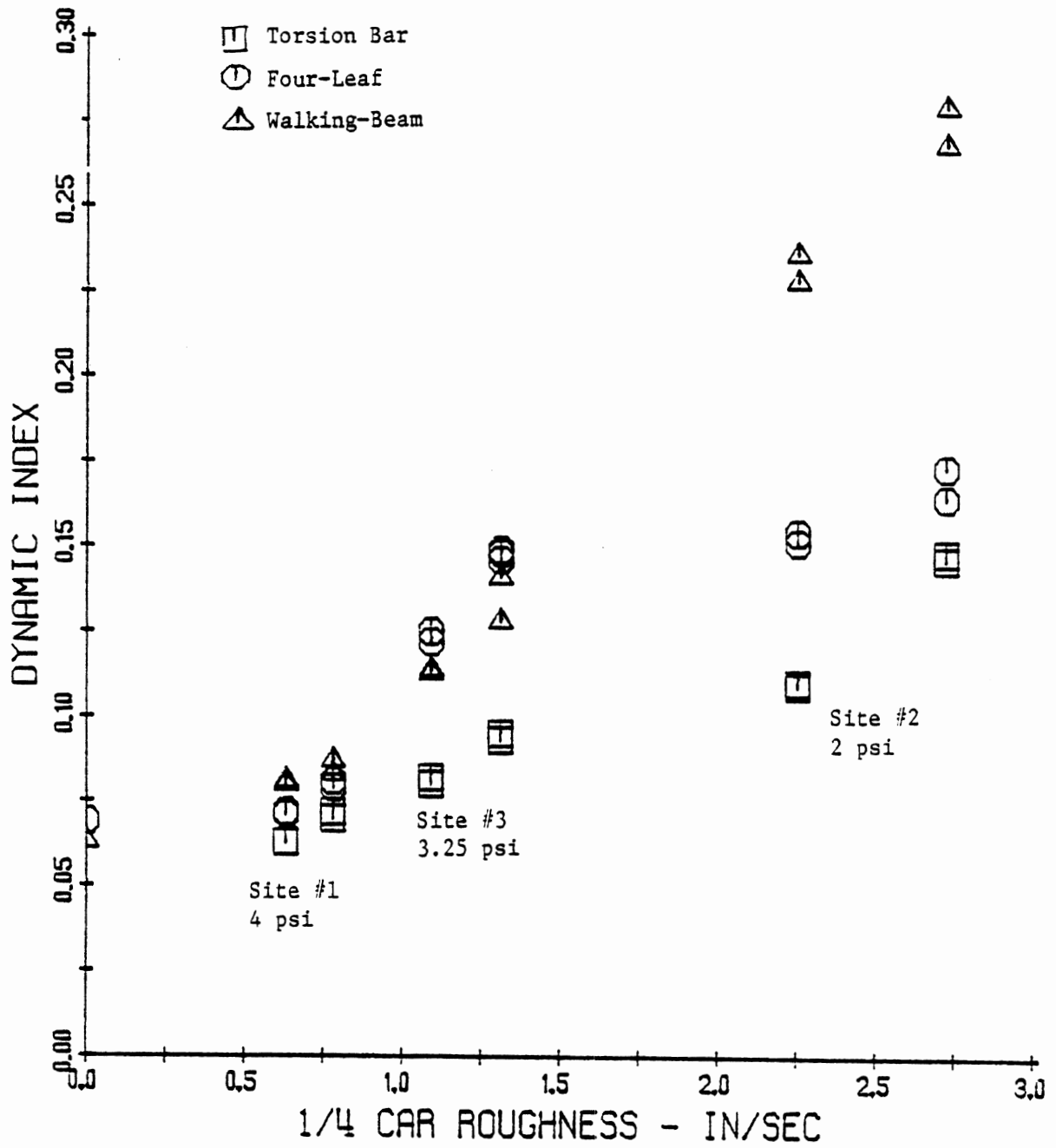


Figure 55. Summary of dynamic indices.

4.4.2 Effect of Suspension Type on Dynamic Index. Figure 55 also shows that the ranking of suspension type agrees with that of Sweatman: the torsion bar produces the least dynamic loading, while the walking beam produces the most. It may be concluded that the dynamic loads imposed on the highways by trucks will be at least 5% (equivalent dynamic index) on the smoothest roads. The dynamic loads increase with roughness to 15-30%, depending on the suspension type on the truck, at roughness levels associated with paved roads in need of repair (approximately 2PSI).

The influence of suspension type as observed in the Australian study is probably understated because the axle acceleration effects were not taken into account in the data reduction. From the measurements made here, it is estimated that the dynamic loads observed for the walking-beam suspension in the Australian study would be underestimated by around 30%, while not seriously influencing the measures for the four-leaf and torsion-bar suspensions.

4.4.3 Effect of Vehicle Speed on Dynamic Index. As speed increases, so does the excitation imposed on a vehicle by a road. Hence, any measure of dynamic response, including dynamic pavement loading, will also increase. In the data reported by Sweatman, the change in dynamic index with speed included both the effects of changing excitation from the road (as a consequence of the way in which roughness was quantified), and the changing dynamic response of the vehicle. In contrast, the results from these tests take into account the way in which the roughness, as perceived by a vehicle, changes with travel speed. The six roughness levels identified in Figure 55 correspond to three test sites and two travel speeds. In comparison, on the Australian scale or the PSI scale only three roughness levels would be defined. By using a roughness definition based on the actual travel speed, the dynamic loads as reported here can be validly attributed solely to vehicle dynamic properties.

4.4.4 Effect of Inter-Axle Load Transfer. Truck tandem suspensions are designed with the general intent of providing load sharing between the axles of the tandem set. These goals are achieved within reason in the static situation, although it has been observed that the mean loads "on-road" will vary with driving or braking forces, vehicle attitude, or other factors. While an accurate measure of inter-axle load transfer requires that both axles in a tandem suspension be instrumented, the load transfer can be estimated by comparing the mean load measured during testing with its supposed "static" value (one-half of the suspension load measured statically on truck axle scales). Sweatman estimated load transfer by this method, and reported figures ranging from 5% to 20%, with the range 5%-10% being "typical." Sweatman's calculations were based on the assumption that all load variations between wheels are negligible compared to the inter-axle transfer in tandem (and triple) suspensions. Given the relatively small changes noted, and the large number of other possible effects (change in pitch or roll angle of vehicle between scales and road; movement of suspension due to free-play in linkages; random variations due to friction hysteresis), the calculated load transfers might contain significant measurement errors. Figures 52-54 show that the variation in the field between tests is on the order of 5%, and that there are no obvious trends between roughness and static load for the three vehicles tested in this survey.

Overall, errors caused by assuming axle loads that are not actually transduced could possibly cause the apparent inter-axle load transfer reported by Sweatman. The significance of inter-axle load transfer relative to dynamic loading is discussed later.

4.4.5 Effect of Tire Inflation Pressure on Dynamic Index. One of the less significant (but most surprising) observations in the Australian study is that dynamic loads are increased by lowering tire pressure. This observation is at odds with what might generally be expected from the analytical understanding of road/vehicle interactions and is also contrary to experimental results reported in England [30]. Decreasing tire inflation pressure will decrease tire stiffness, which under most circumstances lowers the dynamic loads. Only when that change in stiffness allows a particular

vehicle to "tune" one of its dynamic modes to a specific test condition would increased loads be expected. In the Australian study, this latter anomaly could have prevailed on the test vehicles used; however, it is also possible that the absence of corrections for axle accelerations would erroneously indicate an increase in load level at the lower inflation pressure. The decrease in axle resonant frequency at the lower values of inflation pressure would decrease the magnitude of the tire load component which was being "absorbed" through acceleration of the outboard mass, thus causing the load cell to "see" a greater portion of the total tire loading. Such a line of reasoning could explain why Sweatman observed an apparent increase in dynamic load when tire inflation pressure was reduced.

4.5 Relative Importance of Dynamic Loads to Pavement Damage

The primary motivation for investigating the dynamic wheel loads of heavy vehicles is that accelerated pavement deterioration can occur because of actual instantaneous loads that are higher than would be expected from the static wheel loads measured on truck axles. In a statistical sense, occasional high loads are compensated by corresponding low loads (what goes up must come down). But based on the current understanding that pavement stress is proportional to the fourth power of load, the increase in damage during instances of high load is not completely cancelled during the periods of low load. The dynamic stress factor, DS, used by Sweatman is the ratio of the instantaneous load to the fourth power, divided by the mean load to the fourth power. As such, it is a measure of the proportional increase in pavement damage caused by the dynamic load variations. When the forces are random and Gaussian, DS is a function of the dynamic index, s (standard deviation of load, divided by mean load), as shown earlier.

A second factor, when multi-axle suspensions are in use, is an inter-axle load transfer that prevents the suspension load from being equally distributed among the axles. Using the same concept of the DS, the "equivalent damage" can be quantified from this effect as a Load Transfer Pavement Stress Factor LS:

$$LS = [(1 + d)^4 + (1 - d)^4]/2$$

where

$$d = (\text{Mean load} - \text{Static load})/\text{Static load}$$

The above expression can be expanded and rewritten:

$$LS = 1 + 6 * d^2 + d^4$$

The expression for LS is very similar to that for DS, differing only in the fourth-order term. For the range of conditions covered in this study, the effect of this difference is less than 4% for the highest variation observed. Thus, in one sense, the pavement damaging effects of inter-axle load transfer closely parallel those of dynamic loading. For example, a dynamic index of 15% has the same effect as an axle load-sharing imbalance of $\pm 15\%$, except that the load-sharing imbalance constitutes a static force which is continuously applied to the road.

Although dynamic index and inter-axle load transfer (s and d) are seen to be equivalent in the above statistical sense, they describe different mechanisms that are not completely interchangeable. The major difference is that d, the inter-axle load transfer, is approximately constant for different road inputs, whereas s, the dynamic index, involves the direct response of the vehicle to road inputs. On very smooth roads, the dynamic index will be about 5%. Inter-axle load imbalances greater than this (say, 10% or more), will be the main source of "extra" damage not accounted for by regulated static loads. But on rougher roads, the dynamic index of 15-30% will be the primary extra factor in road damage, overwhelming the smaller inter-axle imbalance. (Note that since inter-axle load transfer, d, can result from the reaction of drive torque, the value of d can also be seen to depend upon the roughness level insofar as increased drive torque is needed to maintain speed on rougher roads. Nevertheless, this effect is expected to be weak compared to the direct influence of roughness on the dynamic index.)

Another distinguishing characteristic of dynamic loading is that it is the direct result of road profile. Although summary statistics are most easily used to quantify the magnitude of the excess loads, the actual instantaneous loads are the result of the profile geometry "feeding back" through the mechanism of vehicle response. Figure 56 indicates, for example, that all three of the test vehicles show a minimum dynamic loading approximately 14 seconds into the example test section, and then display a maximum loading 3-4 seconds later. Regardless of the statistical measure for that one-mile section, the pavement area corresponding to approximately 17 seconds into the test takes an extreme beating from all of the vehicles. This effect is mainly amplified by the dynamic responses of the vehicles, rather than by the load-sharing performances of the suspensions.

4.6 The Role of Vehicle Dynamics in Pavement Load

Figures 56 and 57 illustrate the differences in vehicle response to identical road excitation by comparing the actual measured wheel forces of the three test vehicles on the roughest test site. We see in Figure 56 that the responses of the respective vehicles share little in common overall.

On the other hand, the PSD plots shown earlier in Figures 52-54 shed some light on how differences in suspension design cause various levels of dynamic loading. In every case, the PSDs contain most of the dynamic loading within a few narrow "peaks." Peaks such as these, when obtained in response to broad-band road inputs as shown in Figure 51, indicate that lightly-damped modal resonances account for most of the dynamic loading. The resonances tend to be concentrated within two bands, one in the 2-4 Hz range for all vehicles, and one centered around 10 Hz for the vehicle with the walking-beam tandem suspension. Figure 57 shows how these modal vibrations appear as time histories. Although the modal resonance properties of the test vehicles were not investigated in this work, the knowledge of truck vibration properties available from other research can suggest what resonance modes may be involved.

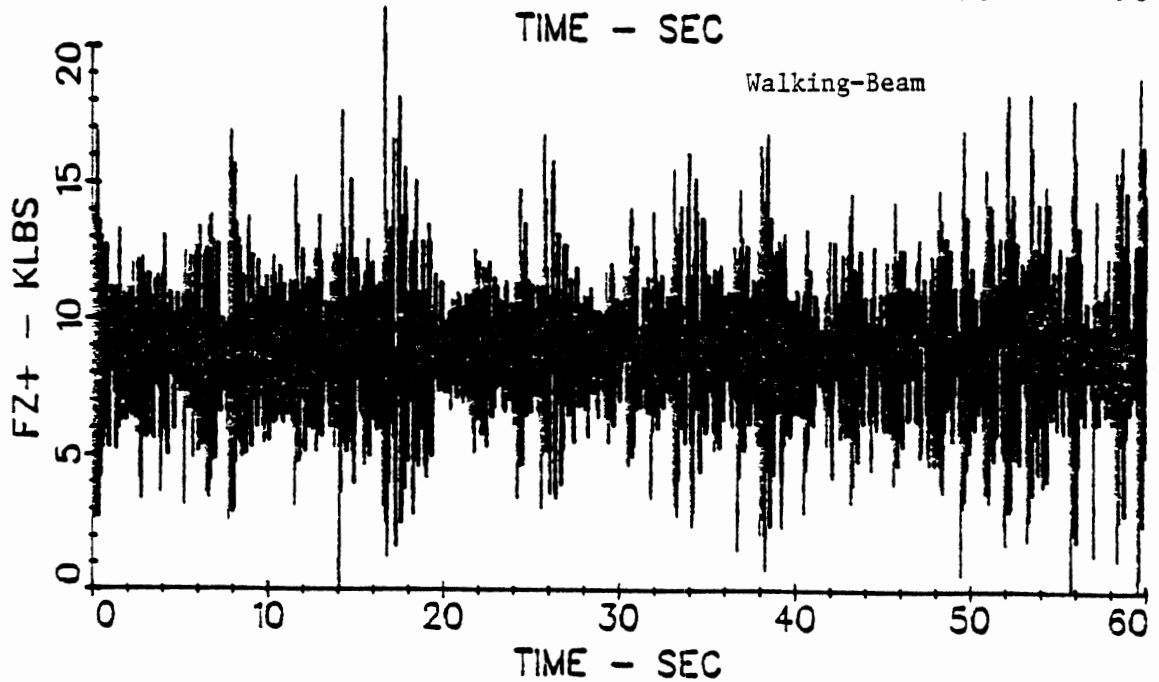
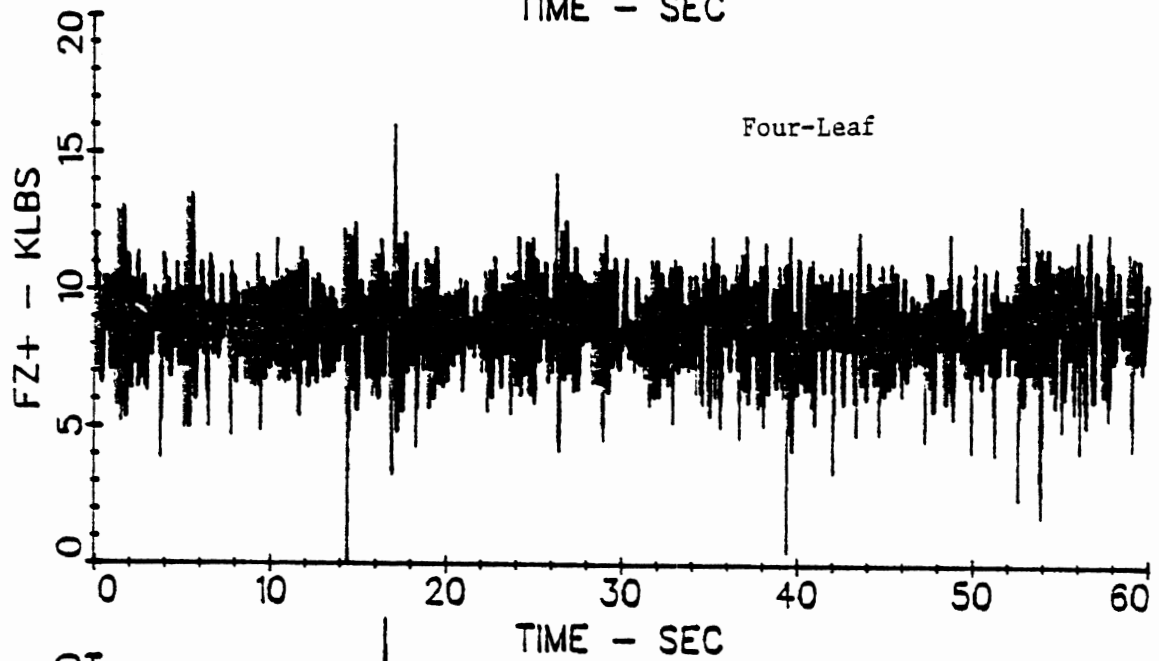
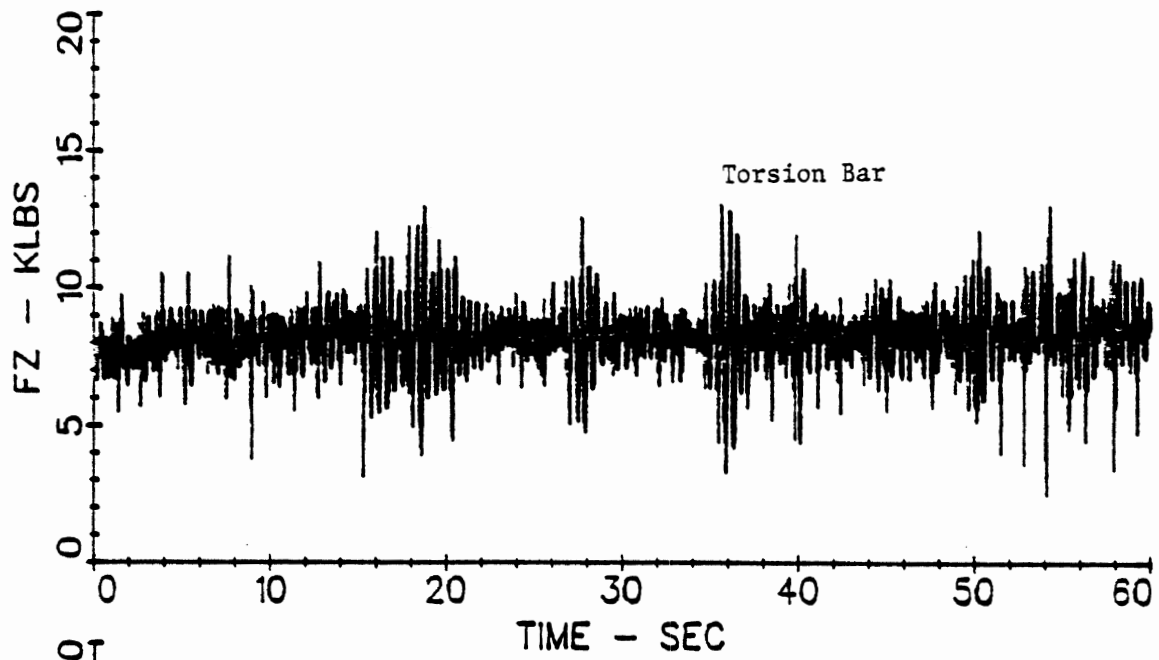


Figure 56. Comparisons of three vehicle responses to the same road input (Note: signals are not accurately synchronized).

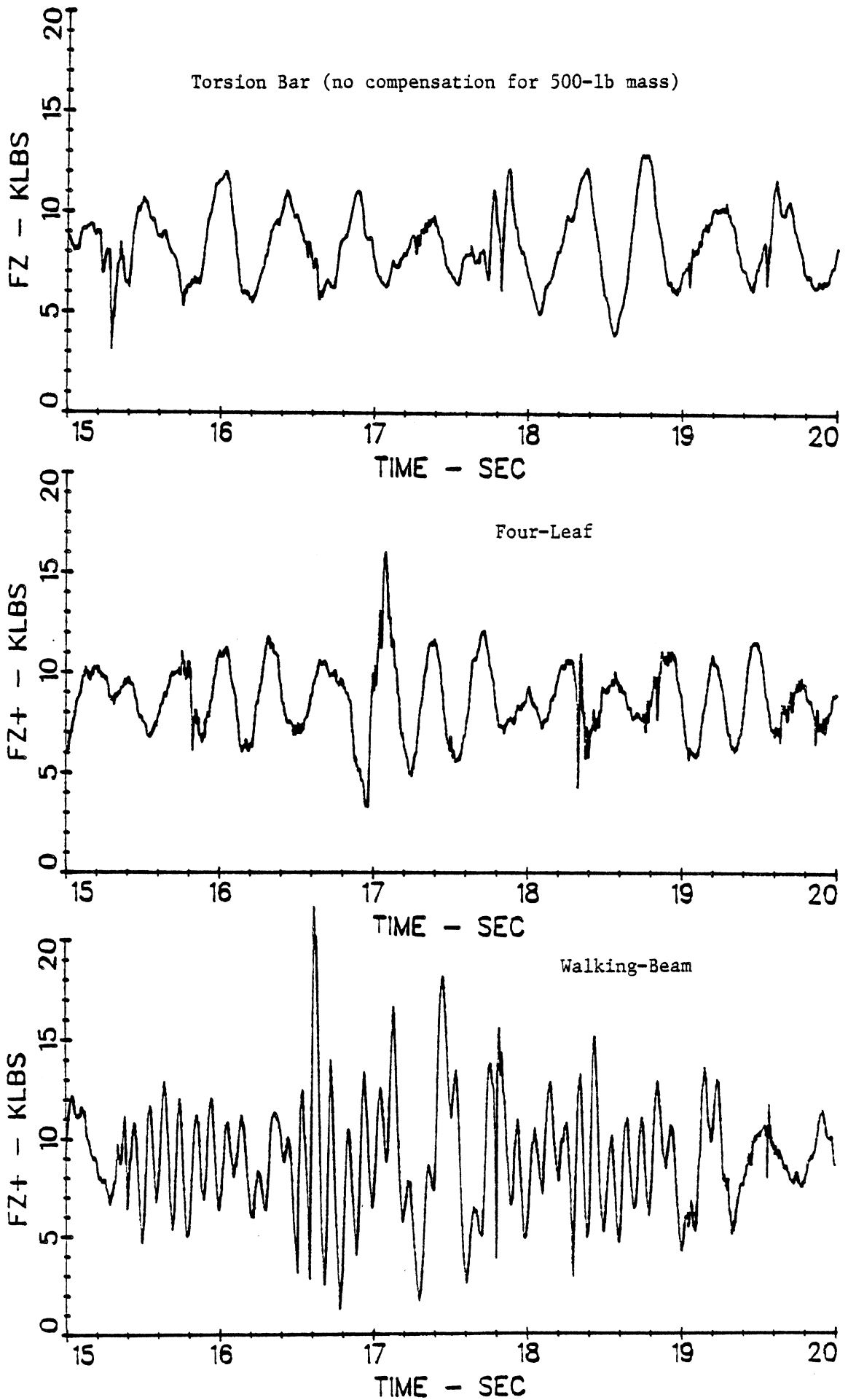


Figure 57. Comparison of three vehicle responses to the same road input (Note: signals are not accurately synchronized).

Resonances in the 2-4 Hz range with heavy commercial vehicles are almost exclusively rigid-body vibration modes involving bounce and/or pitch of the tractor and trailer. These are controlled by the stiffness of suspension systems and tires, the general mass properties, and the overall sizes (lengths) of the tractor and trailer. Although suspension design is but one of many vehicle variables, effects of other variables are held somewhat in check because all of the test vehicles used the same trailer and were loaded so that the instrumented axles always carried the same (maximum rated) load. The rigid-body modes are evident in the spectra for all three vehicles under all conditions, although they do not always dominate on the tractor with the walking-beam suspension. The torsion-bar suspension is clearly best in this mode, being least responsive in causing dynamic loading to occur. The four-leaf suspension tends to be slightly worse than the walking-beam in these modes, although the fact that the four-leaf suspension was installed on a semitrailer, while the walking-beam was installed on a tractor, may strongly influence the relative magnitudes observed (i.e., the dynamic differences between the tractor and trailer may be more significant in this case than the differences between suspension types).

Resonances at 10 Hz and above involve either axle resonances or structural modes of the vehicle (frame-bending modes, etc.). The combined stiffness of the tires and suspension system will normally result in an axle resonant frequency of 15 Hz and above. However, in the special case of the walking-beam type of suspension, there is a vibration mode which does not involve deflection of the suspension, thus resulting in a natural frequency near 10 Hz with tractor drive axles. This mode, often called the "tandem-hop" mode, occurs when the front and rear axles of the tandem pair bounce out of phase. The mode may be excited by the passage of road bumps first under the front and then under the rear axle. With a 10 Hz resonance frequency, for example, this mode will be directly excited when the time delay of road bumps passing under the front, and then rear, axles is 1/20 of a second. With closely spaced tandem-axle sets (typically 4 to 4.5 feet (1.22 m to 1.37 m) apart), excitation of this mode can readily occur at normal highway speeds (say, 80 ft/sec (24 m/sec)). On the roughest road site (see Figures 53 and 57), this mode is seen to be well excited and dominates as a source of dynamic loading for this vehicle.

4.7 Conclusions

The study on dynamic wheel loads generated by loaded tractor-semi-trailers has corroborated earlier findings by P. Sweatman in Australia, confirming that instantaneous loads can be large enough that accelerated pavement deterioration may be expected, and that the magnitude of those loads is influenced by road roughness and vehicle suspension design. Of the three suspension designs represented, dynamic loading was least with a torsion-bar design and greatest with a walking-beam type. A conventional trailer four-leaf suspension fell in the middle. The difference in dynamic pavement loading between the four-spring and the walking-beam can be attributed in this example to high-frequency (10 Hz) axle vibrations, present with the walking-beam but not the four-spring suspension.

Although dynamic wheel loads imposed by a vehicle usually increase with "roughness," the responses of individual vehicles are often different enough that one might "tune in" to a particular road, resulting in high loads, while another might be relatively unresponsive to that same road. The relationship between dynamic wheel load and roughness is generally nonlinear. For example, dynamic loads of about 5% exist even on very smooth roads for the vehicles tested in this study.

Dynamic wheel loads associated with a vehicle/road combination generally increase with speed, but this effect is due mainly to the increased apparent roughness of the road with speed. When the roughness measurements are made at the same speed as used by the truck according to the procedures recommended in NCHRP Report 228, the speed is no longer a primary variable. Rather, the truck response and the corresponding dynamic loads are seen to be only a function of roughness for a specific vehicle.

A wheel-force transducer owned by FHWA was calibrated, evaluated, and found to be suitable for measurement of dynamic loads as they influence pavement stress, although additional instrumentation to measure vertical acceleration of the transducer is also recommended. Without this extra instrumentation (and subsequent data processing), measures of dynamic loads can be up to 30% too low. This is particularly important because the largest errors occurred when the dynamic loading was greatest and therefore most

critical. In the Australian research, a similar transducer was used without the extra instrumentation, with the result that the worst reported dynamic loads may actually be too low.

So far, measurements have been processed to yield simple summary statistics that are indicators of average pavement stress and resulting deterioration. In treating the data this way, the dynamic wheel loads are assumed to be essentially random, occurring with equal likelihood anywhere along a road. Yet the cause-effect relationship between roughness and dynamic loads seen in this data would suggest that the "randomness" feature is not a realistic picture of pavement loading mechanisms relevant to pavement deterioration. Especially on the rougher roads, where dynamic loading has been identified as a much greater problem, the dynamic loads are not random, but are the specific result of an interaction between road profile and the dynamic response of the passing vehicles. The peak loads (which inflict the most damage) resulting from specific road roughness features will therefore occur repeatedly in the same general locations on the pavement (just downstream from each roughness feature) with all traffic. For example, PCC slabs respond to vehicle loading by tilting, and they always tilt according to the direction of vehicle travel, with the leading edge being pushed down. Obviously, this systematic pattern cannot happen with dynamic loads that are completely random in their distribution. Instead, the discontinuity between slabs "feeds back," causing partially deterministic and asymmetric loading responses from the moving vehicles traversing the road. The repeatable asymmetry of the loading history eventually tilts the slab, thereby increasing the discontinuity and accelerating the effect. Similar effects can be expected to exist with other discontinuities, such as potholes or settlements at bridge approaches. Thus the cause-effect relationship demonstrated here should add new insights to the mechanisms of pavement deterioration if applied appropriately.

When measurements of dynamic loading are presented in the form of average summary statistics, such as standard deviation and "dynamic pavement stress factor," very high peak levels are averaged in with lower "background" levels that more closely fit the concept of random vibrations. Yet with dynamic index values (standard deviations) approaching 30%, assuming a

Gaussian distribution, 1% of the road surface must see dynamic loads as high as 170% of the static value, with fourth power stress factors greater than 8; while the extremes, found to exceed 250% (see Figure 56 for the "walking-beam") of the static load level in this study, yield stress factors near 40. By the above reasoning, the pavement locations seeing these high stress levels are not randomly distributed along the length, but because of truck dynamic behavior, will occur repeatedly just downstream of the prominent roughness features.

Increases in pavement stress due to dynamic vehicle response were compared conceptually with increases due to inter-axle load transfer in tandem suspensions. When normalized by static load, the two variations are seen to be statistically identical in terms of pavement stress, although occurring in different patterns on the road surface. On very smooth roads, the inter-axle load transfer may be a more identifiable factor in pavement stress, but on rougher roads in which deterioration is accelerated by "feedback" of roughness through vehicle response, the dynamic loading should be of greater concern.

4.8 Recommendations

Having taken this brief look at dynamic pavement loading by heavy commercial vehicles, many potentially fruitful areas for further investigation become obvious. The needs fall into two categories: investigation of the road surface response to heavy traffic to better understand the mechanisms of distress, and investigation of the dynamic behavior of heavy vehicles to clarify the dynamic loading phenomena and the influence of pavement and vehicle properties on pavement loading.

4.8.1 Road Surface Response. The pioneering effort at quantifying the roadway distress caused by heavy vehicle traffic occurred in the AASHO Road Tests in the late 1950's. From this and subsequent work have emerged the formulas relating roadway deterioration to equivalent axle loads. These equations for estimating pavement damage, however, have been developed without benefit of the current knowledge of how the dynamic loadings are affected by choice of vehicle, or the roughness/speed influences. Thus, the equations

are likely to yield significant errors in predicting the road-damaging effects of truck axle loading with changes in the primary variables. Over the years:

1. truck tire and suspension designs go through normal evolutionary changes,
2. road roughness levels and mean traffic speeds change,
3. fleets respond to changing road conditions in new vehicle specifications (e.g., specifying more rugged suspension systems as the roads deteriorate),
4. truck configurations (wheelbases, number of trailers, axle locations, etc.) change with new road-use laws, and
5. the technology in new highway construction (for example, influencing initial roughness) improves.

With the pressure for improving the efficiency of commercial highway transport by liberalizing the size and weight restrictions, a more complete understanding of the damage caused by truck axle loads is essential if highway costs are to be fairly assessed and distributed.

More recent research on road surface failure arising from traffic loads [36] provides insights on the mechanisms of failure, which, if combined with the understanding of road/vehicle load interactions, can provide more comprehensive models for the equations relating road deterioration to vehicle loadings. For example, the simple cumulative deflection models developed by Harr [36] could be combined with stochastic models of vehicle dynamic behavior to yield simple, yet powerful, models for predicting road deterioration, perhaps even extending to prediction of its location on the highway. Such models would provide valuable contributions in the development of more rational strategies for selective maintenance actions in modern pavement management systems.

4.8.2 Vehicle Response. Inasmuch as vehicle design and operating variables have been shown to have a dominating influence on the dynamic loads imposed on pavements, additional research in this area would be in the direct

interests of the FHWA. A more comprehensive understanding of the variables and mechanisms responsible for accentuating dynamic loads would not only provide a rational basis for truck load regulation, but will provide incentive to truck manufacturers and users to adopt more desirable vehicles.

In either of these research areas, the instrumentation systems the FHWA has acquired are suitable as primary experimental tools. Knowing that instantaneous loads can reach levels 250% higher than the static loads, an important step is to determine when and where these extremely damaging forces arise. Research is needed to determine how existing pavement features interact with the different types of heavy vehicles on the road to result in high instantaneous loads "down the road." Unlike load cells fixed in the road, the FHWA wheel-force transducer offers flexibility by permitting force measurements to be taken continuously over the entire length of a test site, along with the option to include many different sites with no additional instrumentation requirements.

Since the instrumentation needed for measuring dynamic load and longitudinal profile are both mounted in vehicles, a viable approach would be to test vehicles instrumented to measure load and profile simultaneously. This would allow easy identification of those aspects of road profile that induce the highest loads "down the road" through the medium of heavy vehicles, over all types of road disturbances.

REFERENCES

1. Murphy R.W., Bernard, J.E., and Winkler, C.B. "A Computer-Based Mathematical Method for Predicting the Braking Performance of Trucks and Tractor-Trailers." Phase I Report: Motor Truck Braking and Handling Study, Highway Safety Research Institute, Univ. of Michigan, Rept. No. UM-HSRI-PF-72, September 15, 1972.
2. Bernard, J.E., Winkler, C.B., and Fancher, P.S. "A Computer-Based Method for Predicting the Directional Response of Trucks and Tractor-Trailers." Phase II Report, Highway Safety Research Institute, Univ. of Michigan, Rept. No. UM-HSRI-PF-73-1, June 1, 1973.
3. Mallikarjunarao, C. "Road Tanker Design: Its Influence on the Risk and Economic Aspects of Transporting Gasoline in Michigan." Ph.D. Dissertation, University of Michigan, December 1981.
4. Fancher, P.S. "Braking Performance of Commercial Vehicles Equipped with Antilock Systems." Simulation Councils Proceedings Series, Vol. 7, No. 2, December 1977, pp. 167-176.
5. Ervin, R.D., et al. "Ad Hoc Study of Certain Safety-Related Aspects of Double-Bottom Tankers." Final Report, Sponsored by Michigan State Office of Highway Safety Planning, Contract No. MPA-78-002A, Highway Safety Research Institute, Univ. of Michigan, Rept. No. UM-HSRI-78-18, May 7, 1978.
6. Gillespie, T.D. "Validation of the MVMA/HSRI Phase II Straight Truck Directional Response Simulation." Highway Safety Research Inst., Univ. of Michigan, Rept. No. UM-HSRI-78-46, October 1978.
7. "Instrumentation of Test Trucks for Measuring Pavement-Vehicle Interactions." Contract No. FH-11-9289, Systems Technology Inc.
8. Pacejka, H.B. "Simplified Analysis of Steady Turning Behavior of Motor Vehicles. Parts 2 & 3." Vehicle System Dynamics, Vol. 2, No. 4, December 1973.
9. Ervin, R.D. and Mallikarjunarao, C. "A Study of the Yaw Stability of Tractor-Semitrailer Combinations." Proc. 7th IAVSD Symposium on the Dynamics of Vehicles on Roads and Tracks, Cambridge, England, September 7-11, 1981.

10. Tielking, J.T., Fancher, P.S., and Wild, R.E. "Mechanical Properties of Truck Tires." SAE Paper No. 730183, January 1973.
11. Thurman, G.R. and Leasure, W.A., Jr. (Eds.). "Noise and Traction Characteristics of Bias-Ply and Radial Tires for Heavy Duty Trucks." Rept. No. DOT-TST-78-2, October 1977.
12. Office of Heavy Duty Vehicle Research. "Stopping Distance Test Data on Air Braked Vehicles." National Highway Traffic Safety Admin., U.S. Dept. of Transp., February 7, 1980.
13. Federal Register 39:221, November 4, 1974, pp. 4016-4019.
14. Radlinski, R., Machey, J., and Williams, S. "The Importance of Maintaining Air Brake Adjustment." SAE Paper No. 821263, November 1982.
15. Fancher, P.S. "The Transient Directional Response of Full Trailers." SAE Paper No. 821259, November 1982.
16. Mallikarjunarao, C. and Fancher, P. "Analysis of the Directional Response Characteristics of Double Tankers." SAE Paper No. 781064, December 1978.
17. Mallikarjunarao, C., Ervin, R.D., and Segel, L. "Roll Response of Articulated Motor Trucks During Steady-Turning Maneuvers." ASME, Winter Annual Meeting, November 1982.
18. Mallikarjunarao, C. and Segel, L. "A Study of the Directional and Roll Dynamics of Multiple-Articulated Vehicles." Proc. 7th IAVSD Symposium on the Dynamics of Vehicles on Roads and Tracks, Cambridge, England, September 7-11, 1981.
19. MacAdam, C.C., et al. "A Computerized Model for Simulating the Braking and Steering Dynamics of Trucks, Tractor-Semitrailers, Doubles, and Triples Combinations - User's Manual." Final Rept., MVMA Proj. 1197, Highway Safety Research Inst., Univ. of Michigan, Rept. No. UM-HSRI-80-58, September 1, 1980.
20. Gillespie, T.D., et al. "Truck and Tractor-Trailer Dynamic Response Simulation--T3DRS." Final Rept., Contract No. FH-11-9330, Highway Safety Research Inst., Univ. of Michigan, Rept. No. UM-HSRI-79-38, March 1979.
21. Ervin, R.D., et al. "Effects of Tire Properties on Truck and Bus Handling." Final Rept., Contract No. DOT-HS-4-00943, Highway Safety Res. Inst., Univ. of Michigan, Rept. No. UM-HSRI-76-11, December 1976.
22. Fancher, P.S., et al. "Measurement and Representation of the Mechanical Properties of Truck Leaf Springs." SAE Paper No. 800905, November 1980.

23. Fancher, P.S. (Ed.). "Descriptive Parameters Used in Analyzing the Braking and Handling of Heavy Trucks." Vols. 1 and 2, Highway Safety Research Institute, Univ. of Michigan, Rept. No. UM-HSRI-81-19-1 & 2, 1981.
24. Winkler, C.B. and Hagan, M. "A Test Facility for the Measurement of Heavy Vehicle Suspension Parameters." SAE Paper No. 800906, August 1980.
25. Segel, L., et al. "Mechanics of Heavy-Duty Trucks and Truck Combinations." Engineering Summer Conferences, Univ. of Michigan, June 1981.
26. Bernard, J.E. and Vanderploeg, M. "Static and Dynamic Offtracking of Articulated Vehicles." SAE Paper No. 800151, February 1980.
27. Ervin, R.D., Mallikarjunarao, C., and Gillespie, T.D. "Future Configuration of Tank Vehicles Hauling Flammable Liquids in Michigan." Final Rept. to Mich. Dept. of Transp., Agreement #78-2230, Highway Safety Res. Inst., Univ. of Michigan, Rept. No. UM-HSRI-80-73, December 1980.
28. Ervin, R.D., et al. "The Yaw Stability of Tractor-Semitrailers During Cornering." Final Rept., Contract No. DOT-HS-7-01602, Highway Safety Res. Inst., Univ. of Michigan, Rept. No. UM-HSRI-79-21, June 1979.
29. Sweatman, P.F. "Effect of Heavy Vehicle Suspensions on Dynamic Road Loading." ARRB Internal Rept. #AIR 264-3, February 1980.
30. Dickerson, R.S. and Mace, D.G.W. "Dynamic Pavement Force Measurements with a Two-Axle Heavy Goods Vehicle." TRRL Supplementary Report 688, 1981.
31. Gillespie, T.D., et al. "Truck Cab Vibrations and Highway Safety." Univ. of Michigan, Rept. No. UM-HSRI-82-9/2, March 1982.
32. Gillespie, T.D., Sayers, M.W., and Segel, L. "Calibration of Response-Type Road Roughness Measurement Systems." NCHRP Report #228, December 1980.
33. Sayers, M., Gillespie, T.D., and Queiroz, C. "International Experiment to Establish Correlations and Standard Calibration Methods for Road Roughness Measurements." University of Michigan, Rept. No. UMTRI-82-45-1, December 1982.
34. Sayers, M. and Gillespie, T.D. "The Effect of Suspension System Nonlinearities on Heavy Truck Vibration." Proceedings of 7th IAVSD Symposium on Dynamics of Vehicles on Roads and Tracks, Cambridge, England, September 1981.

35. Ilosvai, L., et al. "Random Vehicle Vibrations as Effected by Dry Friction in Vehicle Suspensions." Vehicle System Dynamics, Vol. 1, No. 3-4, December 1972, pp. 197-210.
36. Heighter, W.H. and Harr, M.E. "Cumulative Deflection and Pavement Performance." Transportation Engineering Journal, Purdue University, August 1975.
37. Hazemoto, T. "Analysis of Lateral Stability for Doubles." SAE Paper No. 730688, June 1973.

APPENDIX A

DATA PROCESSING PROGRAM DESCRIPTION

Presented below are outlines of the four subprograms employed in processing raw data tapes obtained in the braking-in-a-turn, trapezoidal-steer, double-lane-change, and sinusoidal-steer tests. A summary of the subprogram for processing the straight-line braking data was presented in the text under Section 2.1.4 "Data Processing."

**** Subprogram #2 (Braking-in-a-Turn) ****

-Duplicates first three items under Subprogram #1.

-Calculates the following numerics over the maneuver interval:

- a) Initial vehicle velocity, V_0 (ft/sec)
- b) Average brake line pressure, P_B (psi)
- c) Stopping distance from integration of forward velocity, corrected for initial velocity variations, D^* (ft)
- d) Average longitudinal deceleration, A_X (g's)
- e) Initial lateral acceleration prior to brake application, A_{Y0} (g's)
- f) Stopping distance from double integration of longitudinal acceleration, corrected for initial velocity variations, D_{AX} (ft)
- g) Stopping time, T (sec)
- h) Tractor yaw rate peak, R_{IP} (deg/sec)
- i) Last trailer yaw rate peak, R_{NP} (deg/sec)
- j) Peak tractor/trailer articulation angle, G_{AM1} (deg)
- k) Peak articulation angle of last dolly with respect to the lead trailer (pintle hook angle), G_{AM2} (deg)

- l) Peak articulation angle of last dolly with respect to the last trailer, GAM3 (deg)
- m) Wheel lock indicator 0.0 (no) or 1.0 (yes) and the corresponding vehicle velocity at which it occurred.
For wheel speeds, $\omega_2, \omega_4, \omega_6, \omega_8, \omega_{10}$
 $\omega_1, \omega_3, \omega_5, \omega_7, \omega_9$

-Writes a header record containing run number, file number, and maneuver information on the output tape.

-Writes the above numerics to both the line printer and the output tape.

-Writes the following variables vs. time histories to both the line printer and the output tape:

- a) time, T (sec)
- b) forward velocity, V5 (mph)
- c) tractor longitudinal deceleration, AX1 (g's)
- d) tractor lateral acceleration, AY1 (g's)
- e) suspension deflections of tractor at wheel locations 1-6, Z1-Z6 (inches)
- f) tractor yaw rate, R1 (deg/sec)
- g) brake line pressure, PB (psi)

-Writes a tape mark on the output tape, closing the output tape file.

-Returns to Main program.

Figure A.1 shows an example printout for Subprogram #2

BRAKING IN A TURN RUMI NO. 320 INPUT FILE 96 OUTPUT FILE 1605 T = 3.5
 V0 = 58.6 PB = 99.2 0* = 110.7 AX = 0.55 AYO = -0.25 DAX = 111.7
 RIP = -7.5 RNP = -6.7 GAM1 = -4.8 GAM2 = 0.0 GAM3 = 0.0
 VEHICLE CONFIGURATION: T3-TR6-C2
 WHEEL LOCKS:

0.0 , 0.0 FT/SEC 0.0 , 0.0 FT/SEC 0.0 , 0.0 FT/SEC 1.0 , 47.2 FT/SEC 0.0 , 0.0 FT/SEC
 0.0 , 0.0 FT/SEC 1.0 , 42.4 FT/SEC 0.0 , 0.0 FT/SEC 1.0 , 47.7 FT/SEC 0.0 , 0.0 FT/SEC

T	V5	AX1	AY1	Z1	Z2	Z3	Z4	Z5	Z6	RI	PB
0.0	40.393	-0.010	-0.253	-1.043	0.650	-0.494	0.140	-0.325	0.215	-6.751	-1.538
0.100	40.302	-0.006	-0.258	-1.103	0.670	-0.450	0.153	-0.340	0.201	-6.950	-1.554
0.200	40.181	-0.008	-0.267	-1.083	0.705	-0.450	0.142	-0.322	0.208	-7.039	-1.704
0.300	40.231	0.017	-0.239	-1.103	0.732	-0.435	0.168	-0.375	0.155	-7.099	-1.704
0.400	40.261	0.026	-0.259	-0.903	0.777	-0.430	0.182	-0.425	0.131	-7.144	-1.644
0.500	40.009	0.034	-0.247	-0.809	0.907	-0.430	0.172	-0.435	0.136	-7.069	2.205
0.600	39.777	0.071	-0.242	-0.895	0.910	-0.390	0.212	-0.472	0.063	-7.104	10.113
0.700	39.131	0.154	-0.230	-0.551	1.166	-0.350	0.268	-0.608	-0.152	-7.393	20.213
0.800	38.888	0.219	-0.231	0.528	2.166	-0.288	0.375	-1.032	-0.553	-6.950	34.770
0.900	38.575	0.377	-0.231	1.416	2.176	-0.250	0.370	-1.502	-1.026	-6.616	51.479
1.000	37.960	0.450	-0.226	1.705	2.178	-0.147	0.372	-1.567	-1.076	-7.139	65.418
1.100	36.536	0.499	-0.179	1.541	2.178	-0.173	0.313	-1.540	-1.116	-7.174	76.241
1.200	35.102	0.559	-0.195	1.505	2.178	-0.163	0.300	-1.638	-1.343	-5.939	83.961
1.300	34.325	0.564	-0.185	1.749	2.179	-0.118	0.325	-1.608	-1.336	-5.869	90.511
1.400	32.871	0.551	-0.167	1.822	2.179	-0.100	0.325	-1.580	-1.316	-5.705	94.696
1.500	31.781	0.543	-0.167	1.844	2.178	-0.096	0.320	-1.590	-1.355	-5.217	97.075
1.600	30.559	0.535	-0.157	1.854	2.181	-0.066	0.332	-1.578	-1.383	-4.953	98.174
1.700	29.196	0.541	-0.149	1.864	2.178	-0.065	0.335	-1.542	-1.370	-4.774	98.986
1.800	27.894	0.529	-0.144	1.839	2.178	-0.065	0.335	-1.510	-1.358	-4.500	99.227
1.900	27.096	0.526	-0.133	1.835	2.179	-0.058	0.325	-1.518	-1.353	-4.520	99.212
2.000	25.763	0.525	-0.124	1.772	2.179	-0.066	0.325	-1.515	-1.355	-4.366	99.257
2.100	24.420	0.519	-0.137	1.825	2.178	-0.088	0.327	-1.510	-1.353	-3.987	99.227
2.200	23.522	0.520	-0.122	1.850	2.179	-0.086	0.323	-1.525	-1.353	-4.062	99.242
2.300	22.250	0.520	-0.109	1.830	2.178	-0.081	0.313	-1.518	-1.348	-3.838	99.242
2.400	21.079	0.533	-0.106	1.956	2.181	-0.035	0.340	-1.510	-1.355	-3.335	99.242
2.500	20.039	0.536	-0.080	2.118	2.181	-0.023	0.343	-1.493	-1.348	-3.330	99.303
2.600	18.847	0.527	-0.055	2.119	2.179	-0.031	0.315	-1.495	-1.348	-3.021	99.257
2.700	17.404	0.537	-0.064	2.089	2.178	-0.010	0.307	-1.500	-1.360	-2.235	99.182
2.800	16.283	0.537	-0.067	2.159	2.178	0.059	0.337	-1.477	-1.361	-2.031	99.167
2.900	15.193	0.550	-0.056	2.218	2.181	0.087	0.327	-1.473	-1.390	-2.339	99.227
3.000	13.971	0.544	-0.034	2.219	2.178	0.092	0.303	-1.473	-1.446	-2.050	99.242
3.100	12.588	0.555	-0.039	2.306	2.178	0.109	0.308	-1.468	-1.471	-1.353	99.212
3.200	11.417	0.572	-0.040	2.378	2.178	0.124	0.303	-1.462	-1.471	-1.393	99.197
3.300	10.306	0.568	-0.023	2.428	2.178	0.147	0.317	-1.432	-1.473	-1.368	99.212
3.400	9.044	0.570	-0.016	2.446	2.178	0.146	0.303	-1.437	-1.492	-1.229	99.197
3.500	7.630	0.569	-0.013	2.461	2.178	0.166	0.290	-1.442	-1.499	-1.219	99.212
3.600	6.490	0.580	-0.005	2.461	2.178	0.166	0.290	-1.442	-1.499	-1.219	99.212
3.700	5.228	0.569	-0.000	2.538	2.181	0.174	0.282	-1.433	-1.494	-1.304	99.182
3.800	3.814	0.574	0.000	2.555	2.178	0.171	0.260	-1.430	-1.499	-0.826	99.212
3.900	2.743	0.574	0.000	2.648	2.178	0.171	0.260	-1.430	-1.499	-0.826	99.212

Figure A.3. Example data processing printout for braking-in-a-turn maneuver.

**** Subprogram #3 (Trapezoidal Steer) ****

- Duplicates first two items under Subprogram #1.
- Detection of start and end of test maneuver (steer application/
5 seconds of test data after steer application).
- Calculates the following numerics over the maneuver interval:
 - a) Initial vehicle velocity, V_0 (ft/sec)
 - b) Average steady-state steering-wheel angle, DSW (deg)
 - c) Average steady-state lateral acceleration of tractor, AY1SS (g's)
 - d) Average steady-state yaw rate of tractor, R1SS (deg/sec)
 - e) Tractor yaw rate response time (50% of steer to 90% of
s.s. yaw rate) TRESP (sec)
 - f) Length of time of processed test data, T (sec)
 - g) Tractor peak lateral acceleration, AY1P (g's)
 - h) Last trailer peak lateral acceleration, AY2P (g's)
(Tractor and last trailer lateral acceleration time histories were
corrected for contributions deriving from roll motions.)
 - i) Tractor peak yaw rate, RIP (deg/sec)
 - j) Tractor peak roll angle, PH1P (deg)
 - k) Last trailer peak roll angle, PHNP (deg)
(Tractor and last trailer roll angles obtained from integration
of roll rates.)
 - l) Peak tractor-trailer articulation angle, GAM1 (deg)
 - m) Peak articulation angle of last dolly with respect to
lead trailer (pintle hook angle), GAM2 (deg)
 - n) Peak articulation angle of last dolly with respect to
last trailer, GAM3 (deg)

-Writes a header record containing run number, file number, and maneuver information on the output tape.

-Writes the above numerics to both the line printer and the output tape.

-Writes the following variables as time histories to both the line printer and the output tape:

- a) time, T (sec)
- b) steering-wheel angle, DSW (deg)
- c) tractor lateral acceleration, AY1 (g's)
- d) last trailer lateral acceleration, AYN (g's)
- e) tractor roll angle, PH11 (deg)
- f) last trailer roll angle, PH1N (deg)
- g) tractor yaw rate, R1 (deg/sec)
- h) last trailer yaw rate, RN (deg/sec)
- i) left front tractor suspension deflection, Z1 (inches)
- j) left rear (single or leading tandem) tractor suspension deflection, Z3 (inches)

-Writes a tape mark on the output tape, closing the output tape file.

-Returns to Main program.

Figure A.4 shows an example printout for Subprogram #3.

TRAPEZOIDAL STEER FUN NO. 609 INPUT FILE 02 OUTPUT FILE 509
 V0 = 67.2 DSW = -102. AYSS = 0.35 RISS = 11.0 TRESP = 0.46 T = 5.0
 AYP = 0.34 AY2P = 0.39 RIP = 11.4 PUIP = 3.2 PIMP = 2.6
 GAM1 = 5.4 GAM2 = -3.2 GAM3 = 0.0

VEHICLE CONFIGURATION: 93-TRC-TR6-127K

T	DSW	AV1	AYH	PHI1	PHIM	F1	FN	Z1	Z3
0.0	-15.255	0.005	0.000	0.021	-0.002	-0.126	-0.282	-0.308	-0.017
0.100	-19.423	0.014	-0.022	0.070	-0.017	-0.019	-0.258	-0.214	0.033
0.200	-17.722	0.009	-0.013	0.078	-0.021	0.184	-0.340	-0.272	-0.007
0.300	-20.546	-0.001	-0.012	-0.001	-0.012	0.261	-0.427	-0.374	0.014
0.400	-23.687	0.023	-0.034	0.313	-0.026	0.242	-0.374	-0.266	0.029
0.500	-31.304	0.027	-0.018	0.056	0.058	0.421	-0.374	-0.274	0.040
0.600	-40.097	0.047	-0.304	0.157	0.125	0.953	-0.263	-0.258	0.017
0.700	-70.207	0.101	-0.020	0.357	0.114	2.430	-0.258	-0.175	0.069
0.800	-94.041	0.153	-0.023	0.623	0.154	4.943	-0.306	-0.059	0.087
0.900	-101.874	0.217	-0.011	0.839	0.259	7.560	-0.311	0.043	0.067
1.000	-101.994	0.230	-0.008	0.981	0.289	8.870	-0.180	0.136	0.079
1.100	-111.922	0.240	-0.006	1.050	0.272	9.814	-0.171	0.122	0.091
1.200	-111.946	0.276	-0.018	1.197	0.237	10.321	-0.272	0.138	0.095
1.300	-101.898	0.206	-0.027	1.430	0.269	10.554	-0.238	0.191	0.075
1.400	-111.874	0.297	-0.010	1.640	0.407	10.529	-0.118	0.245	0.135
1.500	-101.946	0.305	0.011	1.845	0.516	10.505	0.027	0.389	0.103
1.600	-101.779	0.303	0.015	2.041	0.477	10.520	0.240	0.416	0.133
1.700	-101.803	0.321	0.029	2.205	0.417	10.486	0.676	0.531	0.162
1.800	-101.850	0.321	0.037	2.332	0.533	10.529	1.316	0.542	0.156
1.900	-101.803	0.321	0.075	2.413	0.724	10.563	2.267	0.539	0.161
2.000	-101.707	0.333	0.113	2.492	0.918	10.718	3.223	0.613	0.151
2.100	-101.650	0.336	0.130	2.577	1.070	10.703	4.208	0.652	0.103
2.200	-101.822	0.333	0.178	2.656	1.250	10.858	5.183	0.729	0.188
2.300	-111.946	0.349	0.175	2.698	1.404	10.909	5.995	0.692	0.206
2.400	-111.867	0.323	0.219	2.674	1.615	10.858	6.897	0.561	0.209
2.500	-112.066	0.347	0.256	2.698	1.790	11.066	7.612	0.647	0.190
2.600	-101.779	0.349	0.218	2.766	1.875	11.076	8.244	0.755	0.216
2.700	-101.898	0.347	0.288	2.842	1.942	11.226	8.829	0.834	0.225
2.800	-101.850	0.365	0.293	2.860	2.103	11.119	9.260	0.807	0.250
2.900	-101.707	0.340	0.285	2.918	2.216	11.057	9.751	0.760	0.242
3.000	-101.946	0.363	0.318	2.968	2.319	11.139	9.978	0.797	0.240
3.100	-101.395	0.354	0.314	3.018	2.345	11.003	10.383	0.859	0.243
3.200	-101.515	0.344	0.311	3.066	2.357	11.327	10.451	0.825	0.235
3.300	-101.603	0.372	0.313	3.177	2.404	11.264	10.499	0.831	0.251
3.400	-101.659	0.336	0.333	3.050	2.462	11.206	10.601	0.817	0.237
3.500	-101.070	0.376	0.308	3.039	2.474	11.192	10.649	0.851	0.258
3.600	-101.603	0.340	0.327	3.066	2.428	10.820	10.745	0.838	0.254
3.700	-102.130	0.342	0.360	3.136	2.408	11.105	10.905	0.809	0.251
3.800	-102.018	0.352	0.350	3.161	2.435	10.907	10.943	0.833	0.246
3.900	-101.765	0.345	0.320	3.163	2.426	11.119	10.996	0.872	0.254
4.000	-102.900	0.354	0.392	3.198	2.463	10.853	10.866	0.833	0.254
4.100	-101.765	0.321	0.333	3.117	2.525	10.713	11.972	0.755	0.242
4.200	-101.922	0.340	0.354	3.199	2.521	10.795	10.948	0.807	0.243
4.300	-101.946	0.347	0.360	3.165	2.495	10.703	11.073	0.800	0.244

Figure A.4. Example data processing printout for trapezoidal steer maneuver.

4.500	-111.033	0.301	0.308	3.199	2.546	10.507	10.791	0.823	0.232
4.600	-102.186	0.322	0.330	3.166	2.563	10.408	10.789	0.750	0.240
4.700	-102.050	0.329	0.364	3.197	2.616	10.379	10.620	0.817	0.250
4.800	-101.659	0.316	0.351	3.179	2.627	10.462	10.731	0.825	0.237
4.900	-102.042	0.330	0.325	3.138	2.532	10.404	10.470	0.742	0.250
5.000	-102.210	0.328	0.308	3.170	2.464	10.804	10.198	0.878	0.248
5.100	-102.186	0.321	0.326	3.199	2.480	10.404	10.219	0.854	0.242
5.200	-102.114	0.316	0.323	3.164	2.562	10.171	10.292	0.763	0.248
5.300	-102.018	0.306	0.334	3.168	2.485	10.341	10.161	0.706	0.254

Figure A.4 (Cont.)

**** Subprogram #4 (Double Lane Change) ****

- Duplicates first two items under Subprogram #1.
- Detection of start and end of maneuver (steer application/10 seconds after steer application).
- Calculates the following numerics over the maneuver interval:
 - a) Initial vehicle velocity, V_0 (ft/sec)
 - b) Peak steering-wheel angle, $DSWP$ (deg)
 - c) Lag between steering-wheel angle input and tractor yaw rate response corresponding to the maximum cross-correlation, TAU (sec)
 - d) Value of the cross-correlation function for TAU value, $CORR$ (deg²/sec)
 - e) Length of time of processed test data, T (sec)
 - f) Tractor and last trailer peak lateral accelerations, $AY1P$, $AY2P$ (g's)

(Lateral acceleration time histories were corrected for contributions deriving from roll motions.)
 - g) Peak yaw rate of tractor, RIP (deg/sec)
 - h) Peak roll angles of tractor and last trailer, $PH1P$, $PHNP$ (deg)

(Roll angle time histories were obtained by integration of roll rate signals.)
 - i) Peak tractor/trailer articulation angle, $GAM1$ (deg)
 - j) Peak articulation angle of last dolly with respect to the lead trailer (pintle hook angle), $GAM2$ (deg)
 - k) Peak articulation angle of last dolly with respect to the last trailer, $GAM3$ (deg)

Computation of the X (forward) - Y (lateral) path trajectories of tractor rear axle center-line and last trailer rear axle center-line (shown below) are obtained by integration of the axle location lateral accelerations and forward velocities. Input parameters B1, BN, and XACC, printed next, are dimensions between tractor c.g./last axle, last trailer c.g./last axle, and tractor c.g./last trailer c.g. used in the X-Y trajectory calculations.

-Writes a header record containing run number, file number, and maneuver information on the output tape.

-Writes the above numerics to both the line printer and the output tape.

-Writes the following variables as time histories to both the line printer and the output tape:

- a) time, T (sec)
 - b) steering-wheel angle, DSW (deg)
 - c) tractor lateral acceleration, AY1 (g's)
 - d) last trailer lateral acceleration, AYN (g's)
 - e) tractor roll angle, PHI1 (deg)
 - f) last trailer roll angle, PHIN (deg)
 - g) tractor rear axle longitudinal displacement, X1 (ft)
 - h) tractor rear axle lateral displacement, Y1 (ft)
 - i) last trailer rear axle longitudinal displacement, XN (ft)
 - j) last trailer rear axle lateral displacement, YN (ft)
 - k) tractor yaw rate, R1 (deg/sec)
 - l) last trailer yaw rate, RN (deg/sec)
- Path Trajectories {

-Writes a tape mark on the output tape, closing output tape file.

-Returns to Main program.

Figure A.5 shows an example printout for Subprogram #4.

DOUBLE LANE-CHANGE RUN NO. 712 INPUT FILE 116 OUTPUT FILE 530
 VO = 44.5 DSMP = 127. CORR = 411.37 TAU = 0.22 T = 10.0
 AYIP = -0.23 AY2P = -0.20 R1P = -10.6 PHIP = -1.9 PHNP = -1.3
 GAM1 = -7.2 GAM2 = 3.1 GAM3 = -0.5
 BI = 9.13 RN = 15.50 YACC = 80.00

VEHICLE CONFIGURATION: T3-TR5-TR6-127K

T	DSM	AY1	AYN	PHY1	PHYN	X1	V1	KN	YN	R1	RN
0.0	-2.760	0.021	0.002	-0.040	-0.034	-8.208	0.002	-94.608	0.001	-0.069	-0.202
0.100	-4.469	0.024	0.021	-0.041	0.021	-3.761	0.009	-90.161	0.002	-0.030	-0.138
0.200	-8.430	0.022	0.030	-0.045	0.033	0.697	0.013	-85.703	-0.001	0.053	-0.080
0.300	-13.169	0.027	0.023	-0.014	0.050	5.174	0.014	-81.226	-0.008	0.258	-0.104
0.400	-18.832	0.031	0.020	0.030	0.009	9.629	0.013	-76.771	-0.012	0.586	-0.163
0.500	-21.960	0.050	0.049	0.065	-0.038	14.105	0.012	-72.295	-0.016	0.752	-0.133
0.600	-31.008	0.055	0.014	0.093	-0.017	18.565	0.012	-67.835	-0.026	1.396	-0.143
0.700	-40.535	0.079	0.009	0.104	0.029	23.018	0.014	-63.382	-0.041	1.772	-0.094
0.800	-51.398	0.097	0.013	0.157	0.122	27.495	0.027	-58.905	-0.063	2.534	-0.080
0.900	-59.662	0.109	0.025	0.224	0.165	31.959	0.047	-54.441	-0.087	3.491	-0.089
1.000	-66.831	0.133	0.025	0.301	0.150	36.415	0.083	-49.905	-0.110	4.253	-0.080
1.100	-76.115	0.151	0.019	0.375	0.149	40.860	0.141	-45.540	-0.132	5.195	-0.099
1.200	-84.378	0.168	0.017	0.470	0.131	45.280	0.224	-41.120	-0.156	6.040	-0.018
1.300	-87.100	0.177	0.031	0.602	0.116	49.710	0.339	-36.690	-0.190	7.046	-0.050
1.400	-86.541	0.184	0.018	0.700	0.104	54.141	0.493	-32.259	-0.205	7.495	0.033
1.500	-85.983	0.191	0.013	0.802	0.135	58.563	0.694	-27.837	-0.234	7.691	-0.001
1.600	-81.437	0.185	0.023	0.837	0.176	62.991	0.946	-23.409	-0.265	7.788	0.126
1.700	-76.236	0.187	0.035	0.824	0.196	67.413	1.255	-18.987	-0.297	7.295	0.248
1.800	-70.598	0.171	0.046	0.789	0.214	71.850	1.618	-14.550	-0.320	7.031	0.410
1.900	-64.036	0.155	0.059	0.764	0.234	76.302	2.035	-10.098	-0.360	6.274	0.806
2.000	-56.259	0.151	0.079	0.765	0.255	80.756	2.504	-5.644	-0.391	5.918	1.222
2.100	-49.357	0.130	0.074	0.752	0.249	85.212	3.017	-1.188	-0.415	5.264	1.564
2.200	-42.888	0.105	0.078	0.721	0.287	89.663	3.575	3.263	-0.432	4.722	1.900
2.300	-35.528	0.101	0.086	0.654	0.371	94.110	4.170	7.710	-0.442	4.077	2.416
2.400	-26.220	0.101	0.106	0.591	0.460	98.574	4.803	12.174	-0.441	3.198	2.866
2.500	-14.117	0.061	0.111	0.528	0.527	101.051	5.466	16.651	-0.423	2.568	3.301
2.600	1.874	0.040	0.123	0.430	0.575	107.531	6.155	21.131	-0.383	1.435	3.590
2.700	20.539	0.019	0.144	0.341	0.606	112.018	6.865	25.618	-0.317	0.420	3.932
2.800	35.218	-0.021	0.161	0.212	0.578	116.516	7.585	30.116	-0.220	-1.924	4.392
2.900	46.568	-0.036	0.135	0.104	0.562	121.020	8.311	34.620	-0.091	-2.086	4.568
3.000	63.021	-0.063	0.135	-0.052	0.568	125.542	9.035	39.142	0.069	-2.086	4.568
3.100	86.231	-0.106	0.136	-0.204	0.590	130.084	9.747	43.684	0.261	-4.429	4.710
3.200	116.702	-0.152	0.143	-0.402	0.598	134.627	10.441	48.227	0.490	-6.182	4.705
3.300	113.548	-0.156	0.143	-0.639	0.550	139.191	11.105	52.791	0.760	-7.867	4.504
3.400	116.391	-0.179	0.136	-0.772	0.479	143.786	11.729	57.386	1.070	-9.098	4.500
3.500	116.343	-0.190	0.119	-0.900	0.428	148.377	12.258	61.977	1.419	-9.664	4.304
3.600	116.148	-0.199	0.119	-0.993	0.346	152.980	12.806	66.580	1.804	-9.991	4.055
3.700	116.221	-0.190	0.102	-1.122	0.354	157.579	13.246	71.179	2.224	-9.991	3.781
3.800	116.506	-0.190	0.088	-1.220	0.325	162.176	13.613	75.776	2.678	-9.820	3.379
3.900	116.756	-0.205	0.081	-1.320	0.251	166.767	13.907	80.367	3.166	-10.011	2.831
4.000	116.975	-0.202	0.041	-1.422	0.114	171.377	14.129	84.977	3.688	-10.006	2.176
0.100	111.811	-1.009	0.000	-1.866	0.000	175.988	14.377	89.588	4.233	-10.000	1.427

Figure A.5. Example data processing printout for double-lane-change maneuver.

4.300	120.450	-0.213	-0.014	-1.531	-0.163	185.208	14.347	98.808	5.186	-9.933	0.097
4.400	123.464	-0.204	-0.031	-1.563	-0.256	189.830	14.268	103.410	5.974	-9.806	-0.632
4.500	126.477	-0.202	-0.052	-1.611	-0.319	194.411	14.115	108.011	6.564	-9.918	-1.366
4.600	127.489	-0.215	-0.063	-1.718	-0.348	199.039	13.889	112.630	7.140	-10.235	-2.032
4.700	127.231	-0.207	-0.063	-1.807	-0.410	203.632	13.590	117.232	7.721	-10.436	-2.619
4.800	123.707	-0.216	-0.093	-1.884	-0.480	208.247	13.216	121.847	8.280	-10.563	-3.260
4.900	114.447	-0.215	-0.092	-1.892	-0.548	212.861	12.764	126.461	8.818	-10.431	-3.768
5.000	97.119	-0.194	-0.106	-1.914	-0.599	217.472	12.213	131.072	9.332	-10.055	-4.248
5.100	73.180	-0.164	-0.119	-1.908	-0.635	222.079	11.622	135.679	9.817	-8.971	-4.771
5.200	43.633	-0.103	-0.116	-1.826	-0.684	226.685	10.934	140.285	10.270	-7.437	-5.143
5.300	12.446	-0.052	-0.113	-1.662	-0.736	231.262	10.175	144.862	10.687	-5.118	-5.662
5.400	-15.065	-0.025	-0.136	-1.532	-0.803	235.797	9.351	149.397	11.067	-2.662	-6.102
5.500	-41.781	0.042	-0.161	-1.382	-0.872	240.346	8.480	153.946	11.407	-0.288	-6.635
5.600	-65.276	0.099	-0.165	-1.210	-0.933	244.845	7.578	158.445	11.703	-0.099	-7.144
5.700	-86.395	0.158	-0.176	-0.964	-0.999	249.329	6.665	162.929	11.948	4.409	-7.467
5.800	-101.682	0.179	-0.186	-0.608	-1.068	253.804	5.759	167.404	12.141	6.563	-7.927
5.900	-108.001	0.220	-0.184	-0.428	-1.162	258.246	4.870	171.846	12.279	8.111	-8.323
6.000	-107.102	0.220	-0.191	-0.191	-1.239	262.676	4.036	176.276	12.358	9.185	-8.617
6.100	-103.067	0.210	-0.186	0.020	-1.274	267.091	3.244	180.691	12.370	9.532	-8.588
6.200	-95.825	0.218	-0.175	0.157	-1.273	271.509	2.516	185.109	12.313	9.175	-6.558
6.300	-86.079	0.203	-0.175	0.244	-1.224	275.935	1.854	189.535	12.181	8.828	-8.167
6.400	-74.882	0.195	-0.152	0.315	-1.126	280.363	1.259	193.963	11.975	7.886	-7.550
6.500	-63.647	0.163	-0.113	0.350	-1.001	284.802	0.729	198.402	11.698	7.056	-6.885
6.600	-53.464	0.145	-0.085	0.335	-0.887	289.240	0.258	202.840	11.355	5.845	-5.916
6.700	-45.711	0.126	-0.052	0.316	-0.781	293.690	-0.153	207.290	10.952	4.756	-4.952
6.800	-40.097	0.113	-0.021	0.310	-0.686	298.151	-0.521	211.751	10.498	3.970	-3.773
6.900	-37.691	0.106	0.001	0.312	-0.589	302.632	-0.848	216.232	10.002	3.374	-2.746
7.000	-37.084	0.104	0.025	0.305	-0.470	307.109	-1.145	220.709	9.474	3.144	-1.750
7.100	-36.914	0.109	0.053	0.290	-0.359	311.592	-1.413	225.192	8.922	2.915	-0.740
7.200	-37.035	0.101	0.068	0.268	-0.265	316.074	-1.655	229.674	8.358	2.910	0.013
7.300	-36.428	0.081	0.076	0.265	-0.184	320.553	-1.875	234.153	7.787	2.837	0.782
7.400	-36.355	0.102	0.091	0.241	-0.119	325.042	-2.067	238.643	7.217	2.690	1.290
7.500	-36.014	0.092	0.087	0.241	-0.089	329.546	-2.240	243.146	6.655	2.749	1.995
7.600	-35.747	0.093	0.093	0.256	-0.060	334.027	-2.388	247.627	6.107	2.744	1.995
7.700	-35.188	0.102	0.109	0.228	-0.024	338.520	-2.517	252.120	5.574	2.812	2.308
7.800	-34.994	0.108	0.108	0.209	0.035	343.069	-2.622	256.669	5.056	2.641	2.611
7.900	-34.775	0.087	0.106	0.215	0.088	347.574	-2.703	261.174	4.558	2.700	2.734
8.000	-34.945	0.082	0.107	0.219	0.114	352.070	-2.765	265.670	4.081	2.715	2.817
8.100	-34.240	0.084	0.105	0.224	0.138	356.578	-2.805	270.178	3.632	2.681	2.944
8.200	-33.909	0.085	0.098	0.224	0.155	361.075	-2.826	274.676	3.204	2.705	3.047
8.300	-33.827	0.101	0.099	0.206	0.178	365.561	-2.824	279.161	2.800	2.495	3.042
8.400	-33.754	0.085	0.092	0.178	0.229	370.049	-2.799	283.649	2.419	2.422	3.184
8.500	-33.803	0.093	0.120	0.169	0.280	374.538	-2.757	288.138	2.059	2.436	3.277
8.600	-33.390	0.078	0.114	0.167	0.288	379.035	-2.694	292.635	1.730	2.436	3.247
8.700	-32.077	0.072	0.109	0.165	0.275	383.502	-2.614	297.103	1.430	2.402	3.179
8.800	-29.919	0.077	0.104	0.150	0.253	387.999	-2.513	301.599	1.158	2.300	3.189
8.900	-27.022	0.074	0.102	0.127	0.257	392.502	-2.395	306.102	0.912	2.226	3.193
9.000	-24.179	0.087	0.097	0.109	0.270	396.983	-2.257	310.583	0.691	1.953	3.140
9.100	-22.916	0.065	0.093	0.083	0.251	401.467	-2.130	315.067	0.498	1.806	3.017
9.200	-21.360	0.075	0.111	0.039	0.247	405.958	-1.938	319.558	0.332	1.509	2.934
9.300	-21.238	0.058	0.097	-0.005	0.234	410.444	-1.737	324.044	0.194	1.299	2.827
9.400	-21.287	0.098	0.104	-0.007	0.193	414.916	-1.535	328.516	0.084	1.396	2.730
9.500	-21.068	0.061	0.095	0.036	0.143	419.387	-1.321	332.997	0.000	1.455	2.660
9.600	-21.287	0.071	0.080	0.001	0.104	423.885	-1.098	337.485	-0.059	1.426	2.606
9.700	-20.995	0.066	0.037	-0.037	0.114	428.387	-0.860	341.987	-0.097	1.211	2.567
9.800	-20.906	0.052	0.091	0.005	0.085	432.869	-0.611	346.469	-0.112	1.269	2.484
9.900	-20.899	0.064	0.096	-0.019	0.046	437.343	-0.352	350.942	-0.102	1.142	2.372

Figure A.5 (Cont.)

**** Subprogram #5 (Sinusoidal Steer) ****

- Duplicates first two items under Subprogram #1.
- Determines start and end of test maneuver (steer application/ 5 seconds after steer application).
- Calculates the following numerics over the maneuver interval:

- a) Initial vehicle velocity, V_0 (ft/sec)
- b) Peak steering-wheel angle, $DSWP$ (deg)
- c) Lag between steering-wheel angle input and tractor yaw rate response corresponding to the maximum cross-correlation, TAU (sec)
- d) Value of the cross-correlation function for TAU value, $CORR$ (deg²/sec)
- e) Length of time of processed test data, T (sec)
- f) Tractor and last trailer peak lateral accelerations $AY1P$, $AY2P$ (g's)

(Lateral accelerations were corrected for contributions deriving from roll motions.)

- g) Peak yaw rate of tractor, $R1P$ (deg/sec)
- h) Peak roll angles of tractor and last trailer, $PH1P$, $PHNP$ (deg)
(Roll angles were obtained by integration of roll rate signals.)
- i) Peak tractor/trailer articulation angle, $GAM1$ (deg)
- j) Peak articulation angle of last dolly with respect to lead trailer (pintle hook angle), $GAM2$ (deg)
- k) Peak articulation angle of last dolly with respect to last trailer, $GAM3$ (deg)
- l) Ratio of tractor peak lateral acceleration to last trailer peak lateral acceleration, $AMPLIF. RATIO$

- m) Period of driver's "sine-wave" steering-wheel input, PERIOD (sec)
- n) Measure of the quality of the manually-applied steering sine wave, defined as

$$\text{SINBAL} = \frac{1}{(t_f - t_0)} \int_{t_0}^{t_f} \text{DSW} dt, \text{ (deg)}$$

where DSW = steering-wheel input.

-Writes a header record containing run number, file number, and maneuver information on the output tape.

-Writes the above numerics to both the line printer and the output tape.

-Writes the following variables as time histories to both the line printer and the output tape:

- a) time, T (sec)
- b) steering-wheel angle, DSW (deg)
- c) tractor lateral acceleration, AY1 (g's)
- d) last trailer lateral acceleration, AYN (g's)
- e) tractor roll angle, PH11 (deg)
- f) last trailer roll angle, PHIN (deg)
- g) tractor yaw rate, R1 (deg/sec)
- h) last trailer yaw rate, RN (deg/sec)
- i) tractor left front suspension deflection, Z1 (inches)
- j) tractor left rear (single axle/leading tandem) suspension deflection, Z3 (inches)

-Writes a tape mark on the output tape, closing output tape file.

-Returns to Main program.

Figure A.6 shows an example printout for Subprogram #5.

SINUSOIDAL STEER RUN NO. 678 INPUT FILE 81 OUTPUT FILE 499
 V0 = 69.4 DSWP = 147. CORR = 413.76 TAU = 0.16 T = 5.0
 AV2P = -0.36 AV2P = -0.30 RIP = 15.0 PHIP = -1.6 PUMP = -1.9
 GAM1 = 5.5 GAM2 = -5.3 PERIOD = 2.0 SIRBAL = 5.2
 AMPLIF. RATIO = 0.8
 VEHICLE CONFIGURATION: T3-THE-TR6-177K

T	DSW	AV1	AVH	PHI1	PHI	P1	RN	Z1	Z3
0.0	-3.090	-0.000	-0.025	0.201	-0.017	0.453	0.011	-0.364	-0.032
0.100	-3.041	-0.007	-0.003	0.110	0.110	0.182	0.045	-0.374	-0.064
0.200	-2.283	-0.001	0.029	-0.006	0.053	0.127	0.109	-0.471	-0.116
0.300	2.408	-0.002	0.066	-0.039	-0.115	0.275	0.223	-0.503	-0.073
0.400	15.700	-0.020	-0.037	-0.037	-0.210	0.266	0.218	-0.404	-0.064
0.500	38.178	-0.038	-0.035	0.014	-0.231	-0.001	0.252	-0.382	-0.089
0.600	69.306	-0.003	-0.015	-0.079	-0.038	-1.150	0.154	-0.463	-0.015
0.700	134.123	-0.162	0.016	-0.180	0.056	-3.660	0.168	-0.511	-0.086
0.800	137.450	-0.240	0.033	-0.732	-0.041	-7.211	0.257	-0.608	-0.089
0.900	146.881	-0.311	-0.007	-1.067	-0.217	-10.737	0.360	-0.902	-0.063
1.000	144.927	-0.307	0.008	-1.291	-0.230	-12.265	0.454	-1.006	-0.150
1.100	128.483	-0.330	0.002	-1.435	-0.139	-13.281	0.553	-0.955	-0.209
1.200	96.622	-0.331	0.004	-1.549	-0.047	-12.650	0.626	-0.933	-0.148
1.300	59.093	-0.257	0.033	-1.570	-0.065	-10.022	0.572	-0.940	-0.193
1.400	12.181	-0.169	0.002	-1.586	-0.155	-6.624	0.410	-1.079	-0.195
1.500	-45.994	-0.071	-0.014	-1.442	-0.191	-2.457	0.173	-0.971	-0.267
1.600	-138.348	0.071	-0.071	-1.208	-0.231	2.667	-0.324	-0.757	-0.269
1.700	-143.532	0.172	-0.071	-0.681	-0.405	9.049	-1.289	-0.422	-0.176
1.800	-141.580	0.229	-0.103	-0.650	-0.650	12.994	-2.579	-0.075	-0.112
1.900	-142.114	0.312	-0.166	-0.178	-0.866	14.291	-4.071	0.001	-0.078
2.000	-129.336	0.331	-0.233	0.390	-1.159	15.021	-5.987	0.001	-0.013
2.100	-99.625	0.304	-0.244	0.729	-1.486	14.101	-7.550	0.074	0.015
2.200	-64.392	0.251	-0.202	0.992	-1.758	11.707	-8.779	0.138	-0.013
2.300	-30.186	0.195	-0.209	1.027	-1.915	8.371	-9.109	0.037	-0.005
2.400	-7.218	0.149	-0.278	0.974	-1.927	4.724	-9.035	-0.006	0.021
2.500	-1.941	0.107	-0.292	1.021	-1.830	2.466	-8.080	0.011	0.008
2.600	-4.507	0.083	-0.203	1.061	-1.591	0.340	-6.135	-0.009	0.024
2.700	-5.044	0.061	-0.128	1.016	-1.144	-0.198	-3.300	-0.009	0.016
2.800	-3.954	0.047	-0.035	0.893	-0.553	-0.435	0.011	-0.202	0.031
2.900	-2.112	0.018	0.084	0.766	0.041	-0.159	2.921	-0.194	-0.018
3.000	0.600	0.010	0.152	0.730	0.526	0.216	5.408	-0.149	-0.000
3.100	2.310	0.010	0.212	0.614	0.816	-0.030	7.304	-0.176	0.011
3.200	2.921	0.005	0.246	0.532	1.038	-0.025	8.446	-0.232	-0.010
3.300	3.312	0.005	0.251	0.496	1.183	-0.085	8.943	-0.220	0.001
3.400	3.849	-0.004	0.272	0.452	1.262	-0.085	8.904	-0.252	0.003
3.500	4.411	-0.003	0.264	0.395	1.234	-0.168	8.397	-0.210	-0.007
3.600	4.460	0.001	0.225	0.331	1.151	-0.405	7.619	-0.293	-0.018
3.700	4.460	-0.009	0.219	0.252	1.060	-0.262	6.442	-0.291	0.003
3.800	4.436	-0.003	0.183	0.183	0.923	-0.405	5.240	-0.285	-0.017
3.900	4.411	-0.016	0.117	0.156	0.787	-0.435	3.915	-0.280	-0.015
4.000	4.405	-0.019	0.119	0.147	0.680	-0.223	2.908	-0.263	-0.013
4.100	4.400	-0.019	0.119	0.147	0.680	-0.223	2.908	-0.263	-0.013

Figure A.6. Example data processing printout for sinusoidal steer maneuver.

4.300	0.005	0.015	0.109	-0.252	0.494	-0.286	-0.028
4.400	0.008	0.019	0.147	-0.302	0.114	-0.270	-0.050
4.500	-0.009	-0.009	0.060	-0.297	-0.211	-0.311	-0.020
4.600	-0.010	-0.029	0.047	-0.292	-0.304	-0.351	-0.038
4.700	-0.020	-0.024	0.041	-0.242	-0.516	-0.371	-0.032
4.800	-0.017	-0.006	0.008	-0.267	-0.595	-0.333	-0.035
4.900	-0.027	-0.037	-0.010	-0.252	-0.580	-0.337	-0.030

Figure A.6 (Cont.)

